On focusing of strong shock waves

by

Veronica Eliasson

December 2005
Technical Reports from
Royal Institute of Technology
KTH Mechanics
SE-100 44 Stockholm, Sweden

Akademisk avhandling som med tillstånd av Kungliga Tekniska Högskolan i Stockholm framlägges till offentlig granskning för avläggande av teknologie licentiatexamen torsdagen den 15 december 2003 kl 10.15 i S40, Teknikringen 8, Kungliga Tekniska Högskolan, Vallhallavägen 79, Stockholm.

Universitetsservice US–AB, Stockholm 2005

Veronica Eliasson 2005, **On focusing of strong shock waves**
KTH Mechanics, SE-100 44 Stockholm, Sweden

Abstract

Focusing of strong shock waves in a gas-filled thin test section with various forms of the reflector boundary is investigated. The test section is mounted at the end of the horizontal co-axial shock tube. Two different methods to produce shock waves of various forms are implemented. In the first method the reflector boundary of the test section is exchangeable and four different reflectors are used: a circle, a smooth pentagon, a heptagon and an octagon. It is shown that the form of the converging shock wave is influenced both by the shape of the reflector boundary and by the nonlinear dynamic interaction between the shape of the shock and the propagation velocity of the shock front. Further, the reflected outgoing shock wave is affected by the shape of the reflector through the flow ahead of the shock front. In the second method cylindrical obstacles are placed in the test section at various positions and in various patterns, to create disturbances in the flow that will shape the shock wave. It is shown that it is possible to shape the shock wave in a desired way by means of obstacles. The influence of the supports of the inner body of the co-axial shock tube on the form of the shock is also investigated. A square shaped shock wave is observed close to the center of convergence for the circular and octagonal reflector boundaries but not in any other setups. This square-like shape is believed to be caused by the supports for the inner body. The production of light, as a result of shock convergence, has been preliminary investigated. Flashes of light have been observed during the focusing and reflection process.

Descriptors: Shock focusing, imploding shock, converging shock, reflected shock, annular shock tube

Preface

The thesis is divided into two parts. The first part, starting with an introductory section, is an overview and summary of the present contribution to the field of fluid mechanics. The second part consists of three papers, which are adjusted to comply with the present thesis format for consistency. However, their contents have not been changed compared to published or submitted versions except for minor refinements.

November 2005, Stockholm
Veronica Eliasson

Contents

Abstract iii

Preface iv

Chapter 1. Introduction 1

Chapter 2. Theoretical Preliminaries 3
2.1. Euler Equations 3
2.2. Shock Tube Theory 4
2.3. Shock Wave Reflections 6
2.4. Visualization by the Schlieren Optics Method 7
2.5. Theoretical Methods of Shock Propagation 8
2.6. Numerical Methods for Shock Propagation 11
2.7. Definition of Stability for Converging Shock Waves 11
2.8. Previous Work in the Field of Shock Wave Focusing 11

Chapter 3. Experimental Facility and Setup 19
3.1. The Shock Tube 19
3.2. The Shock Visualization 22

Chapter 4. Results 25
4.1. Shock Speed Sensor Signals 25
4.2. Temperature Measurements 25
4.3. The Forming of the Shock Wave by Reflector Boundaries 27
4.4. The Forming of the Shock Wave by Obstacles 30
4.5. Production of Light 34

Chapter 5. Conclusions 35

Chapter 6. Papers and Authors Contributions 37

Acknowledgements 40

References 41

Paper 1 47

Paper 2 77

Paper 3 89

Part I

Overview and Summary

CHAPTER 1

Introduction

A shock wave is a thin region in a fluid where the thermodynamic properties, for example pressure and temperature, of the fluid has changes abruptly. In nature, shock waves occur in many phenomena for example in volcanic eruptions, tsunamis, and sonic booms caused by thunder. Shock waves are also important in many technological applications ranging from medical industry to sonic booms caused by airplanes or by a high speed train entering a tunnel.

An interesting branch of the research on shock waves is the focusing of shock waves. Experimental studies of shock wave focusing has been an active research area since the 1950's. The most common experimental device for the study of shock wave focusing is the shock tube. In a shock tube high temperatures and pressures can be produced in the vicinity of the center of convergence of the shock shock wave. Therefore a shock tube is a useful tool for the study of thermodynamic and chemical properties of gases.

One example of medical use of shock wave focusing is Extra corporeal Shock Wave Lithotripsy (ESWL) which uses ultra sound waves to break kidney stones into small pieces. An elliptical shock wave generator creates a shock wave at the first focal point of the ellipse and then the shock wave focuses at the second focal point. The second focal point is located within the patient, thus it is possible to shatter the kidney stone. This method has decreased the need for surgery. More applications, both for shock waves and shock wave focusing, can be found in the review article by Takayama K. & Saito T. (2004).

In this introduction we consider an experimental study of shock wave focusing in the new shock tube facility at KTH Mechanics. We apply two different methods to change the shape of the shock wave, either by changing the outer reflector boundary of the test section or by introducing disturbances in the test section of the shock tube. Also, the presence of light during the convergence and reflection process is preliminary investigated.

The main purposes of the present work is to study

- the influence of the shape on the stability of the shock wave during the focusing and reflection process,
- the influence of disturbances introduced in the flow on the shape of the shock wave during the convergence and reflection process.

The remainder of the thesis is organized as follows. In chapter 2 we discuss some useful concepts concerning shock waves, shock tubes and in particular focusing of shock waves. In chapter 3 the experimental equipment and setup used in the present investigation is presented. In chapter 4 the results are presented and in chapter 5 we conclude and summarize. Finally, in chapter 6 we give a summary of the included papers.

CHAPTER 2

Theoretical Preliminaries

The analysis of compressible flow is based on three fundamental equations, see for instance Anderson J.D. (1990). They are the continuity equation, the momentum equation and the energy equation, presented here in integral form,

$$\iiint_{\mathcal{V}} \frac{\partial}{\partial t}\rho \mathrm{d}\mathcal{V} + \iint_{S} \rho \mathbf{V} \cdot \mathrm{d}\mathbf{S} = 0, \tag{2.1}$$

$$\iiint_{\mathcal{V}} \frac{\partial}{\partial t}\Big[\rho \mathbf{V}\Big] \mathrm{d}\mathcal{V} + \iint_{S} (\rho \mathbf{V} \cdot \mathrm{d}\mathbf{S})\mathbf{V} = \iiint_{V} \rho \mathbf{f} \mathrm{d}\mathcal{V} - \iint_{S} p \mathrm{d}\mathbf{S}, \tag{2.2}$$

$$\begin{aligned} &\iiint_{\mathcal{V}} \frac{\partial}{\partial t}\left[\rho\left(e + \frac{V^2}{2}\right)\right] \mathrm{d}\mathcal{V} + \iint_{S} \rho\left(e + \frac{V^2}{2}\right)\mathbf{V} \cdot \mathrm{d}\mathbf{S} \\ &= \iiint_{\mathcal{V}} \dot{q}\rho \mathrm{d}\mathcal{V} - \iint_{S} p\mathbf{V} \cdot \mathrm{d}\mathbf{S} + \iiint_{\mathcal{V}} \rho(\mathbf{f} \cdot \mathbf{V}) \mathrm{d}\mathcal{V}. \end{aligned} \tag{2.3}$$

Here $\mathcal{V}$ is a fixed volume, $\mathbf{V}$ is the velocity vector $\mathbf{V} = (u, v, w)$ in the x, y and z direction, ρ is the density, S is the surface area of the volume $\mathcal{V}$, p is the pressure acting on the surface S, $\dot{q}$ is the heat rate added per unit mass, f represents the body forces per unit mass and e is the internal energy. The above system of equations, (2.1)- (2.3), are closed with an equation of state, the ideal gas law

$$p = \rho R T, \tag{2.4}$$

where R is the specific gas constant and T is the absolute temperature. These equations, (2.1)- (2.4) are enough to analyze continuous compressible flows.

Because a shock wave has a width of only a few mean free paths it can be described as a discontinuity. A shock wave is an irreversible process and by the second law of thermodynamics the entropy is increasing across the discontinuity. This cannot be seen from equations (2.1)- (2.4) and an entropy relation must be added, see Courant R. & Friedrichs K.O. (1948).

2.1. Euler Equations

The Euler equations are a simplification of equations (2.1) – (2.3), neglecting the viscosity, body forces and heat transfer. When the heat conductivity and

and viscosity are very small, this simplification is a good approximation to observations in reality. The Euler equations in two dimensions are given by

$$\mathbf{U}_t + \mathbf{F}_x + \mathbf{G}_y = 0, \tag{2.5}$$

where the state vector, $\mathbf{U}$, and the fluxes, $\mathbf{F}, \mathbf{G}$ are given by

$$\mathbf{U} = \begin{bmatrix} \rho \\ \rho u \\ \rho v \\ \rho e \end{bmatrix}, \mathbf{F} = \begin{bmatrix} \rho u \\ \rho u^2 + p \\ \rho vu \\ \rho eu + pu \end{bmatrix}, \mathbf{G} = \begin{bmatrix} \rho v \\ \rho uv \\ \rho v^2 + p \\ \rho ev + pv \end{bmatrix}. \tag{2.6}$$

The subscripts t, x and y denote derivatives in time and space directions x and y. These equations are used together with an equation of state, such as equation (2.4), to obtain a closed system of equations. This set of equations can be used in numerical analysis to describe the flow in a shock tube and the converging and reflecting process.

2.2. Shock Tube Theory

A shock tube is a device for studying shock waves as well as thermodynamic and chemical properties. Also, a shock tube is useful in producing very high temperatures and pressures in a fairly simple way. A shock tube consists of a long tube closed at both ends separated into two parts by a membrane. The two parts are the high pressure part, called the driver section, and the low pressure part, called the driven section. The pressure in the low pressure part, p_1, is usually lower than the atmospheric pressure, often of the order of kPa. The high pressure part has as high pressure, p_4, as possible, usually of the order of MPa. See Fig. (2.1) for explanations of the initial conditions for the pressure.

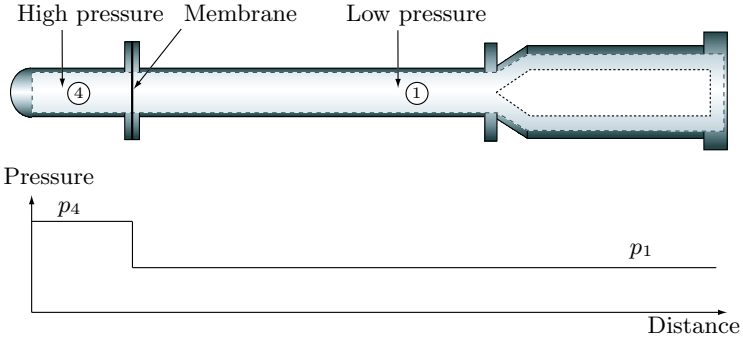

FIGURE 2.1. Initial conditions in a shock tube.

To produce a shock wave the low pressure part is evacuated from gas to a given pressure. The high pressure part is filled with gas and at a given

pressure difference between the two parts, the membrane rapidly breaks and the compressed gas in the high pressure part rushes into the low pressure part. A shock wave travels through the low pressure part and a rarefaction wave, starting at the broken membrane, travels through the high pressure part. See Fig. (2.2) for the flow conditions in the shock tube when the membrane is broken. The shock wave separates region 1 from region 2, which means that in region 1 the initial conditions are still undisturbed. The interface between the driver gas and the driven gas, separating region 2 and 3, is called the contact surface. Across the contact surface there is no flow of gas. Between region 3 and 4 a rarefaction wave is propagating upstream. The different regions are shown in Fig. (2.2).

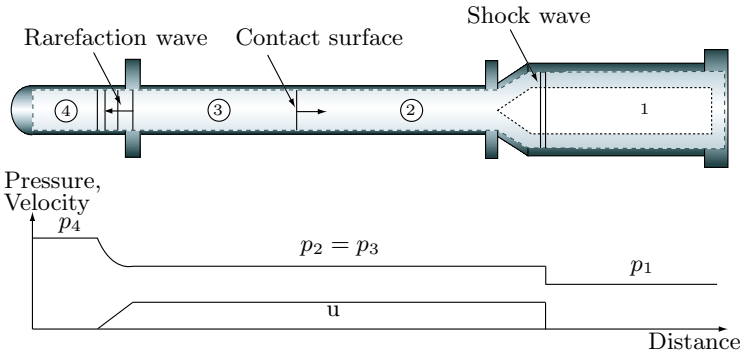

FIGURE 2.2. Flow in a shock tube after the membrane is broken.

The Mach number the shock travels downstream with is called the shock Mach number and is denoted M_s. The shock Mach number depends on the pressure ratio between the high and the low pressure part, p_4/p_1, the choice of gas used in the different parts of the tube and the temperatures of the gases respectively. The relation between the pressures p_1 and p_4 can be derived from equations (2.1) – (2.3) and is given by equation (2.7). The derivation can be found in e.g. Liepman H.W. & Roshko A. (1957).

$$\frac{p_4}{p_1} = \frac{2\gamma_1 M_s^2 - (\gamma_1 - 1)}{\gamma_1 + 1}\left[1 - \frac{\gamma_4 - 1}{\gamma_1 + 1}\frac{a_1}{a_4}\left(M_s - \frac{1}{M_s}\right)\right]^{-\frac{2\gamma_4}{\gamma_4 - 1}} \tag{2.7}$$

Here $\gamma = c_p/c_v$ is the ratio between the specific heats for constant pressure and constant volume respectively, and a is the speed of sound. The subscripts denote the region in which the property is valid.

For a more detailed explanation of shock tubes and the conditions during operation see Anderson J.D. (1990).

2.3. Shock Wave Reflections

There are two different types of reflections that can occur when a shock wave is reflected, *regular reflections* and *Mach reflections*. These two types of reflections are important to understand when studying the converging and reflection process for shock waves.

We first consider regular reflections. Consider an oblique shock wave reflected from a wall, Fig. 2.3. The flow in region 1 is deflected by an angle θ_1 at point A. If the angle θ_1 and the properties in region 1 are known then it is possible to calculate the properties in region 2 by using shock relations derived from the earlier mentioned equations (2.1) – (2.3). At point B, the shock wave meets the upper wall and a reflected shock wave is created. The flow properties in region 3 are determined by the Mach number in region 2, M_2, and the angle θ_1. A condition at point B is that the flow in region 3 has to be parallel to the upper wall, hence, θ_2 in region 3 is known. The Mach number in region 2, M_2, is less than the Mach number in region 1, M_1 and hence the reflected shock is weaker than the incident shock.

The above mentioned scenario applies for regular reflections and only possible if the angle θ is smaller than θ_{max} for M_2. See Fig. 2.3 for a θ-β-M diagram with maximum angles for M_1 and M_2. The θ-β-M-relation is given by

$$\tan\theta = 2\cot\beta\left(\frac{M_1^2\sin^2\beta - 1}{M_1^2(\gamma + \cos 2\beta + 2)}\right). \tag{2.8}$$

A derivation of the θ-β-M-relation can be found in e.g. Anderson J.D. (1990).

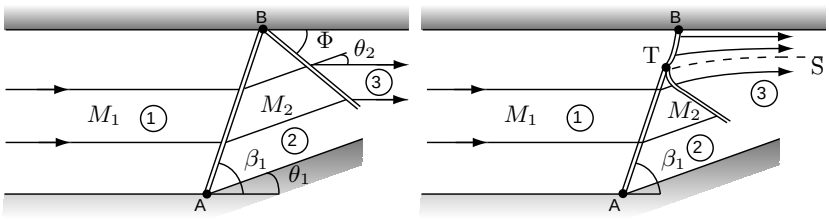

(a) Regular Reflection (b) Mach Reflection

FIGURE 2.3. Flow pattern and definitions of angles and regions for (a) a regular reflection and (b) a Mach reflection.

It is found that a regular reflection from the wall is no longer possible when $\theta > \theta_{max}$ for M_2. Instead, a normal shock is created by the wall to turn the flow parallel to the wall. The normal shock transforms into an in general curved shock and intersects the incoming shock and a curved shock is reflected

downstream. The point of intersection is called a triple point and the normal shock wave to the wall is called a Mach stem. A slip line, denoted S in Fig. 2.3, is attached to the triple point. The velocity of the gas on different sides of the slip line is in the same direction but necessarily not of the same magnitude. Furthermore, the density and entropy levels respectively are different on each side of the slip line since the gases have passed through shocks of different strength. This kind of reflection is called a Mach reflection and typically for this reflection is that there are large areas with subsonic flow behind the normal shocks.

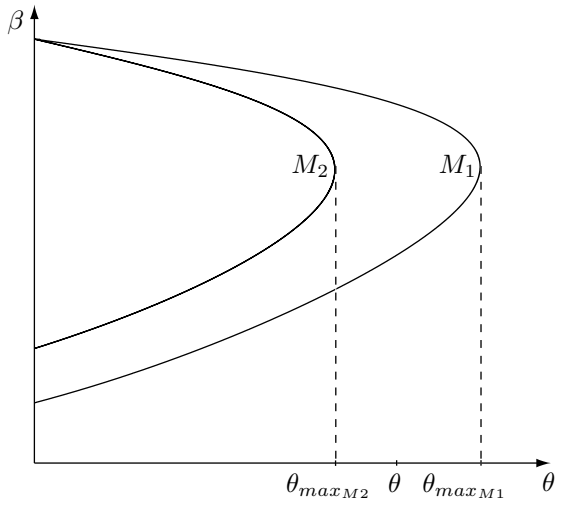

FIGURE 2.4. θ-β-M curves.

2.4. Visualization by the Schlieren Optics Method

To visualize the shocks a schlieren optics method is usually used. This method is an optical technique that visualizes density gradients in a fluid flow. The method is rarely used for quantitative measurements of density gradients but is useful for the qualitative understanding for the flow.

The speed of light, c, and the refraction index, n, will vary with the density, ρ, of the medium in which it is passing through. This means that light that passes through a region of compressible flow is diffracted due to the density changes in the gas. The refraction index, n, can be written as a function of the density, ρ,

$$n \equiv \frac{c}{c_0} = 1 + \beta \frac{\rho}{\rho_n}. \tag{2.9}$$

Here β is a dimensionless constant, c_0 is the speed of light in vacuum and ρ_n is the density at standard state. The idea of the schlieren method is to cut off part of the deflected light before it reaches the camera and hence produce darker (or brighter) regions on the photograph. If the density change takes place over a distance which is less than the wave length of the light then the optical method is sufficiently accurate. A schematic diagram of the schlieren method is shown in Fig. (2.5). A light source is placed at *(A)* and parallel light is achieved after passing the lens L_1. After passing the test section the light is focused by the lens L_2. The focal plane of L_2 is where the image of the light source appears. There are two focal planes, one for the source and one for the test section. The camera is placed in the focal plane of the test section.

More specifically, consider a pencil *abc* emitted from point *a* which covers the whole test section and is focused on *a'*, *(A')* the image plane of the light source. Other points from the light source similarly focus on *(A')*. Thus, every point in the image plane receives light from every point in the test section. In this plane all pencils from the light source overlap. If one of the pencils were passing through a region where the density is changing it would be deflected and no longer overlap the other pencils in *(A')*. When placing a schlieren edge in *(A')* to cut off parts of the light, the pencils that are deflected will appear darker or brighter at the image plane of the test section depending on how the light is intercepted. It is important to notice that *the point* where the light hits the focal plane of the test section does not change, it is just *the amount of light* that changes. More detailed information about visualization methods for compressible flow can be found in Liepman H.W. & Roshko A. (1957).

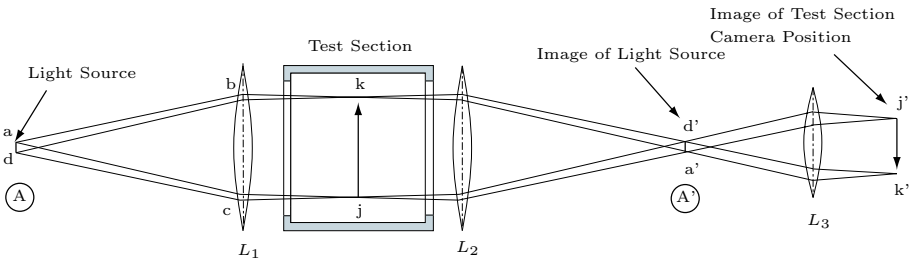

FIGURE 2.5. Schematic diagram of a schlieren system.

2.5. Theoretical Methods of Shock Propagation

Two methods that can be used to approximately solve shock propagation problems are geometrical acoustics theory and geometrical shock dynamics. The methods are constructed to study the flow field on or in the vicinity of the shock front and will be briefly discussed below.

2.5.1. *Geometrical Acoustics*

Geometrical acoustics is a linear theory which can be applied to propagation of weak shock waves. The shock speed is assumed equal to the speed of sound. The general idea of the method is that each element of the shock front propagates through a ray tube with variable area, A. The ray tubes are straight lines and orthogonal to the shock front. When the shock front reflects off a surface, the Mach number and angle for the incident ray are equal to the Mach number and angle for the reflected ray, similar to that of geometrical optics. The method is fairly simple to use considering the above mentioned assumptions but it can not be used for problems with stronger shocks for which the nonlinear effects become important. For a more detailed explanation and some examples on how to use the method, see Whitham G.B. (1974).

2.5.2. *Geometrical Shock Dynamics*

Geometrical Shock Dynamics (GSD) was introduced by Whitham G.B. (1957). The method is a non-linear extension of the geometrical acoustics theory. In GSD, the shock front propagates in a ray tube and the speed of propagation depends on shock the Mach number and the area of the ray tube at each position, $A(x)$. The governing equations are: the quasi 1D equation of conservation of mass, the momentum equation and the energy equation,

$$\rho_t + u\rho_x + \rho u_x + \rho u \frac{A'(x)}{A(x)} = 0, \tag{2.10}$$

$$u_t + uu_x + \frac{p}{\rho_x} = 0, \tag{2.11}$$

$$p_t + up_x - a^2(\rho_t + u\rho_x) = 0. \tag{2.12}$$

Here body forces and viscous forces are assumed small and hence they are neglected. The specific heats are assumed constant. The subscripts t and x denote the derivatives in time and x direction respectively.

The C_+ characteristic, representing equations (2.10) – (2.12), is given by

$$\frac{dp}{dx} + \rho a \frac{du}{dx} + \frac{\rho a^2 u}{u+a} \frac{1}{A} \frac{dA}{dx} = 0. \tag{2.13}$$

Using the following shock conditions,

$$u = \frac{2a_0}{\gamma+1}(M - \frac{1}{M}), \tag{2.14}$$

$$p = \rho_0 a_0^2 \left(\frac{2}{\gamma+1} M^2 - \frac{\gamma-1}{\gamma(\gamma+1)} \right), \tag{2.15}$$

$$\rho = \rho_0 \frac{(\gamma+1)M^2}{(\gamma-1)M^2+2}, \tag{2.16}$$

where $a_0^2 = \gamma p/\rho$, in equation (2.13) gives the relation between the Mach number and the area, also called the A-M relation and is given as

$$\frac{M}{M^2-1}\lambda(M)\frac{dM}{dx} + \frac{1}{A}\frac{dA}{dx} = 0, \tag{2.17}$$

where

$$\lambda(M) = \left(1 + \frac{2}{\gamma+1}\frac{1-\mu^2}{\mu}\right)\left(1 + 2\mu + \frac{1}{M^2}\right) \tag{2.18}$$

and

$$\mu^2 = \frac{(\gamma-1)M^2+2}{2\gamma M^2 - \gamma + 1}. \tag{2.19}$$

The quantity μ is the Mach number of the shock relative to the flow behind it.

In general, a weak shock is defined as one for which the normalized pressure ratio over the shock is very small,

$$\Delta p = \frac{p_2 - p_1}{p_1} << 1.$$

Subscripts 1 and 2 denote the regions just downstream and upstream of the shock. The shock speed for a very weak shock is about the speed of sound in the region downstream of the shock. A very strong shock is defined as one for which the pressure ratio, p_2/p_1, is very large.

The limiting cases, for weak and very strong shocks respectively, are

$$M \to 1, \qquad \lambda \to 4, \tag{2.20}$$

$$M \to \infty, \qquad \lambda \to 1 + \frac{2}{\gamma} + \sqrt{\frac{2\gamma}{\gamma-1}}. \tag{2.21}$$

These limiting cases can be used in the above mentioned A-M relation, to simplify the analysis.

In a 2D system, the shock front position, $\mathbf{r}(x, y)$, is related to the A-M relation, equation (2.17), by a system of non-linear equations,

$$\frac{d}{dt}\mathbf{r}(t) = M(t)\mathbf{j}(t),$$

where $\mathbf{j}(t)$ is the normal of the shock front.

Whitham's version of the GSD does not take the influence of the flow ahead of the shock into account. A later version of GSD, introduced by Whitham G.B. (1968), deals with uniform conditions in the flow field ahead of the shock. Apazidis N. & Lesser M.B. (1996), extended the GSD method to deal with non-uniform media ahead of the shock with a technique based on the invariance properties of Galilean transformations. New terms appear in the equations since there is a gradient in the flow conditions and the ray tubes are no longer orthogonal to the shock front.

2.6. Numerical Methods for Shock Propagation

Shock front propagation problems are often solved numerically using, either the previously mentioned methods, geometrical acoustics or geometrical shock dynamics, or the full set of Euler equations. A detailed explanation on how to use GSD for shock propagating problems can be found in Henshaw W.D. *et al.* (1986). They show results from different cases of shock propagation, such as shock wave diffraction, shock waves in channels and shock wave focusing.

Two numerical methods have been used in the present study. The first method is an Artificially Upstream Flux vector Splitting scheme for the Euler equations, AUFS, suggested by Sun M. & Takayama K. (2003). This numerical scheme discretizes the Euler equations according to the direction of wave propagation. Results obtained with the AUFS are presented in Paper 1 and Paper 3.

CLAWPACK (Conservation LAW PACKage) is a free software package suitable for solving hyperbolic partial differential equations numerically. The software can solve linear and nonlinear problems in one, two and three space dimensions. It can be downloaded from the CLAWPACK site at the University of Washington, `http://www.amath.washington.edu/~claw/`. In the present study CLAWPACK has been used to solve the 2D Euler equations in a simulation of a converging and reflecting shock wave. Typical examples of results from octagonal shaped converging shock waves are shown in Fig. 2.6.

2.7. Definition of Stability for Converging Shock Waves

A stable shock wave is said to maintain its shape at all times during the entire converging (or diverging) process. If a symmetric n-gonal structure is artificially imposed on the shock it will develop n plane sides and sharp corners. Then the shock wave transforms from an n-gonal to a double n-gonal form which now is oriented opposite to the original one. This process continues during the whole process of convergence. In the present thesis this behavior is referred to as stable since the shock wave keeps the symmetry during the focusing (or reflecting) process.

Examples of unstable and stable behaviors are shown in Fig. 2.7. An unstable process is for example when a circular (or cylindrical in 2D) shock wave is perturbed and transforms into a non-symmetrical circle-like shape. An example of a stable converging shock wave is when a heptagonal shock wave transforms into a double heptagon and then back to a heptagon, repeating this behavior in successive intervals.

2.8. Previous Work in the Field of Shock Wave Focusing

Guderley (1942) was first to analytically investigate the convergence of cylindrical and spherical shock waves. Guderley derived a self similar solution for the radius of the converging shock wave as a function of time. Guderley's self

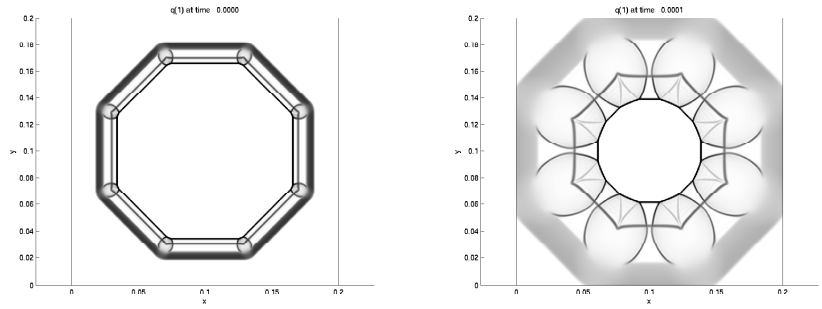

(a) (b)

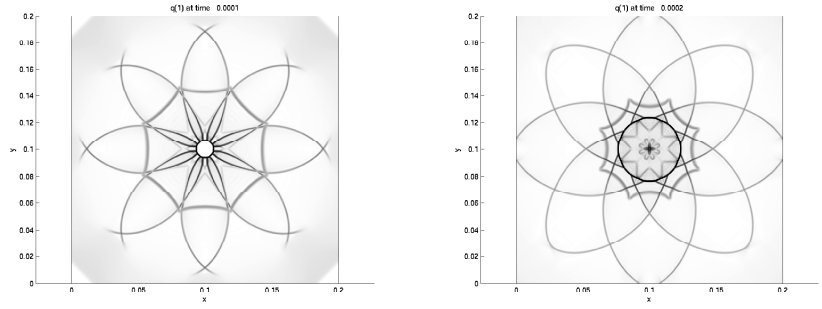

(c) (d)

FIGURE 2.6. Typical examples of CLAWPACK results. Schlieren plots, showing density gradients of octagonal shaped shock waves, (a), (b) and (c) are converging and (d) are diverging. The size of the computational domain is 500 x 500 gridcells.

similar solution can be written as

$$\frac{R}{R_c} = \left(1 - \frac{t}{t_c}\right)^{\alpha}. \tag{2.22}$$

Here R is the radius of the converging shock wave, R_c is the radius of the outer edge of the test section, t is the time and t_c is the time when the shock wave arrives at the center of convergence. The self similar power law exponent for cylindrical shock waves was found to be $\alpha = 0.834$.

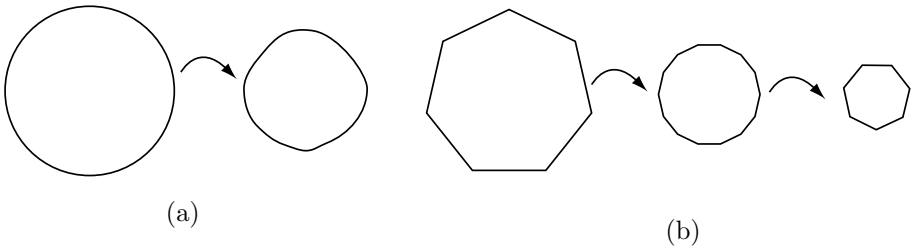

FIGURE 2.7. The definition of stability for a shock wave, (a) represents an unstable shock wave and (b) represents a stable shock wave convergence.

The first experiment with shock wave focusing was done by Perry R.W. & Kantrowitz A. (1951). Perry & Kantrowitz were interested in cylindrical converging shock waves as to their ability to produce high temperatures and pressures during the focusing process. The increase in pressure and temperature depends on the shape of the shock wave, rendering the goal to produce perfect cylindrical shock since it would achieve the highest temperatures and pressures. Perry & Kantrowitz used a horizontal shock tube with a tear-drop inset in the test section to create cylindrical shocks. They studied converging and reflecting shocks, visualized by the schlieren technique, at two different shock Mach numbers (1.4 and 1.8). They found that creating perfect cylindrical shocks was more difficult for higher Mach numbers since the shock strength was increased. Perry & Kantrowitz suggested that this could be explained by irregular membrane opening times and bad membrane material. Also, an obstacle, a rod, was placed in the flow and the result showed that the center of convergence was displaced toward the disturbed side of the shock wave. Another interesting observation was the presence of light in the center of the test section during the focusing process. This was taken as an indicator of the presence of high temperatures as the light was believed to be caused by ionized gas.

Sturtevant B. & Kulkarny V.A. (1976) performed experiments on plane shock waves which focused in a parabolic reflector mounted at the end of a shock tube. Different shapes of parabolic reflectors were used. Results showed that weak shock waves focused with crossed and looped fronts while strong shocks did not. Conclusions where that the shock strength governed the behavior during the focusing process and that non-linear phenomena where important near the center of focal point.

Knystautas R. *et al.* (1969) performed experiments with cylindrical imploding detonation waves. Their experimental setup was a 25 mm thick plane chamber with an inner diameter of 250 mm and 30 holes along its periphery.

The holes where connected to tubes with spark-gaps placed at the end. A detonation wave was created by each of the spark-gaps and together they formed a polygonal shock wave. As the polygonal shaped shock wave approached the center of convergence it transformed into a smooth cylindrical form. Knystautas *et al.* concluded from the experiment that converging detonation waves were stable due to the shape of the shock wave. This conclusion was also reached on the basis that large-scale vorticity production behind the shock wave was absent in this experiment. Spectroscopic measurements indicated temperatures as high as $1.89 \cdot 10^4$ K during the focusing process which indicated that the experimental method could be used to generate plasma for basic studies.

Takayama K. *et al.* (1984) used a horizontal annular shock tube to produce converging shock waves with initial shock Mach numbers in the range of 1.10 – 2.10. A double exposure holographic interferometer was used to visualize the converging shock wave and the flow behind it. One observation was that close to the center of convergence the shock wave was shaped like a square. This was referred to as a mode-four instability.

Takayama K. *et al.* (1987) used two different horizontal annular shock tubes to investigate the stability and behavior of converging cylindrical shock waves. One of the goals was to find out if a stable converging cylindrical shock wave could be produced. The results showed that the shape of the shock wave was very sensitive to disturbances in the flow. Both shock tubes where equipped with supports for the inner body and these supports caused disturbances that changed the shape of the shock wave. (One shock tube was located in the Stoßwellenlabor, RWTH Aachen, and one in the Institute for High Speed Mechanics, Tohoku University in Sendai.) The Aachen shock tube had three supports and near the center of convergence the shock wave was always triangular, showing a mode-three instability. The Sendai tube had two sets of four supports. Although the area contraction from these supports was rather small the converging shock was still affected by these and the converging shock wave showed a mode-four instability. To investigate the effect of disturbances, cylindrical rods where introduced upstream of the test section in the Sendai shock tube. It was found that the shock wave was significantly affected by these rods during the first part of the converging process. Later, as the shock wave reached the center of convergence, the mode-four instability was again observed. Takayama *et al.* concluded that the disturbances caused by the supports could not be suppressed by the cylindrical rods. Also, the instability, i.e. the deviation from a cylindrical shape, was found to be more significant for stronger shocks.

To avoid disturbances in the flow caused by supports for the inner body a vertical shock tube was used by Watanabe M. *et al.* (1995). This shock tube had no supports for the inner body. Further, special care was taken to minimize possible disturbances in the shock tube to enable production of perfect cylindrical converging shock waves. The results showed that the cylindrical

shock waves tend to keep their form more uniformly than in horizontal shock tubes with supports. Still, when the shock wave reached the center of convergence it was not perfectly cylindrical. This was believed to be caused by small changes of the area in the co-axial channel between the inner and outer body of the shock tube. To study the influence of artificial disturbances, a number of cylindrical rods were introduced in the flow. Different numbers of rods were used and Watanabe *et al.* concluded that when there was a combination of modes, the lowest mode was strongest and suppressed the other ones.

All the previously mentioned experiments have been performed for cylindrical shock waves. Production of spherical, converging, shock waves were studied by Hosseini S. H. R. & Takayama K. (2005). A test section with transparent walls and inner diameter of 150 mm was used. The shock wave was generated by small explosives in the center of the test section. Immediately after the explosion the shock wave was not spherical but as it propagated further out it approached a spherical shape quickly. Hosseini & Takayama concluded that a diverging shock wave was always stable. The diverging shock wave reflected off the wall of the test section and started to converge. The converging shock wave kept its spherical shape until it started to interact with the detonation products. Comparisons were made with both Guderley's similarity law and the Chester-Chisnell-Whitham (CCW) method (Whitham G.B. (1974)). These two methods showed a reasonable agreement with the experimental data. The methods overestimated the speed of the shock wave though, since neither of them take into account the flow ahead of the shock wave. The shock wave in the experiments was visualized in two different ways, both by double-exposure holographic interferometry and with high-speed video camera (100 sequential images with a frequency of 1000 000 images/s) with the shadowgraph method. The usage of a high speed camera was a new method to visualize the entire focusing process for an individual shock wave. Earlier, each photograph was usually taken for an individual shock wave. Hence it was hard to keep exactly the same conditions in the experiment to get the same Mach number, pressure etc. for each shock wave.

Schwendeman D.W. & Whitham G.B. (1987) used the approximate theory of Whitham G.B. (1957), (geometrical shock dynamics), to study the behavior of converging cylindrical shocks. They showed that a regular polygon will keep reconfiguring with successive intervals and that the shock Mach number will increase exactly as that for a circular converging shock. They also showed that perturbed polygonal shaped shock waves, with smooth corners as well as without plane sides, first form plane sides and sharp corners. Then the shock wave starts to reconfigure until it reaches the center of convergence and starts to reflect. This behavior was later confirmed by Apazidis N. & Lesser M.B. (1996) and Apazidis N. *et al.* (2002) for a smooth pentagonal converging shock wave.

At KTH Mechanics experiments with converging shock waves has been performed since 1996. Experiments with polygonal shock waves in a confined reflector were performed by Johansson (2000). The experimental setup consisted of a thin cylindrical chamber were the shock waves where created, reflected and focused. The chamber had a specific boundary in the shape of a pentagon with smooth corners, given by

$$r = \frac{r_0}{1 + \varepsilon \cos(5\theta)}, \tag{2.23}$$

where r is the radius, $\varepsilon = 0.035$ and $r_0 = 77$ mm. The chamber and the pentagonal boundary can be seen in Fig. 2.8. The chamber was filled with gas,

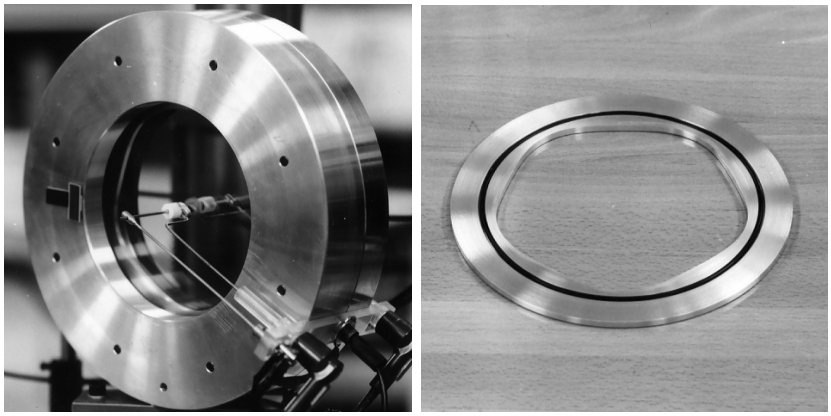

(a) The cylindrical chamber.

(b) The pentagonal shaped boundary.

FIGURE 2.8. The chamber and pentagonal boundary used by Johansson (2000). Reprinted with permission from Johansson (2000).

either air or argon, at atmospheric pressure and the shock wave was generated in the center of the chamber, either by an igniting spark or by an exploding wire. Weak or moderately strong shocks with shock Mach numbers in between $1.1 \leq M_s \leq 1.7$ were produced. An outgoing cylindrical shock wave was created and after reflection from the boundary of the chamber the shock wave was transformed into a smooth pentagonal shape. The shock waves were visualized by schlieren optics and photographs from these experiments can be seen in Fig. 2.9. In Fig. 2.9 (a) the weak shock has just been reflected from the boundary and still maintains a smooth pentagonal shape. In (b) corners and plane sides have developed and the diffracted shocks can be seen behind the corners.

Moderately strong shocks at the center of the chamber are shown in (c) and (d). As seen in the figure the disturbance zone grows when the Mach number is raised. Observations for the weak shock waves, $M_s = 1.1$, showed that the corners of the reflected shock wave became sharper with time. This meant that the curvature was increasing and hence an increase in speed of the shock was occurring at these points. Shock-shocks where formed behind the corners and due to this diffracted shocks where also formed. The focusing of moderately strong shocks, $M_s = 1.35$, showed a similar behavior as in the focusing process of weak shock waves. The outgoing shock wave was similar to the weak shock but when it reflected off the wall the plane sides were straighter than before. A larger shock Mach number at the reflector boundary gives, according to the shock reflection relation, a smaller reflection angle and hence initially straighter sides. For the moderately strong shock case it was more obvious that the corners started to transform into plane sides. However, it was not possible to see a fully transformed reoriented pentagon with corners pointing toward the sides of the reflector due to the size of the disturbance zone. The shock Mach number was then increased to 1.5 but the results showed no major changes. Raising the shock Mach number even more produced even larger disturbances that covered almost the entire central part of the chamber and hence no results were obtained. A drawback of the above method to create shock waves is that it creates a disturbance zone which prevents visualization of the most important part of the focusing process, the disturbed zone can be seen in Fig. 2.9 in the center of the photographs. For weaker shock waves, the disturbance zone was less than for stronger shock waves. The size of the disturbance zone depended on the various techniques used to create the shock waves in the experiment. The experimental results were compared to numerical calculations to a good agreement. The numerical analysis was based on geometrical shock dynamics of Whitham G.B. (1957) with the assumption of no flow ahead of the shock wave. More results and discussions are presented in Apazidis N. & Lesser M.B. (1996) and Apazidis N. *et al.* (2002).

To be able to study the full focusing process, without disturbances ahead of the flow, a new experimental setup has been built at KTH Mechanics. The setup consists of a horizontal annular shock tube similar to those in the above mentioned experiments. Compared to the chamber used by Johansson (2000) there are no disturbances ahead of the shock wave and hence it is possible to visualize the whole focusing and reflection process. Another improvement with this new shock tube facility is that the test section has an exchangeable outer boundary and hence it is possible to use different shapes for the reflector boundaries. The present experimental setup is also able to produce significantly stronger shock waves.

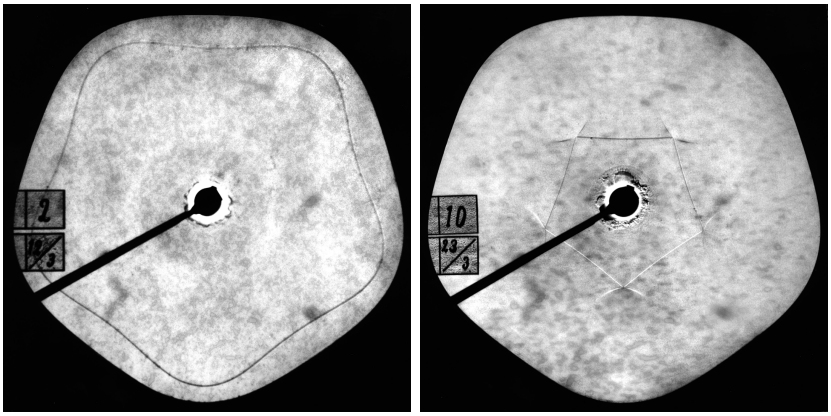

(a) $M_0 \approx 1.1$ $\Delta t = 199\mu s$.

(b) $M_0 \approx 1.1$ $\Delta t = 300\mu s$.

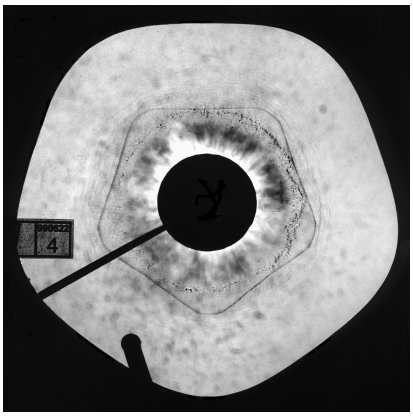

(c) $M_0 \approx 1.35$ $\Delta t = 181\mu s$.

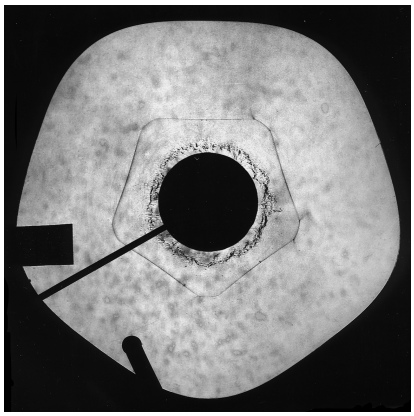

(d) $M_0 \approx 1.35$ $\Delta t = 229\mu s$.

FIGURE 2.9. Converging shock waves at different Mach numbers and time delays. The Mach number, M_0, is defined as the Mach number when the diverging shock wave hits the reflector boundary. The time Δt is the time from the creation of the shock wave to the time when the photograph is taken. Reprinted with permission from Johansson (2000).

CHAPTER 3

Experimental Facility and Setup

The experimental setup consists of the light source, here a laser, a horizontal shock tube and a schlieren optics system. The shock tube has a test section where shock waves are focused and reflected. That process is visualized by the schlieren system with a camera. The experimental setup is shown in Fig. 3.1.

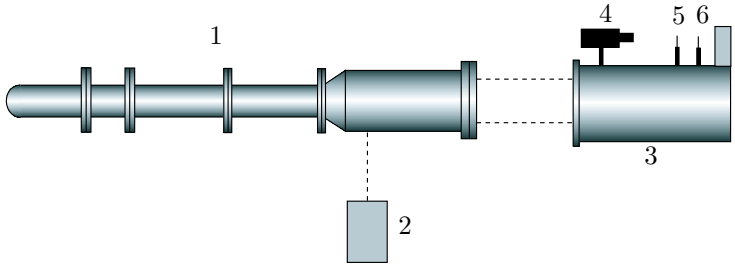

FIGURE 3.1. Schematic overview of the experimental setup: 1. Shock tube, 2. Pulse laser, 3. Schlieren optics, 4. PCO CCD camera, 5. Lens, 6. Schlieren edge.

3.1. The Shock Tube

The 2.4 m long circular shock tube consists of two main parts, the high pressure part and the low pressure part which are separated by a 0.5 mm thick aluminum membrane. An illustration of the shock tube and its main elements is shown in Fig. 3.2. To create a shock wave the low pressure part is evacuated of gas to a given pressure. The high pressure part is filled with gas and at a given pressure difference between the two parts the membrane bursts, creating a shock wave which becomes planar in the inlet section of the low pressure part. The pressures in the high and low pressure parts are monitored by senors, see Fig. 3.2.

To control the membrane opening, a knife-cross is placed in the inlet of the low pressure part. The knife-cross helps the membrane to open evenly, shortens the time until a fully developed shock has formed and prevents unnecessary disturbances as well as it helps to prevent pieces come loose from the membrane.

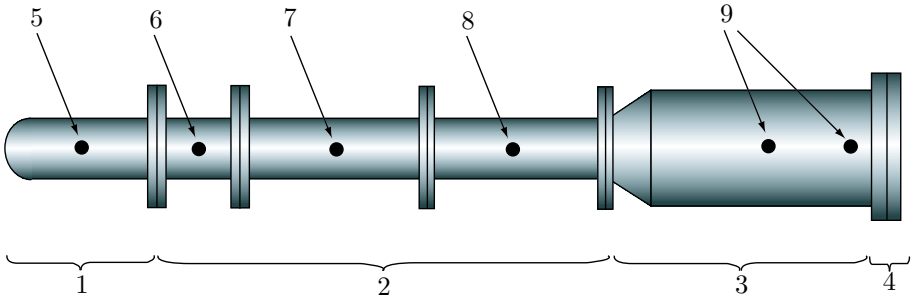

FIGURE 3.2. Schematic overview of the shock tube setup: 1. High pressure part, 2. Low pressure part: inlet section, 3. Low pressure part: transformation section, 4. Low pressure part: test section, 5. High pressure sensor, 6. Low pressure sensor, 7. Vacuum valve, 8. Vacuum pump, 9. Shock speed sensors.

When the plane shock wave reaches the transformation section, the shock wave is forced to become annular by a conically diverging section where the diameter increases from 80 mm to 160 mm, see Fig. 3.3. The cross-section area is held constant from the inlet section through the transformation section. The annular section is formed by an inner body mounted coaxially inside the wider diameter outer tube.

The 490 mm long inner body, with a diameter of 140 mm, is held in place by two sets of four supports. These supports are shaped as wing profiles to minimize flow disturbances. The second set of supports is rotated 45° as compared to the first set. The shock speed, U_s, is measured by sensors placed in in the annular section. The sensors are triggered by the temperature jump caused by the passage of the shock wave.

The test section is mounted at the end of the annular part of the shock tube. After a sharp 90° bend the annular shock wave enters the test section and the focusing and reflection process begins. The initial shape of the shock wave is determined by the shape of the reflector boundary. The gap between the two facing glass windows in the test section is 5 mm, reducing the cross sectional area to half of that in the annular part.

The outer boundary of the test section is exchangeable and four different reflector boundaries have been used in the present experiments: a circle, a smooth pentagon, a heptagon and an octagon. The radius for the circular reflector boundary is 80 mm. The shape for the smooth pentagonal boundary is given by equation (2.23). The radius for the circumscribed circle is 80 mm both for the heptagonal and the octagonal reflector boundary. The four boundaries are shown in Fig. 3.4.

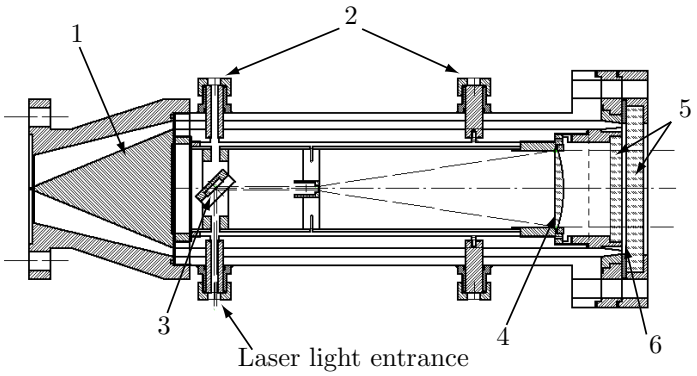

FIGURE 3.3. The annular part of the shock tube: 1. Inner body with a cone, 2. Supports, 3. Mirror, 4. Lens, 5. Glass windows for visualization, 6. Obstacle positioning area.

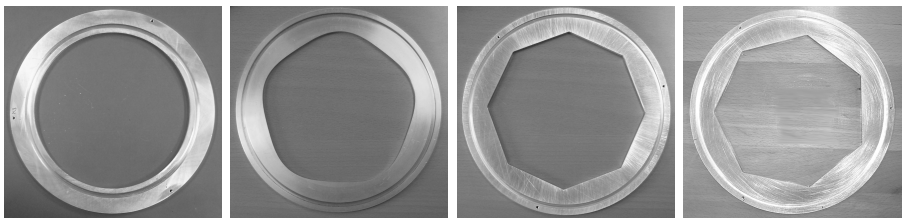

(a) Circular. (b) Pentagonal. (c) Octagonal. (d) Heptagonal.

FIGURE 3.4. The four reflector boundaries for the test section used in the experiments.

To create disturbances in the flow field 1-16 cylinders, with three different diameters of 7.5, 10 and 15 mm, are placed in various patterns and positions between the two facing glass windows in the test section. The cylinders can be placed at two different radial positions, $r_1 = 46$ mm and $r_2 = 66$ mm in both regular and irregular patterns, using a template with holes in it, see Fig. 3.5(a). The cylinders are equipped with rubber rings in one end and glue on the other end and are then held in place by the pressure between the two facing glass windows. The method to place these cylindrical obstacles in the test section is both safe and easy to use. In Fig. 3.5(b) an example where 16 cylinders with diameters of 10 mm and 15 mm are placed in a circle with the radius $r = r_1$ can be found.

A difference between the experiments with the heptagonal reflector boundary and the three other reflector boundaries is worth to mention. The supports

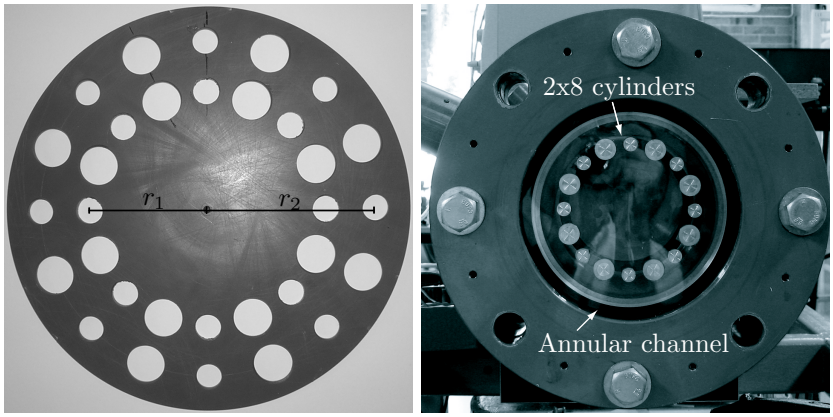

(a) (b)

FIGURE 3.5. (a) Template for cylinder positioning, $r_1 = 46$ mm and $r_2 = 66$ mm. (b) Rear part of the shock tube with 2x8 cylinders placed in the test section at $r = r_1$.

where adjusted to produce a minimal disturbance for the experiments with the heptagonal reflector boundary while for the rest, two of the supports where not in optimal position.

3.2. The Shock Visualization

The facing surfaces in the test section consist of glass windows and the convergence and reflecting process is visualized by schlieren optics method. As a light source an air-cooled Nd:Yag (NewWave Orion) laser is used. The laser can be operated in single shot mode with 5 ns long light pulses. The laser is placed outside the shock tube, either parallel or normal to the axis of the shock tube. If the laser is placed parallel to the shock tube then a mirror is used to deflect the light through the laser light entrance on the shock tube.

The laser light entrance is a hole with a diameter of 6 mm through one of the upstream positioned supports for the inner body. When the laser light beam has entered the shock tube it is deflected in the axial direction by a mirror placed inside the inner body. It then enters a beam expander that produces parallel light. The beam expander consists of two lenses. The first lens is biconcave with a diameter of 6 mm and a focal length of -8 mm. The second lens is plane convex with a diameter of 95 mm and a focal length of +300 mm. After the beam expander the parallel light passes the first glass window, enters

the test section and then leaves the shock tube via the rear end glass window to enter the schlieren optics system.

3.2.1. *The schlieren optics*

The receiver part of the schlieren optics system is placed 1150 mm from the rear glass window at the shock tube. The receiver system consists of a large lens 185 mm in diameter, with a focal length of 1310 mm and two mirrors that deflect the light into the section located at the top of the system.

The schlieren edge is placed in the image plane of the light source to cut off parts of the deflected light beams. Usually, the schlieren edge is a razor's edge but in this experiment a spherical needle-point with a radius of 1 mm was used. The reason for this form of the schlieren edge is to match the shape of the shock wave.

After passing the schlieren edge the light passes through a lens and then enters the camera. The camera is a CCD PCO SensiCam (12 bits, 1280 x 1024 pixels, pixel size: 6.7 x 6.7 μm) equipped with a Canon lens with a focal length of 80 mm.

For experiments with the heptagonal reflector boundary special care was taken to avoid light reflections inside the inner body by adding a light absorbing coating material in the interior of the inner body. This was done to obtain a better quality of the photographs.

3.2.2. *The shock speed measuring device and time control*

Two units, containing sensor and amplifier, are placed in the wall of the outer tube in the annular part of the shock tube. The sensor element is a 70 mm long glass plug with a diameter of 17 mm with a thin strip of platinum paint at the end. It is mounted in a hole so that its end surface, with the platinum paint, is flush with the inner surface of the tube.

The resistance of platinum is temperature dependent and when the shock wave passes the sensor, the resistance of platinum is changed due to the temperature increase caused by the shock wave. This change in resistance is transformed via an electric circuit to a voltage pulse which can be monitored on an oscilloscope. The electric circuit consists of an amplifier, an AD845 operational amplifier with a settling time of 350 ns to 0.01%. The sensor can be seen in Fig. 3.6 and the circuit diagram of the electric circuit is shown in Fig. 3.7.

A time delay unit (Stanford Research System, DG535) is used to control the laser and the camera to enable exposure at a predetermined position in the test section.

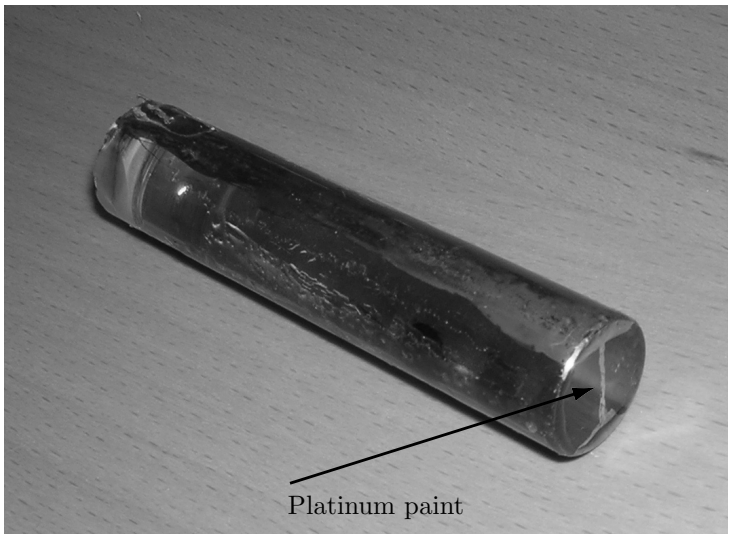

FIGURE 3.6. A sensor for shock speed measurement with a thin strip of platinum paint at the end surface.

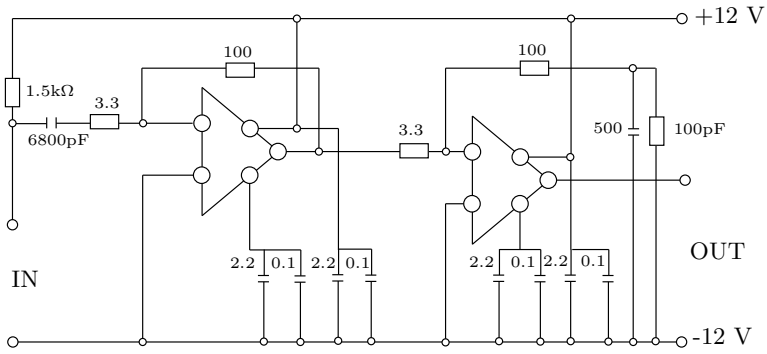

FIGURE 3.7. Circuit diagram for the amplifier. Resistances in $k\Omega$ and capacitances in μF.

CHAPTER 4

Results

In this chapter we present results from three types of experiments; shock wave focusing by using four different reflectors boundaries, shock wave focusing with cylindrical obstacles in the test section and preliminary experiments with light flashes observed during the focusing and reflection process. More details of the results are found in Papers 1-3.

4.1. Shock Speed Sensor Signals

For each run the time instants, t_1 and t_2, when the shock wave passes the first and the second sensor, are recorded. From these time instants, the shock speed, U_s, can be determined since the distance between the sensors is known and is 25 cm. These measurements have high repeatability, thus, yielding a low error level. For a typical shock wave speed of 800 m/s the average of the passage time $t_2 - t_1$ and the rms-value are 312 μs and 1.32 μs respectively, i.e the accuracy is within 0.5%. The sensors are very fast and the time response is less than 1 μs.

A typical time history of signals is shown in Fig. 4.1. The upper curve is the signal from the first sensor, upstream. The first peak in this signal corresponds to the time t_1 and the second peak corresponds to the reflected shock wave. The lower curve represents the signal from the second sensor, downstream. The first peak in the lower signal corresponds to the time t_2 and the second peak to the reflected shock wave. The resolution used for the measurement of the time signals is 2 μs.

4.2. Temperature Measurements

The speed of sound, a, in the annular part of the shock tube is found from the equation $a = \sqrt{\gamma RT}$, where R is the specific gas constant, $\gamma \equiv c_p/c_v = 1.4$, for standard air conditions, and T is the temperature.

Since the speed of sound depends on the temperature, which changes during operation, the temperature has been measured using a cold wire. A plot of the measured temperature as a function of time during the evacuation phase of the low pressure part can be found in Fig. 4.2. Before the first peak (I), the pressure is 13.3 kPa, in the low pressure part. At (II) air is let in. At (III) the vacuum pump is started and air is evacuated and when the pressure in the

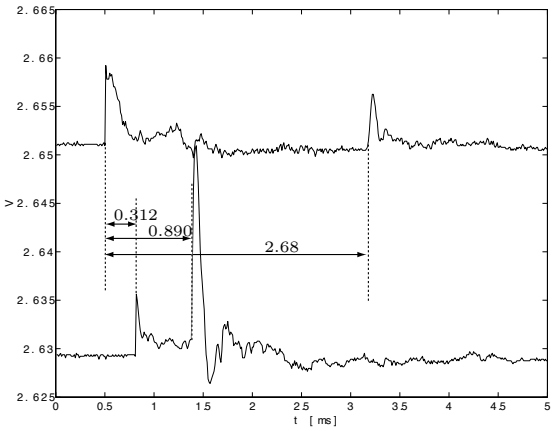

FIGURE 4.1. The signals from the two sensors showing the shock wave passage and reflection, at $M_s = 2.3$. The upper curve is the signal from the first, upstream, sensor and the lower curve is the signal from the second, downstream sensor.

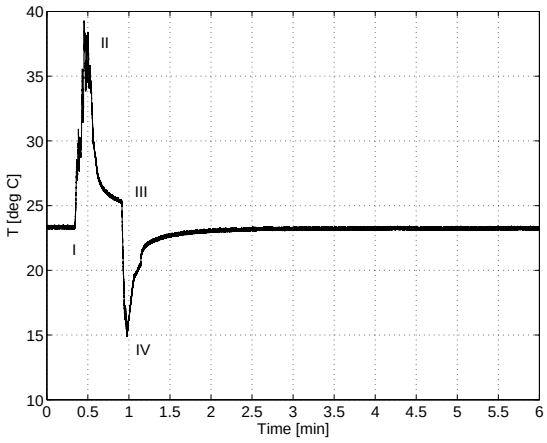

FIGURE 4.2. Measurement of the temperature in the low pressure part during evacuation of air.

low pressure part reaches 13.3 kPa the pump is shut down (IV). It can be seen in Fig. 4.2 that the temperature to stabilizes well within one minute. Since it takes more than one minute from the moment when vacuum pump is shut

down until the moment when the membrane breaks, the temperature in the low pressure part can be considered as well known.

4.3. The Forming of the Shock Wave by Reflector Boundaries

In this thesis four different reflector boundaries, see Fig. 3.4, have been used to shape the shock wave. In Figs. 4.3 and 4.4, schlieren photographs of a typical focusing and reflecting process for the heptagonal reflector boundary are presented. When the shock wave enters the test section it assumes the heptagonal shape of the reflector boundary, see Fig. 4.3(a) and (b). In the time interval between Fig. 4.3(b) and (c) the shock wave transforms into a double heptagonal shape. In Fig. 4.3(c) the shock wave has again assumed a heptagonal shape but now with opposite orientation as compared to its original orientation, compare Fig. 4.3(b) and (c). This reconfiguring process, from heptagonal to double heptagonal back to heptagonal with an opposite orientation, continues during the whole focusing process. This can be seen in Fig. 4.3(d) and Figs. 4.4(a)-(b).

As the shock wave starts to reflect, it initially assumes a circular shape, see Fig. 4.4(c). In the later stages of the reflection process the shock wave interacts with the flow ahead of it, which is still directed toward the center of the test section, thus the shock wave changes from a circular shape into a perturbed heptagonal shape, see Fig. 4.4(d).

The focusing behavior of polygonal shaped shock waves has been studied analytically and numerically by Schwendeman D.W. & Whitham G.B. (1987) and Apazidis N. & Lesser M.B. (1996). The results of Schwendeman & Whitham and Apazidis & Lesser agree with our experiments during the focusing process. However, the above theories cannot be used to study the reflecting process, therefore our experiments provides new results.

The present experiments with differently shaped reflector boundaries, circular, smooth pentagonal, heptagonal and octagonal, are described in detail in Paper 1 and 2.

Similar to Takayama K. *et al.* (1984) and Takayama K. *et al.* (1987) the annular shock tube used in the present study has supports for the inner body. These supports create disturbances in the flow field that have been attributed the change of the shape of the shock wave during the final stage of the focusing process. In the present experiments, the annular part of the shock tube is equipped with two sets of four supports and the disturbances of the shape of the shock wave is only observed when the circular and octagonal reflector boundaries are used. The disturbance from the supports is small and therefore we believe that a substantially stronger disturbance is required to change a shock wave with an uneven number of corners into a shock wave with even number of corners. In Paper 2 the influence of the supports are investigated.

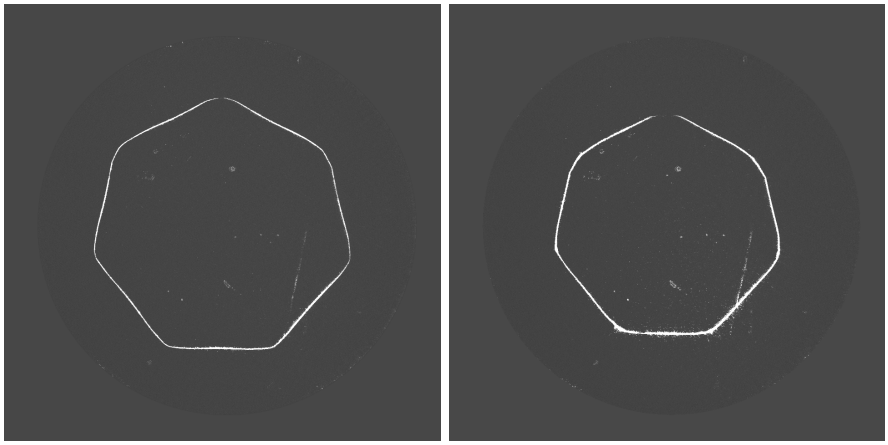

(a) Δt=195 μs.

(b) Δt=200 μs.

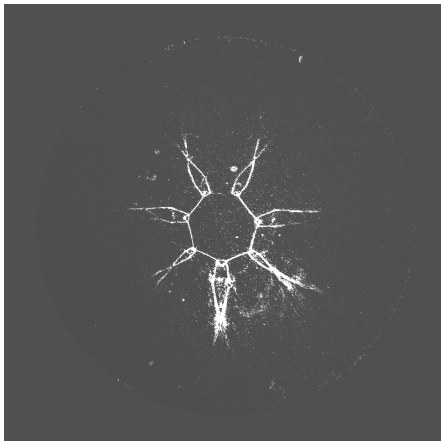

(c) Δt=210 μs.

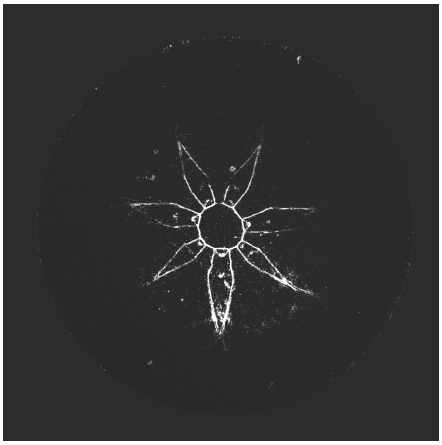

(d) Δt=215 μs.

FIGURE 4.3. Schlieren photographs of the shock wave for shock Mach number $M_s = 2.3$ at different time instants for the heptagonal reflector boundary. Each photograph is from an individual run in the shock tube.

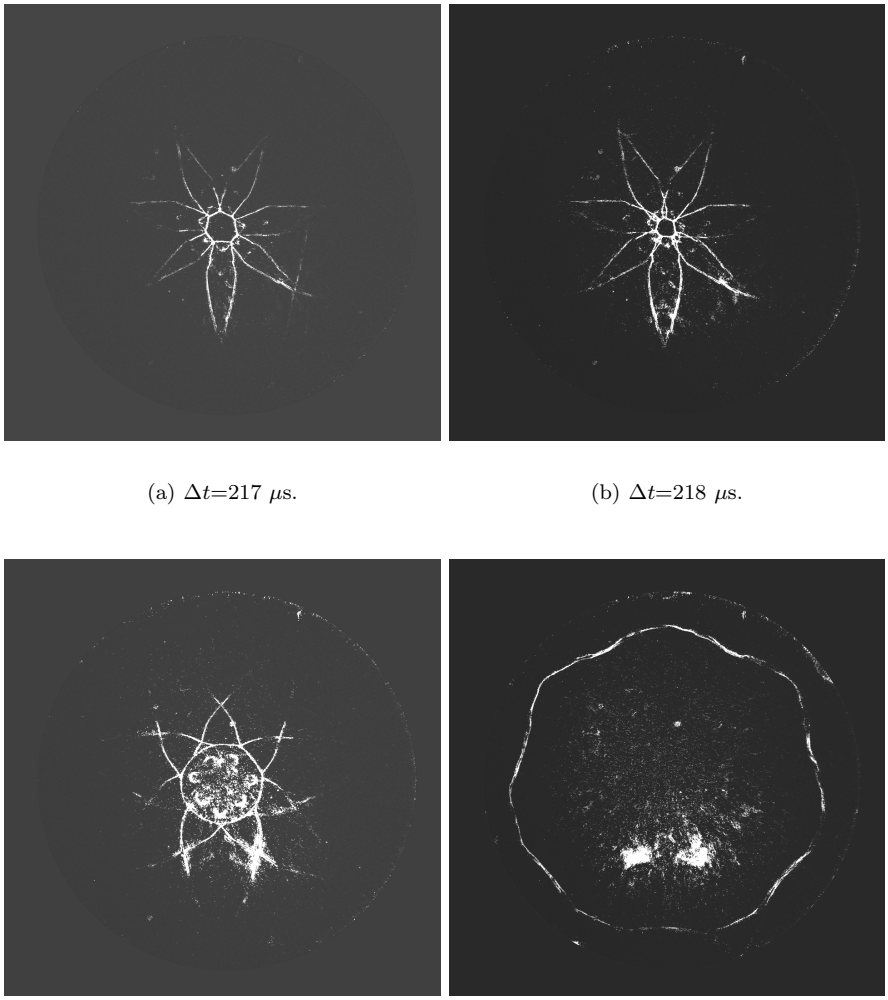

(a) Δt=217 μs. (b) Δt=218 μs.

(c) Δt=230 μs. (d) Δt=270 μs.

FIGURE 4.4. Schlieren photographs of the shock wave for shock Mach number $M_s = 2.3$ at different time instants for the heptagonal reflector boundary. Each photograph is from an individual run in the shock tube.

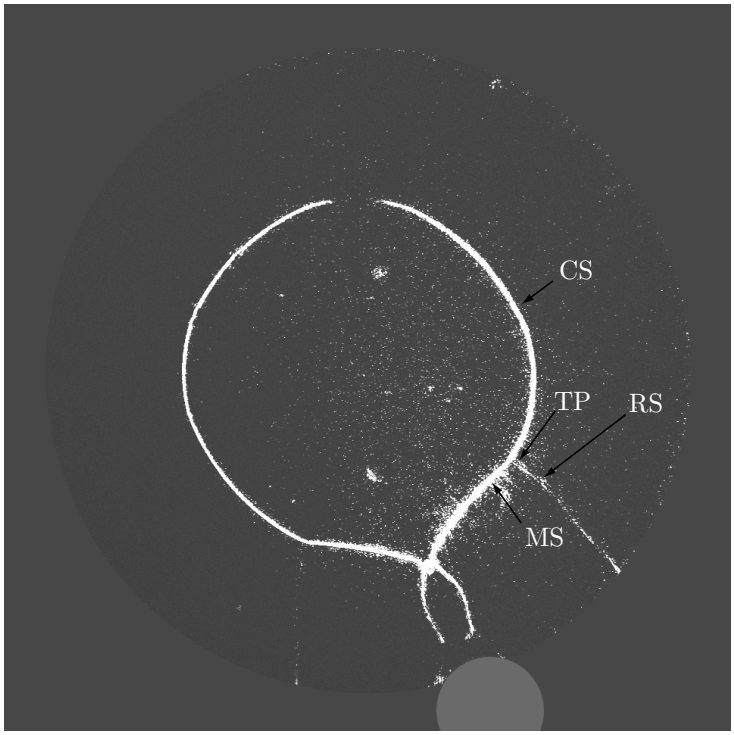

FIGURE 4.5. Schlieren photograph of a shock wave passing a single cylinder, with a diameter of 15 mm. M_S=3.2. CS, converging cylindrical shock, RS, reflected shock from the cylinder, MS, Mach shock and TP, triple point. The filled grey circle shows the position of the cylindrical obstacle.

4.4. The Forming of the Shock Wave by Obstacles

To investigate the influence of disturbances in the flow, cylindrical obstacles where placed in various patterns and positions using the template seen in Fig. 3.5(a). In all the experiments with cylindrical obstacles the circular reflector boundary was used.

In Fig. 4.5 a schlieren photograph shows the converging shock wave after passing a single cylinder. The cylinder with a diameter of 15 mm is placed at $r = r_1 = 44.6$ mm. A reflected shock wave (RC) is created when the converging shock hits the cylinder. Mach shocks and the triple point (TP) between these and the converging shock (CS) are seen in Fig. 4.5. The observed flow field is similar to the flow field from diffraction on a cylinder by a plane shock wave, see photographs in Bryson A.E. & Gross R.W.F. (1960). The main difference is the circular shape of the converging shock wave.

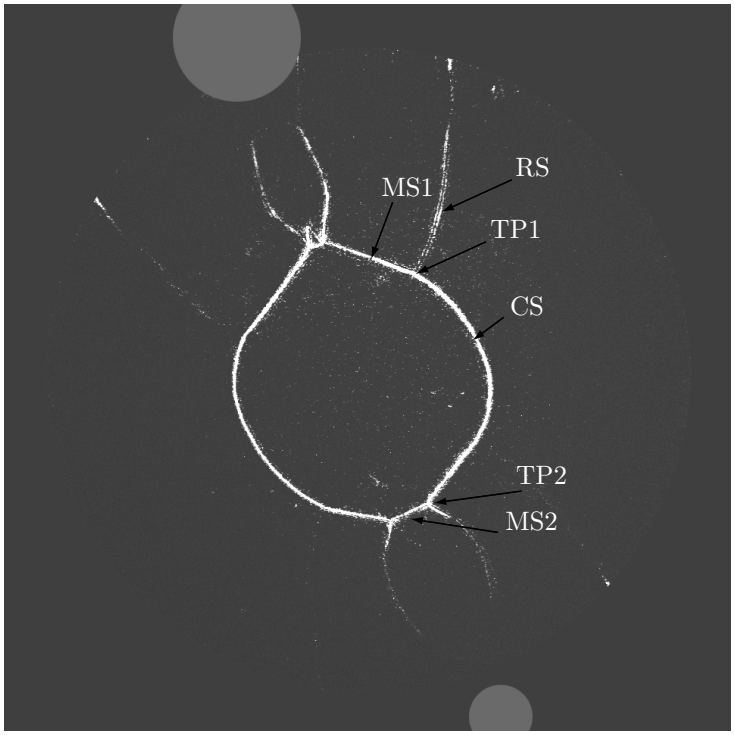

FIGURE 4.6. Schlieren photograph of a shock wave passing two cylinders, with diameters of 15 mm and 7.5 mm respectively. M_S=3.2. CS, converging cylindrical shock, RS, reflected shock from the cylinder, MS, Mach shock and TP, triple point. The filled grey circles show the positions of the cylindrical obstacles.

To study the effect of the size of the diameter of the cylindrical obstacles, two cylinders with different diameters, 7.5 and 15 mm respectively were placed opposite each other at $r = r_1$. In Fig. 4.6 it can be seen how the size of the diameters of the cylinders affects the focusing shock wave. Behind the smaller cylinder a second Mach shock (MS2) and triple point (TP2) are visible. This is consistent with results of Bryson A.E. & Gross R.W.F. (1960). In the latter work, the second Mach shock appears when the incoming shock wave has reached a position about 0.5 to 1.0 diameters behind the cylinder. The second Mach shock originates from the collision between the two first Mach shocks. The diameter of the cylindrical obstacle is influencing the disturbance on the shock wave. A larger diameter of the cylinder gives a more significant disturbance. This agrees with the results of Takayama K. *et al.* (1987).

It is possible to create polygonal shaped shock waves using obstacles. An example can be found in Fig. 4.7 where eight cylinders, with diameters of 15 mm, have been placed at $r = r_1$ in an octagonal pattern. The focusing and reflection process, seen in Figs. 4.7(a)-(d), has the same large scale features as when an octagonal reflector boundary is used. A difference is that the flow field behind the shock front is more complicated with more structures.

In summary, the results in Paper 3 show that a regular pattern of perturbations produces a regular shock wave with plane sides and corners which will repeat its shape in successive intervals. The results agree with earlier analytical, numerical and experimental results obtained from Schwendeman D.W. & Whitham G.B. (1987); Apazidis N. & Lesser M.B. (1996) and Apazidis N. *et al.* (2002) where it is seen that regular polygonal shock waves will repeat in successive intervals during the convergence process.

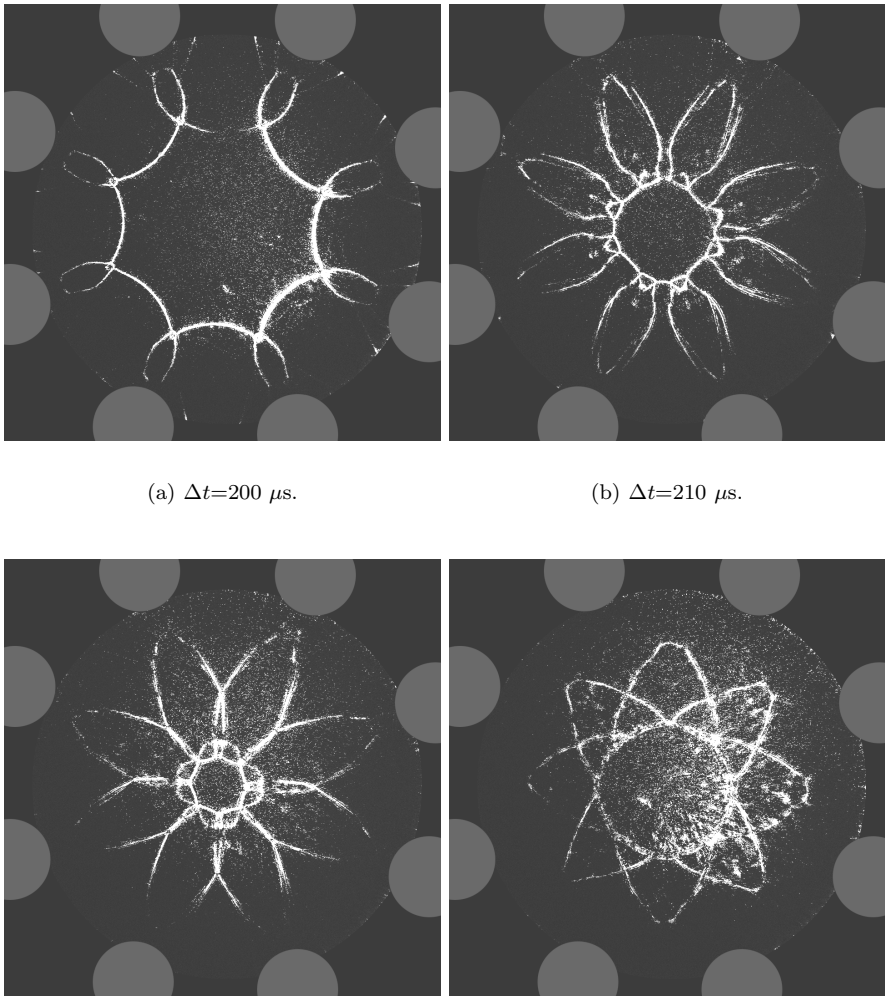

(a) Δt=200 μs.

(b) Δt=210 μs.

(c) Δt=216.5 μs.

(d) Δt=240 μs.

FIGURE 4.7. Schlieren photographs of shock waves at different time instants passing eight cylinders, with diameters of 15 mm). The filled grey circles show the positions of the cylindrical obstacles.

4.5. Production of Light

The production of light, as a result of shock convergence, has been preliminary investigated. In these experiments the low pressure part is filled with argon instead of air. Flashes of light have been observed during the focusing and reflection process. Fig. 4.8 shows a pattern of luminescence during shock convergence when the pentagonal reflector boundary is used. In Fig. 4.8(c) the inner of the argon-filled test section is illuminated by glowing spots and the pentagonal reflector boundary is clearly seen. Luminescence has previously been observed in experiments with shock wave focusing by Perry R.W. & Kantrowitz A. (1951) and Knystautas R. *et al.* (1969).

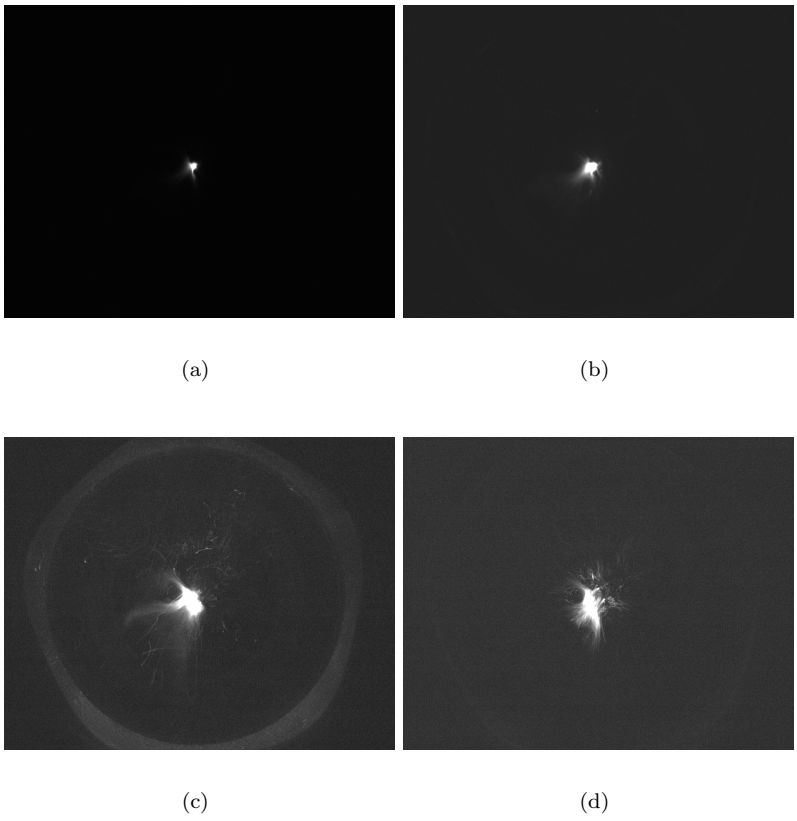

(a) (b)

(c) (d)

FIGURE 4.8. Luminescence patterns, when a pentagonal reflector boundary is used, during the converging and reflection process. Argon is used as test gas.

CHAPTER 5

Conclusions

A new type of a a horizontal co-axial shock tube was used to investigate the properties of converging and reflected shocks with various initial shapes. Two methods where used to generate shock waves with various geometrical shapes. The first method was to use the reflector boundary in the cylindrical test section mounted at the rear part of the co-axial shock tube. Four different shapes of boundaries have been used in the present study: a circle, a smooth pentagon, a heptagon and an octagon. The second method was to introduce disturbances in the test section in the form of cylindrical rods. The cylindrical rods where placed at various positions and in various patterns to create disturbances in the flow.

Numerical calculations have been performed to simulate the described experimental configurations and the results have been compared to the experimental observations.

A preliminary investigation of the light emission observed during the convergence and reflection process is performed.

We summarize the major results of the present investigation.

1. The initial form of the converging shock can be tailored by an appropriate choice of the form of the reflector boundary or by introducing obstacles in a specific pattern in the flow.

2. The nonlinear dynamics of the shock convergence is observed in the present experimental study. The form of the shock undergoes a transformation from an original n-gonal form through a double n-gonal back to an n-gonal, this time with opposite orientation compared to the original orientation. This is due to the nonlinear coupling between the form of the shock and the velocity of shock propagation. The above feature is confirmed experimentally for the pentagonal, heptagonal and octagonal shaped shock waves.

3. The final form of the converging shock, close to the center of the convergence center, is square-like for circular and octagonal reflector boundaries. This is believed to stem from the perturbations in the flow due to the four supports in the annular part of the shock tube. The shock strength is increasing as it approaches the center of the test section and the disturbances in the initial flow are amplified. This is in agreement with earlier experimental studies.

It is interesting to note that the square-like shape is not present when the pentagonal and heptagonal reflector boundary is used. A possible explanation is that a disturbance with an even number of modes can not overtake a disturbance with an uneven number of modes if the size of the disturbance is approximately the same in both cases. Also, the square-like shape is missing in all cases when the cylindrical obstacles were present. This means that the disturbances from the obstacles are stronger than the disturbances from the supports.

4. The reflected shock has initially a circular symmetry for all four reflector boundaries. The shock wave retains its circular symmetry in the case of the circular reflector. In the case of the other reflectors the form of the outgoing shock is influenced by the flow field created by the converging shock. In the heptagonal case the shock is transformed into a heptagonal-like form, in the octagonal case the shock is transformed to an octagon-like form, while in the case of a pentagon it attains a pentagon-like shape. This shows that the flow ahead of the shock front influences the shape of the reflected shock. This behavior is not seen when the cylindrical obstacles are present and the explanation should be that no photographs where taken as late as needed to show this feature.

5. The numerical simulation of the flow in the test section was performed by the numerical solution of the full set of Euler equations. The numerical calculations were based on the artificially upstream flux vector splitting scheme (AUFS), introduced by Sun M. & Takayama K. (2003). Several flow parameters obtained from the numerical computations have been compared with the experimental data. The first one is the average radius of the converging and reflected shocks as function of time. The experimental data was obtained from the schlieren images of the shocks. Also the shape of the shock fronts in the test section at various instants of the convergence and reflection processes as well as the density profiles obtained by the numerical calculations were compared with the schlieren images. The numerical results were found to be in good agreement with the experimental data and were also able to reproduce the major features of the flow in the test section. Numerical results indicate further that the maximum Mach number at the center of the test section is obtained for the circular reflector and is lower for a reflector with a polygonal form, decreasing with the number of sides of a polygon. For the case with cylindrical obstacles placed in the test section the AUFS scheme was able to reproduce the major features of the shock propagation process in the test section. The flow patterns produced in the calculations compare well with the experimental observations.

6. Preliminary results show production of light as a result of shock convergence. The amount of light was greater when argon was used as gas in the low pressure part as compared to the case with air.

CHAPTER 6

Papers and Authors Contributions

Paper 1

Focusing of strong shocks in an annular shock tube.
V. Eliasson (VE), N. Apazidis (NAP), N. Tillmark (NT) & M. Lesser (ML)
Accepted for publication in Shock Waves

In this paper an experimental and numerical study is performed for converging and diverging shock waves of three different shapes: circular, smooth pentagonal and octagonal. The experiments were conducted in a new shock tube facility at KTH Mechanics. The influence of the shape of the shock wave during both the converging and diverging process is investigated. The results show that it is possible to shape the converging shock wave by changing the reflector boundary of the test section in the shock tube. Close to the center of convergence the shock obtains a square-like form in case of a circular and octagonal reflector boundary. This is attributed to the instability of the converging shock front triggered by disturbances in the flow field. These disturbances are caused by the supports for the annular part of the shock tube. It is also shown that the shape of the diverging shock wave is influenced by the choice of reflector boundary. The general idea was suggested by ML. The experimental investigation was performed by VE. The numerical calculations were performed by NAP. The paper was written by VE, NAP and NT jointly.

Paper 2

The production of strong converging shocks.
V. Eliasson

In this paper the converging and diverging process of differently shaped shock waves are investigated. Two different methods to produce various geometrical shapes of shock waves are tested. In the first method the reflector boundary of the test section is exchangeable and four different reflectors are used: a circle, a smooth pentagon, a heptagon and an octagon. It is shown that the form of the converging shock wave is influenced both by the shape of the reflector boundary and by the nonlinear dynamics between the shape of the shock and the velocity of the shock front. In the second method cylindrical obstacles are placed in

the test section at various positions and patterns, to create disturbances in the flow that will shape the shock wave. It is shown that it is possible to shape the shock wave in a desired way with these obstacles. The influence of the supports of the inner body of the co-axial shock tube is also investigated. The experimental investigation was performed by the author. The paper was written by the author. This work will be presented at the Second International Conference on flow Dynamics in Sendai, November 2005.

Paper 3

On control of the form of strong converging shocks by means of disturbances.
V. Eliasson, N. Apazidis & N. Tillmark

In this paper an experimental and numerical study is performed for cylindrical converging shock waves shaped by disturbances in the flow. The disturbance elements consist of cylindrical objects placed in various patterns and positions in the test section of the shock tube. Their influence on the convergence and reflection process is investigated. It is found that disturbances arranged in a symmetrical pattern will produce a converging shock with a symmetric shape. For example a square formation will produce a square-like shock and an octagon formation a shock with an octagonal boundary. The experimental investigation was performed by VE. The numerical calculations were performed by NAP. The paper was written by VE, NAP and NT jointly.

Acknowledgements

First of all I would like to thank my supervisor Dr Nicholas Apazidis for his support and guidance throughout this work. I appreciate the opportunity to participate in this project.

Secondly, I would like to thank my co-supervisor Dr Nils Tillmark for guidance and great patience during the long hours when the experimental setup was tested and adjusted.

Prof. Martin Lesser is greatly acknowledged for initiating this project. Without this, I would not have had the chance to discover how beautiful fluid mechanics can be. Prof. Henrik Alfredsson is acknowledged for sharing his genuine interest and knowledge in fluid mechanics and compressible flow.

I would also like to thank Ulf Landén and Marcus Gällstedt for manufacturing the shock tube and other experimental equipment. It is always a pleasure to visit the workshop. Thanks to Ramis Örlü for help with the cold wire experiments and for always being a source of positive energy.

Many thanks to Michael and Timmy for reading and commenting the manuscript. Jens, Fredrik, Gabriele, Enrico, Allan and all other friends at KTH Mechanics are also acknowledged.

Thanks to my brother Micke for help with lifting all the heavy weights and to Eivysan and Larsa for all support during the years.

Tusen och åter tusen tack till Daniel.

The Swedish Research Council (VR) is acknowledged for the financial support. The funding from Göran Gustafsson Foundation provided means for the construction of the shock tube and for acquisition of the experimental equipment which is gratefully acknowledged.

References

Anderson J.D. 1990 *Modern Compressible Flow*, New York, McGraw-Hill Publishing Company.

Apazidis N. & Lesser M.B. 1996 On generation and convergence of polygonal-shaped shock waves. *J. Fluid Mech.* **309**, 301–319.

Apazidis N., Lesser M.B., Tillmark N. & Johansson B. 2002 An experimental and theoretical study of converging polygonal shock waves. *Shock waves* **12**, 39–58.

Bryson A.E. & Gross R.W.F. 1960 Diffraction of strong shocks by cones, cylinders and spheres. *J. Fluid Mech.* **09**, 301–319.

Courant R. & Friedrichs K.O. 1948 Intersciences publishers Inc. New-York. *Supersonic Flow and Shock Waves*.

Eliasson V., Apazidis N., Tillmark N. & Lesser M. 2005 Focusing of strong shocks in an annular shock tube. *Accepted for publication in Shock waves*

Guderley. 1942 Starke kugelige und zylindrische Verdichtungsstöße in der Nähe des Kugelmittelpunktes bzw. der Zylinderachse. *Luftfahrt Forsch.* **19**, 302–312.

Henshaw W.D., Smyth N.F. & Schwendeman D.W. 1986 Numerical shock propagation using geometrical shock dynamics *J. Fluid Mech.* **171**, 519–545.

Hosseini S. H. R. & Takayama K. 2005 Implosion from a sperical shock wave reflected from a spherical wall *J. Fluid Mech.* **530**, 223–239.

Johansson B. 2000 Experimental study of shock wave focusing in a confined reflector. *Licentiate Thesis, KTH, Stockholm, TRITA-MEK Tech. Rep. 2000:04*

Knystautas R., Lee B.H.K, & Lee J. H. S. 1969 Diagnostic experiments on converging detonations. *Phys. of Fluids Suppl.* **1**, 165–168.

Liepman H.W. & Roshko A. 1957 Elements of gasdynamics John Wiley & Sons Inc.

Perry R.W. & Kantrowitz A. 1951 The production and stability of converging shock waves. *J. Appl. Phys.* **22**, 878–886.

Schwendeman D.W. & Whitham G.B. 1987 On converging shock waves. *Proc. R. Soc. Lond. A.* **413**, 297–311.

Sturtevant B. & Kulkarny V.A. 1976 The focusing of weak shock waves. *J. Fluid Mech.* **73**, 651–671.

Sun M. & Takayama K. 2003 An artificially upstream flux vector splitting scheme for the Euler equations. *J. Comput. Phys.* **189**, 305–329.

Takayama K., Onodera O. & Hoshizawa Y. 1984 Experiments on the stability of converging cylindrical shock waves. *Theor. Appl. Mech.* **32**, 117-127.

Takayama K., Kleine H. & Gröning H. 1987 An experimental investigation of the stability of converging cylindrical shock waves in air. *Exp. Fluids* **5**, 315–322.

Takayama K. & Saito T. 2004 Shock wave/geophysical and medical applications *Annu. Rev. Fluid Mech.* **36**, 347–379.

Watanabe M. & Takayama K. 1991 Stability of converging cylindrical shock waves. *Shock waves* **1**, 149–160.

Watanabe M., Onodera O. & Takayama K. 1995 Shock wave focusing in a vertical annular shock tube *Shock Waves @ Marseille IV. Editors Brun R, Dimitrescu LZ. Springer-Verlag*, 99–104.

Whitham G.B. 1957 A new apporach to problems of shock dynamics. Part 1. Two-dimensional problems. *J. Fluid Mech.* **2**, 145–171.

Whitham G.B. 1959 A new apporach to problems of shock dynamics. Part 2. Three-dimensional problems. *J. Fluid Mech.* **5**, 369–386.

Whitham G.B. 1968 A note on shock dynamics relative to a moving frame. *J. Fluid Mech.* **31**, 449–453.

Whitham G.B. 1974 *Linear and Nonlinear Waves*, New York, John Wiley & Sons Inc.

Part II

Papers

1

Paper 1

Focusing of strong shocks in an annular shock tube

By V. Eliasson, N. Apazidis, N. Tillmark and M. Lesser

KTH Mechanics, SE-100 44 Stockholm, Sweden

Accepted for publication in *Shock Waves*

Focusing of strong shock waves in a gas-filled thin convergence chamber with various forms of the reflector boundary is investigated experimentally and numerically. The convergence chamber is mounted at the end of the horizontal co-axial shock tube. The construction of the convergence chamber allows the assembly of the outer chamber boundaries of various shapes. Boundaries with three different shapes have been used in the present investigation - a circle, an octagon and a smooth pentagon. The shock tube in the current study was able to produce annular shocks with the initial Mach number in the range $M_s = 2.3 - 3.6$. The influence of the shape of the boundary on the shape and properties of the converging and reflected shock waves in the chamber has then been investigated both experimentally and numerically. It was found that the form of the converging shock is initially governed by the shape of the reflector and the nonlinear interaction between the shape of the shock and velocity of shock propagation. Very close to the center of convergence the shock obtains a square-like form in case of a circular and octagonal reflector boundary. This is believed to stem from the instability of the converging shock front triggered by the disturbances in the flow field. The outgoing, reflected shocks were also observed to be influenced by the shape of the boundary through the flow ahead as created by the converging shocks.

1. Introduction

High pressures, temperatures and densities may be achieved in a region of gas compressed by means of a converging shock wave. This feature in connection with various technological applications is one of the main reasons for continuing interest in the problem of shock focusing. The highly nonlinear nature of the process presents a major challenge to its study. At the same time it serves as a source of the non-triviality of this phenomenon.

Two aspects of a converging shock are of special interest. The first one being the connection between the local strength of the shock and the shape evolution of the converging shockfront. The second issue, which is however

closely related to the first one is the the question of the stability of converging shocks.

Guderley (1949) was first to investigate theoretically the convergence of an initially cylindrical shock wave. Guderley used a similarity power law assumption for the radius of the converging shock as function of time. He was thus able to transform the governing equations to an ordinary differential equation which was integrated numerically. For a cylindrical shock the power law exponent was found to be $\alpha = 0.834$. Over the years a large number of mainly theoretical and numerical investigations were dedicated to similar problems.

Perry and Kantrowitz (1951) were the first to produce experimentally a converging cylindrical shock. The cylindrical shock in their experiment was generated in a shock tube with a tear-drop inserted in the test section. The behavior of the converging cylindrical shock was studied in detail in this pioneering investigation. It was observed that for a shock strength exceeding $M = 2.4$ the cylindrical form of the shock was distorted as the shockfront approached the center of the cavity. This was attributed to the instability of the converging shock resulting from a growth of small perturbations of the cylindrical shape. Another important observation of this study was the luminescence observed in the center of the cavity at the final stages of the shock collapse.

In a later investigation Sturtevant and Kulkarny (1976) used a parabolic reflector to study the complex behavior of shock waves in a focal region. In this extensive experimental study shocks were brought to a focal region by reflecting an initially plane shock from a surface of the reflector. One of the important results of this study was that it showed a tendency of curved shocks to build planar sections. This tendency to planarity as a result of the nonlinear interaction between the form and the local strength of the shock was later investigated and confirmed in a series of experimental, theoretical and numerical investigations, see e.g. Schwendeman and Witham (1987), Apazidis and Lesser (1996), Apazidis *et al.* (2002).

Takayama *et al.* (1984), (1987) and Watanabe and Takayama (1991) studied the convergence of initially cylindrical shock waves in shock tubes with an annular section. One of the interesting observations of these studies was the formation of square-formed shocks in the final stages of the convergence process. This was attributed to a 4 symmetrical perturbations introduced in the flow by the supports holding the annular section of the shock tube. This tendency of the converging shock to build n-gonal structures corresponding to the same number of perturbations in the flow was further confirmed by an introduction of artificial perturbations in the flow field. Takayma *et al.* (1987) referred to this as the mode-n instability. An alternative way would be to describe this as an inherent dynamic stability of the shock in the sense that the curved sections tend to transform to planar ones. In other words the form of the shock may be considered as unstable since it diverges from the original circular form and at

the same time stable since it tends to build a natural for the shock dynamics n-gonal form with plane sides and sharp corners. Once the the n-gonal shape is formed it will be periodically transforming, repeating itself during the convergence process, see e.g. Schwendeman and Whitham (1987), Apazidis and Lesser (1996), Apazidis *et al.* (2002). The condition for such stable periodic behavior is that the perturbations in the flow influencing the shock form are symmetric. This results in a symmetric polygonal form, periodically repeating itself. If, on the other hand, the perturbations lack symmetry the formed polygon will reflect this and the periodicity would therefore be lost.

The influence of the disturbances on the convergence of a cylindrical shock was investigated in an experimental study by Watanabe *et al.* (1995). This study was performed in a vertical co-axial annular shock tube. Special care was taken in the design of this shock tube to minimize the possible disturbances in the flow. Thus this facility lacked the supports for the inner tube known to introduce disturbances in the flow. The results of this study showed that the cylindrical shock wave converge more uniformly towards the center than in a similar co-axial shock tube with supports.

In the previous paper by Apazidis et al. (2002) a 2D chamber was used to study the convergence of a reflected shock wave. Shock waves were created in a plane chamber which had a specific geometric boundary, in the form of a pentagon with "smooth" corners. The shocks were produced by two different methods, by means of an igniting spark as well as an exploding wire, placed at the center of the chamber. Thus an outgoing cylindrical shock was created. After reflection from the chamber boundary the shock was transformed to a converging pentagonal shock. The Mach number range for the converging reflected shock was 1.1 to 2.0, producing weak to moderately strong shock waves. The above experimental method was able to produce highly symmetrical converging pentagonal shock waves. One of the disadvantages of the method was the creation of a disturbance zone in the center of the chamber due to the initial spark creation. It was therefore not feasible to continue the study of the converging shock as it approached the center of the chamber. This was unsatisfactory since the main nonlinear focusing effects become more pronounced as the strength of the shock increases in the vicinity of the center.

To be able to study this process in full, a new experimental setup was built at KTH Mechanics. This setup consists of a horizontal annular shock tube similar to those used in the earlier mentioned experiments. Compared to the chamber used in Apazidis et al (2002) there are no disturbances ahead of the shock wave and hence the whole converging-reflection process is visible.

Another improvement of the new shock tube facility is that it can produce converging shock waves of various shapes. The present shock tube differs from the previous annular shock tubes by the construction of the thin convergence chamber, perpendicular to the tube. The construction of the chamber allows

the mounting of the outer boundaries of various shapes. Three different shapes of the outer boundary have been tested in the present experiment including a circular boundary, an octagonal boundary and a boundary with a smooth pentagonal shape. The purpose of the present work is therefore to study the influence of the form of the shock on the process of shock convergence and reflection. This influence of the shape of the boundary on the form and properties of the resulting shocks have been investigated both experimentally and numerically.

2. Experimental apparatus

The experimental apparatus consists of a 2.4 m long shock tube where the shock is generated, focused and reflected. The focusing and reflection process is visualized by means of a schlieren system with a camera. The shock speed is measured before the shock converges by sensors placed on the annular part of the shock tube. The experimental setup is shown in Fig. 1.

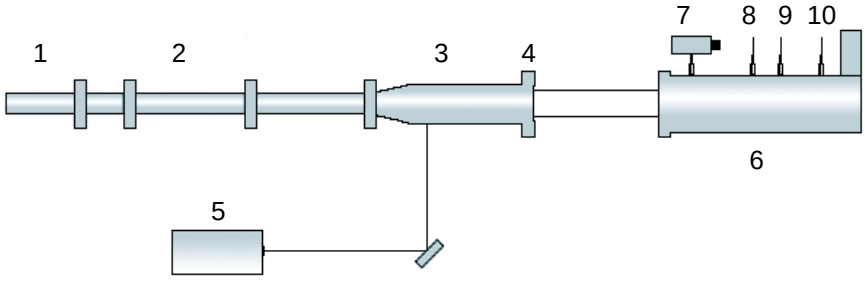

FIGURE 1. Schematic overview of the experimental setup: 1. The high pressure part, 2. Low pressure part: inlet section, 3. Low pressure part: transformation section, 4. Low pressure part: test section, 5. Pulse laser, 6. Schlieren optics, 7. PCO CCD camera, 8. Damping filter, 9. Lens, 10. Schlieren edge.

2.1. *The shock tube*

The horizontal shock tube consists of two main parts, the high pressure part or the driver and the driven or low pressure part. The low pressure part is divided into three sections: the inlet section with a constant cross-section area where a plane shock is formed, the shock transforming section where the shock becomes annular and finally the plane test section in the rear end of the shock tube. The shock tube has a circular cross-section. In the experiments, the test gas is air and the pressure in the low pressure part ranges from 0.133 kPa to 13.3 kPa, while the pressure in the high pressure part is kept almost constant at

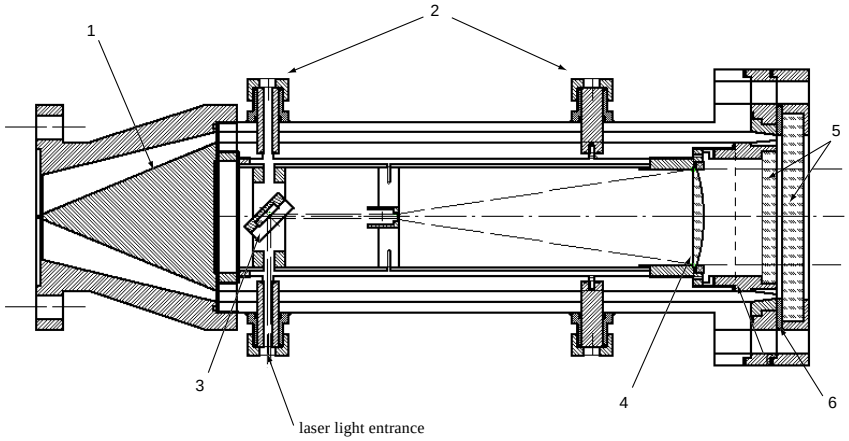

FIGURE 2. The annular part of the shock tube: 1. Inner body with a cone, 2. Supports, 3. Mirror, 4. Lens, 5. Glass windows for visualization, 6. Convergence chamber with replaceable reflector plates.

1500 kPa. This yields shock Mach numbers between 2.3 and 3.1 in the annular section of the tube.

The high and low pressure parts are separated by an aluminum membrane with a thickness of 0.5 mm. As the pressure is increased in the high pressure part, the membrane is forced against a knife-cross placed in the inlet of the low pressure part. When the membrane bursts, a shock is formed and starts to propagate down the 80 mm wide and 1300 mm long inlet section. The inlet section of the low pressure part is sufficiently long to establish a plane shock. The plane shock is transformed into an annular shape in the transforming section which consists of a conically diverging section where the inner diameter increases from 80 to 160 mm. A 490 mm long cylindrical inner body (ϕ=140 mm) is mounted coaxially in the interior of the outer tube thus forming an annular channel. The cross-sectional area is maintained constant from the inlet section, through the transformation section. The inner body is mounted by means of two sets of four supports. To minimize the disturbance from the supports, they are shaped as wing profiles. Also, the second set of supports is rotated in the plane of the shock 45° with respect to the first set, see Fig. 2. The speed of the shock, U_s, that impacts upon the test section is determined by two sensors mounted in the wall of the outer tube along the axis of the transforming section. The temperature jump from the shock wave passage triggers the sensors and gives a measure of the shock speed with an accuracy within 0.5%.

At the end of the shock tube the flow turns at a sharp 90° bend and enters radially into the plane test section. The gap between the two facing surfaces is 5 mm and the cross-section area is decreased by a factor of two as compared to the annular section. The outer boundary of the test section is exchangeable and three reflector plates of different shapes are used in the experiments, a circular, a pentagonal and an octagonal plate, see Fig. 3. The radius for the circular reflector plate is 80 mm. The shape for the pentagonal boundary is given by

$$r = \frac{r_0}{1 + \varepsilon \cos(5\theta)}, \tag{1}$$

where ε=0.035 and r_0=77 mm and r is the radius. Focusing of pentagonal shock waves, given by (1), has previously been studied by Apazidis et al. (2002). The octagonal plate has $R = 80$ mm, which is the radius of the outer circumscribed circle.

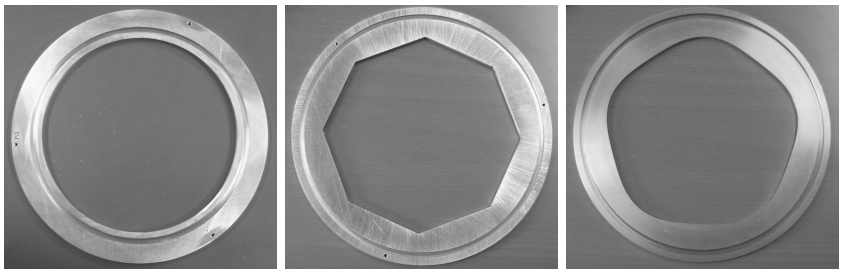

(a) Circular. (b) Octagonal. (c) Pentagonal.

FIGURE 3. The three reflector plates used in the experiments.

2.2. *The shock visualization*

The facing surfaces in the test section have glass windows and the flow is visualized by schlieren technique. The inner body contains an adjustable beam expander to provide axial parallel light through the test section. An Nd:Yag (NewWave Orion) laser that provides single shot operation, with 5 ns long light pulses, is used as light source for the schlieren optics. It is mounted outside the shock tube and the light beam from the laser is reflected by mirror before entering the shock tube. As the laser beam enters the tube through an orifice in one of the inner body supports, it is deflected in the axial direction, see Fig. 1. The parallel light obtained by means of the beam expander passes the test section and leaves the shock tube via the rear end glass window. The light is then focused by schlieren optics. A schlieren edge, a pin-head with r=1 mm, is

placed in the focal plane of the source and intercepts parts of the light before it reaches the camera. The camera, (PCO SensiCam, 12 bits, 1280 x 1024 pixels, pixel size: 6.7 x 6.7 μm, CCD) is placed in the focal plane of the test section. The camera is triggered by the same signal as the laser. A time delay unit (Stanford Research System, DG 535) is used to control the laser and the camera to enable exposure of the shock wave at predetermined positions in the test section.

3. Experimental Results

The present light source system allows one exposure at each run. To resolve the process of shock focusing and reflection in time, single exposures are taken with different time delays. For each run the time instants t_1 and t_2 when the shock wave passes the sensors are recorded. From these, the shock speed, U_s, can be determined. These measurements have a high repeatability giving low error level. For a typical shock speed around 800 m/s the average of the passage time $t_2 - t_1$ and the rms-value are 312 μs and 1.32 μs respectively i.e. the error is less than 0.5%. In Fig. 5 a typical time history of signals recorded by the two sensors is shown. The upper curve is the signal from the first sensor. The first peak corresponds to the time t_1 and the second peak is the reflected shock wave. The lower curve is the signal from the second sensor. The resolution used in the measurements of the time signals is $2\mu s$.

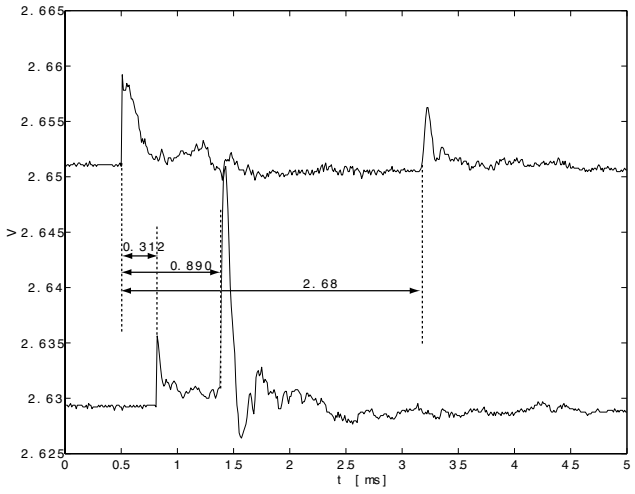

FIGURE 4. The signal from the two sensors showing the shock wave passage and reflection, $M_s = 2.3$, octagonal reflector.

Typical sets of pictures are shown in Fig. 4, 7 and 6. The size of the visualized area is 70 mm in diameter, e.g. that is ca 50% of the test section. In Fig. 4, where the circular reflector plate is used, the shock wave is seen to maintain a slightly perturbed circular form during the main part of the focusing process. Very close to the center the shock wave loses its circular shape and becomes square-shaped, see Fig. 4c. The reflected shock propagates into a flow field created by the converging shock. Although the final form of the converging shock is square-like the reflected shock wave regains its circular symmetry after focusing. The circular symmetry of the outgoing shock is then maintained through the rest of the reflection process, see Fig. 4e-d.

In Fig. 7 the shock focusing and reflection using an octagonal reflector plate is shown. Initially the shape of the shock wave is octagonal and has the same orientation as the reflector boundary, see Fig. 7a. During the focusing process the octagonal shaped shock wave transforms first into a double octagon and then obtains again an octagonal form, see Fig. 7c. This time, however the orientation of the shock front differs from that of the boundary in the sense that corners of the shock are now positioned against the plane sides of the reflector and vice versa. That is the octagonal shape is now reoriented as compared to the initial shape, compare Fig. 7b and 7c. This behavior was predicted earlier in the numerical studies of polygonal shock convergence, see e.g. Schwendeman and Whitham (1987) and Apazidis and Lesser (1996). The above phenomenon originates from the nonlinear coupling between the shape of the shock and the velocity of the shock propagation. Due to the high curvature in the vicinity of the corner areas these propagate with higher velocities than the plane parts of the shock front. This leads to a transformation and reorientation of the shock front shape with new plane portions replacing the corners and new corners being built at the middle positions of the previous plane sides. To our knowledge this feature has not been observed experimentally earlier. Numerical studies indicate that this process would repeat itself through several cycles.

The present experimental observations show however that close to the center of convergence the shock obtains a square-like form, see Fig. 7d. We believe that this is attributed to the disturbances in the flow introduced by the supports holding the inner body of the shock tube. It seems that the 4-mode instability mentioned earlier in Takayama (1984) and Takayama *et al.* (1987) plays an important role here.

Although the final form of the converging shock is square-like just before the focusing the reflected shock obtains a circular form in the beginning of the reflection process just as in the case of a circular reflector, see Figs. 7f-g. The difference as compared to the circular case is a more complicated structure of the flow field created by the converging shock seen in these figures. In the later stages of the reflection process the outgoing shock transforms from a circular to an octagonal form, now as the result of the interaction with the flow ahead of the shock, see Fig. 7h.

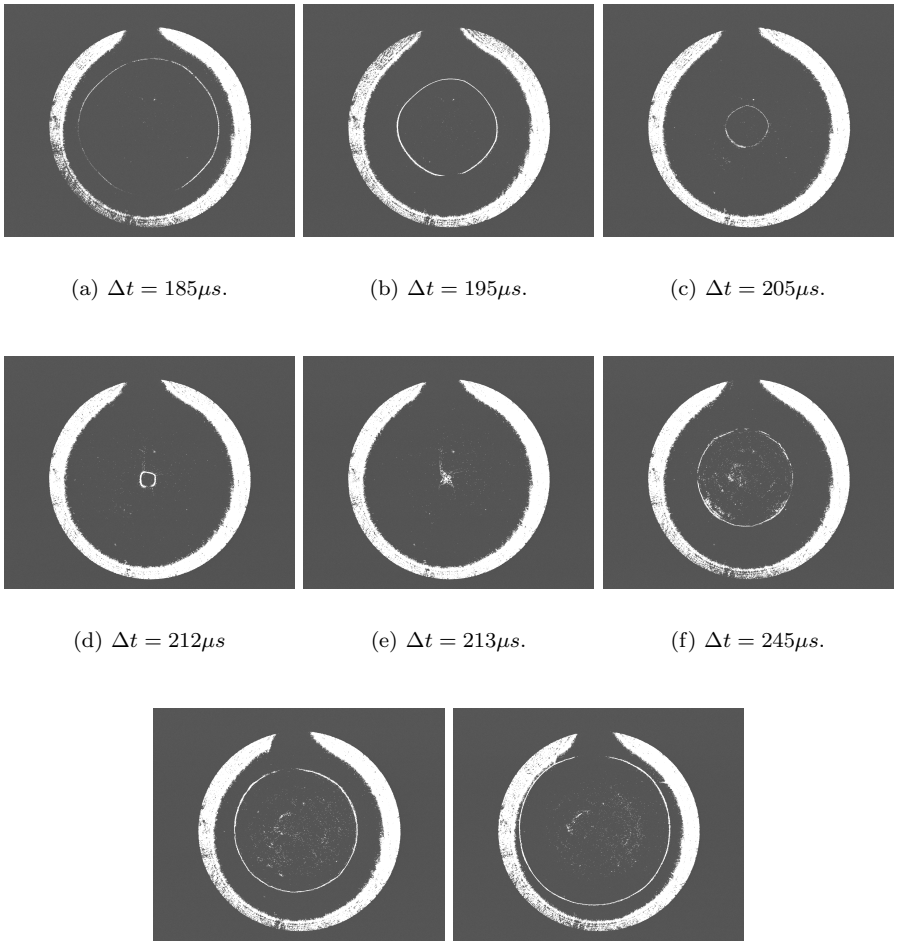

(a) $\Delta t = 185\mu s$. (b) $\Delta t = 195\mu s$. (c) $\Delta t = 205\mu s$.

(d) $\Delta t = 212\mu s$ (e) $\Delta t = 213\mu s$. (f) $\Delta t = 245\mu s$.

(g) $\Delta t = 255\mu s$. (h) $\Delta t = 265\mu s$.

FIGURE 5. The shock wave for the annular Mach number $M_s = 2.3$ at different instants for the circular reflector plate.

Finally, Fig. 6 shows the focusing and reflection process for the pentagonal reflector plate. The shock behavior in this case is similar to that of the octagonal case. The shape of the converging shock initially resembles the form of the reflector boundary, see Fig. 6a. As the converging shock approaches the center of the test section its form is transformed to that of an reoriented smooth pentagon as in Fig. 6c. The reflected shock is influenced by the flow

ahead of it, as created by the converging shock. This influence transforms the shock from a more circular-like form at the beginning of the reflection to a pentagon-like form at the later stages of the process, as seen in Fig. 6h. The orientation here is the same as in Fig. 6c, that is opposite to the orientation of the reflector boundary.

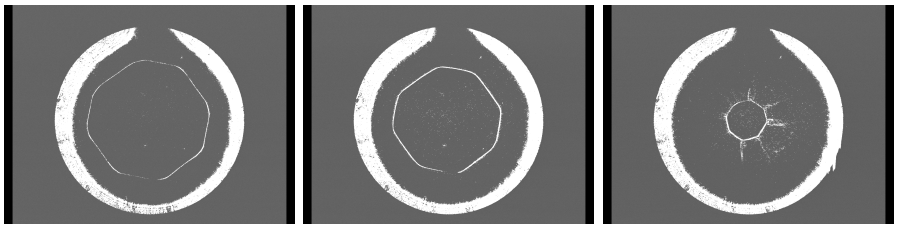

(a) $\Delta t = 185\mu s$. (b) $\Delta t = 190\mu s$. (c) $\Delta t = 202\mu s$.

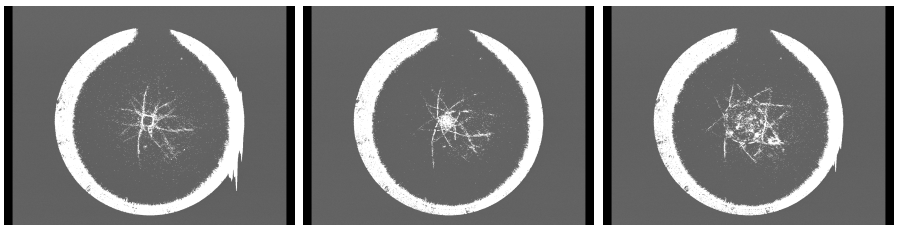

(d) $\Delta t = 210\mu s$. (e) $\Delta t = 215\mu s$. (f) $\Delta t = 230\mu s$

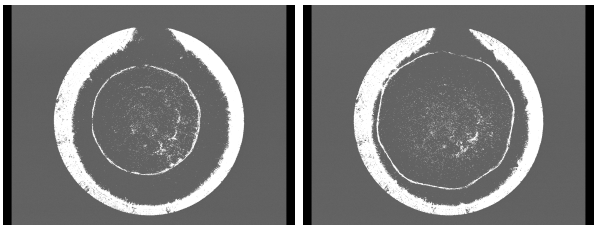

(g) $\Delta t = 250\mu s$. (h) $\Delta t = 265\mu s$.

FIGURE 6. The shock wave for the annular Mach number $M_s = 2.3$ at different instants for the octagonal reflector plate.

Near the center of convergence the shock wave is observed to attain a square shape, for the circular and octagonal reflector case. It is likely that

this is caused by the disturbances in the flow introduced by the second set of supports to the inner body. The corners of the square shaped shock wave correspond to the location of the second set of supports. As mentioned earlier this phenomenon was observed in the experiments performed by Takayama (1984) and Takayama *et al.* (1987).

The present experimental study shows that the flow field behind the shock influences not only the converging shock but is equally important for the shape of the the reflected shock.

Fig. 8 shows a blow up of the center of convergence for different reflector forms and Mach numbers, all showing the square shape of the shock wave. In Fig. 8d the initial Mach number was increased to $M_s = 3.68$ by using helium as the driver gas instead of air.

To be able to make comparisons of the shock speed of the three different shaped shock waves, a concept of equivalent radius is introduced. This radius is defined as the mean value of the smallest circle surrounding the shock and largest contained inside the shock wave. The equivalent radius for four different pressure ratios corresponding to Mach numbers (measured in the annular section), $M_{s1} = 3.10$, $M_{s2} = 2.71$, $M_{s3} = 2.51$ and $M_{s4} = 2.36$ are plotted in Fig. 9. The visualization technique is not satisfactory when using low pressures in the low pressure part, (< 4kPa), which explains the reduction of points for the converging shock with $M_s = 3.10$ in Fig. 9.

In Fig. 10 the radius of the shock wave is plotted versus the delay time for the three reflector plates at the same annular Mach number, $M_s = 2.3$.

In Fig. 11 - 13 the radius of the shock wave is plotted versus the time delay for the circular, pentagonal and octagonal reflector respectively.

To estimate the error in the shock wave position the time delay was set to $\Delta t = 200\mu s$ and a series of 5-9 runs were performed for the three different reflectors. The rms values and the equivalent radius are presented in Table 1. As seen from Table 1, the errors are about 10% for the pentagonal and the octagonal reflectors and about 5% for the circular reflector. Possible sources of errors are fluctuations in temperature and variations in the light pulse emission in the laser. These errors could be effectively reduced if equipment allowing several exposures per run were used, as in Takayama *et al.* (1984).

Reflector	rms	mean radius (mm)
Circle	$\sigma = 1.20$	$\bar{R}$=22.9
Pentagon	$\sigma = 2.12$	$\bar{R}$=19.4
Octagon	$\sigma = 1.89$	$\bar{R}$=18.6

TABLE 1. Error estimation for $\Delta t = 200\mu s$ for all three reflectors, $p_1 = 13.3kPa$.

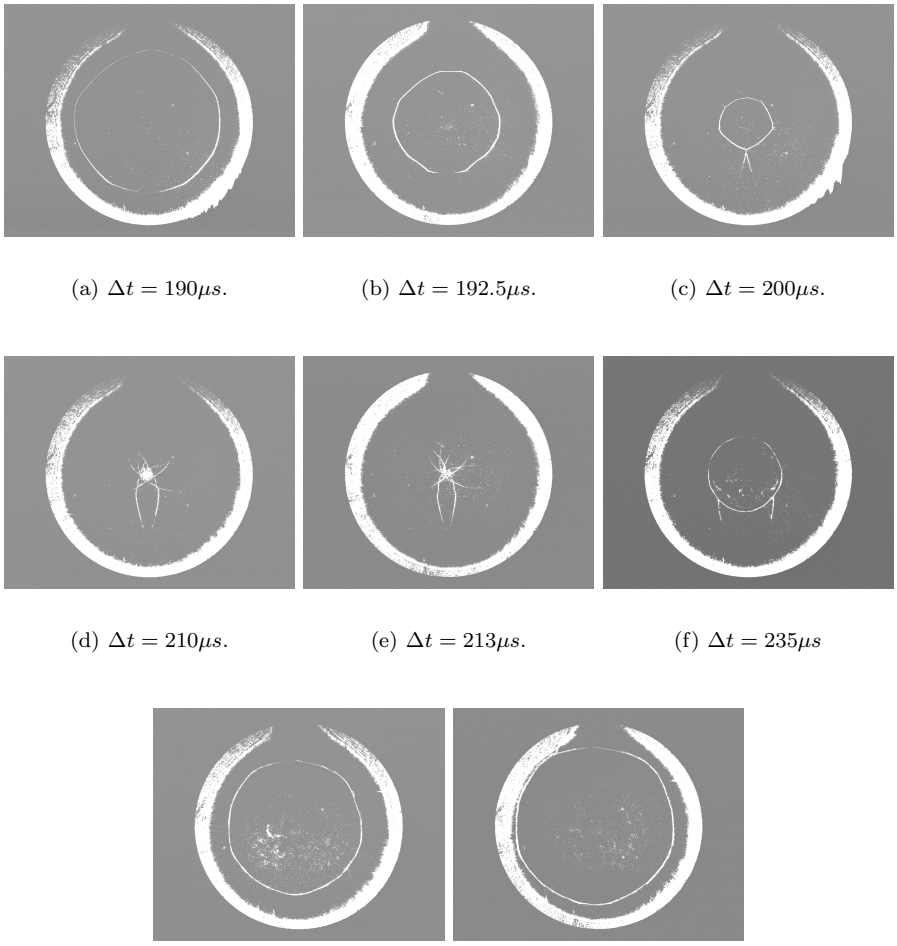

(a) $\Delta t = 190\mu s$. (b) $\Delta t = 192.5\mu s$. (c) $\Delta t = 200\mu s$.

(d) $\Delta t = 210\mu s$. (e) $\Delta t = 213\mu s$. (f) $\Delta t = 235\mu s$

(g) $\Delta t = 255\mu s$. (h) $\Delta t = 270\mu s$.

FIGURE 7. The shock wave for the annular Mach number $M_s = 2.3$ at different instants for the pentagonal reflector plate.

An attempt was made to compare the experimental data for the converging shock wave radius with the similarity solution obtained by Guderley (1942),

$$\frac{R}{R_c} = \left(1 - \frac{t}{t_c}\right)^{\alpha}, \tag{2}$$

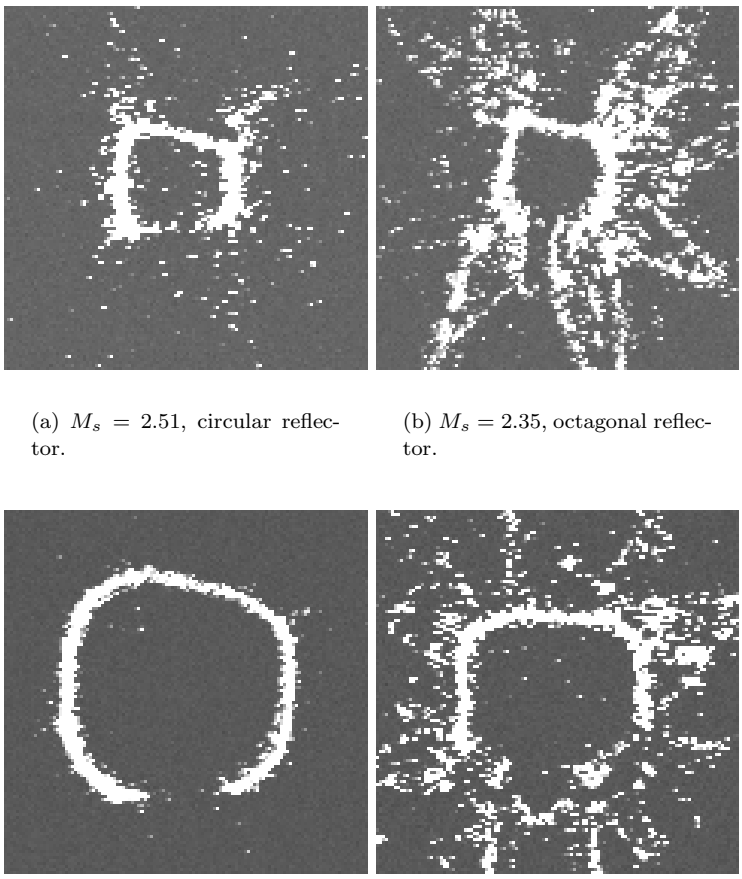

(a) $M_s = 2.51$, circular reflector.

(b) $M_s = 2.35$, octagonal reflector.

(c) $M_s = 2.35$, circular reflector.

(d) $M_s = 3.68$, octagonal reflector.

FIGURE 8. Square shaped shock waves near the center of convergence for circular and octagonal reflectors for various values of the annular Mach number M_s.

where R_c is the outer radius of the test section and t_c is the time when the converging shock wave arrives at the center. By a nonlinear least square fit to the experimental data, R_c, t_c and α are found. The single run procedure used in the estimation of the shock position makes the determination of the R_c, t_c and α difficult. Despite the low level of variation of the Mach number value between various runs it was not possible to determine an accurate value based on the present experimental results. This is due to the sensitivity of the α-value on

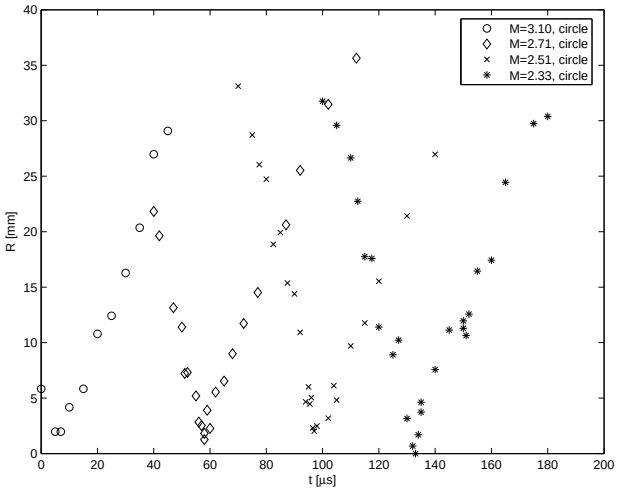

FIGURE 9. Radius as function of the delay time for the circular reflector plate and four various values of the annular Mach number.

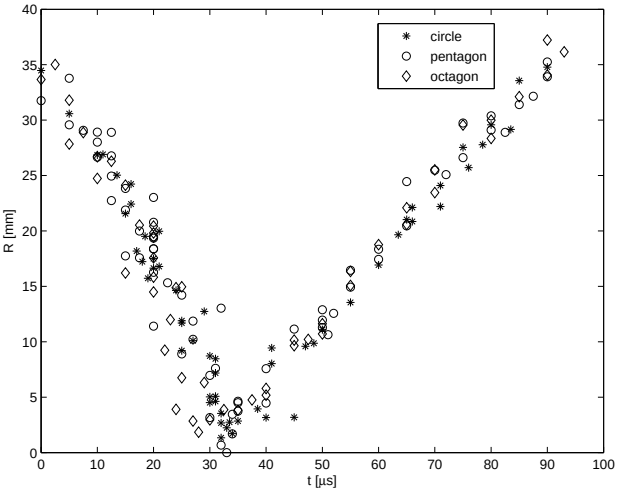

FIGURE 10. Comparison between octagonal, pentagonal and circular reflector plates for the annular Mach number $M_s = 2.3$.

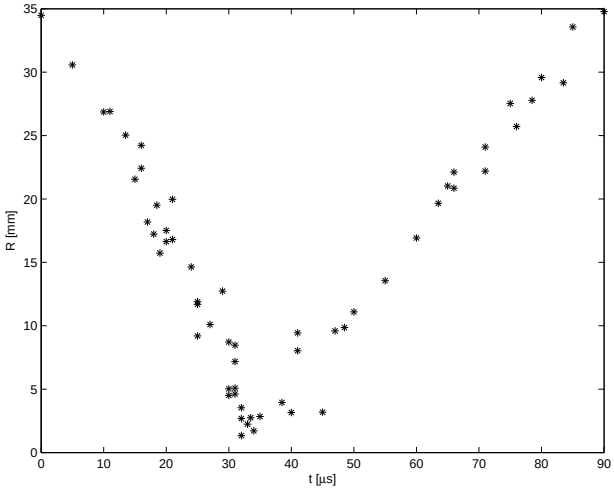

FIGURE 11. Converging and reflected shock wave for the circular reflector for the annular Mach number $M_s = 2.3$.

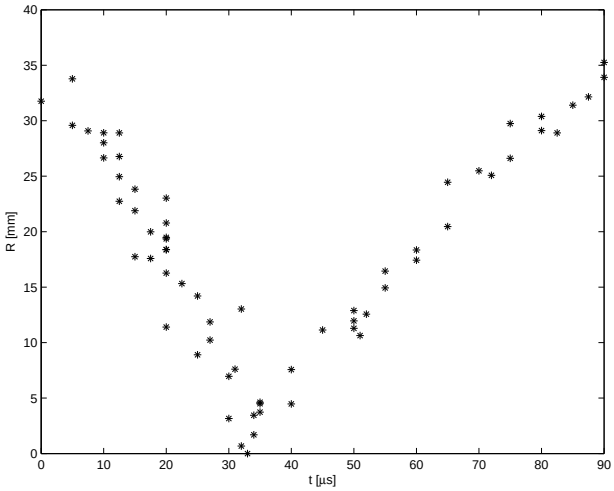

FIGURE 12. Converging and reflected shock wave for the pentagonal reflector for the annular Mach number $M_s = 2.3$.

even small variations in the experimental data between the runs, especially in

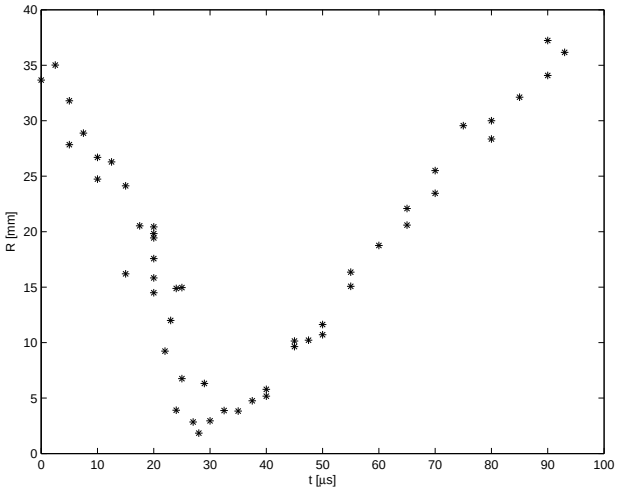

FIGURE 13. Converging and reflected wave for the octagonal reflector for the annular Mach number $M_s = 2.3$.

the vicinity of the convergence center. In the next section we give a comparison of the present numerical results with the similarity power law assumption (2) for both numerical and experimental data obtained by previous investigators.

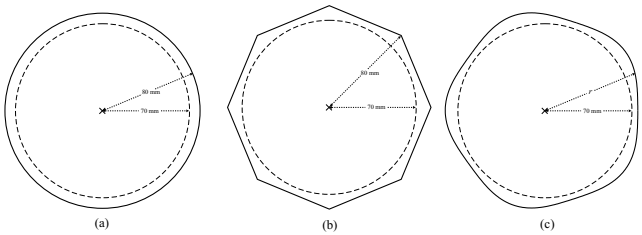

FIGURE 14. Initial high pressure zone adjacent to the chamber boundary. (a) - circular boundary, (b)- octagonal boundary (c) - smooth pentagon defined by $r = r_0 \diagup (1 + \varepsilon \cos(5\theta))$ where $r_0 = 77mm$ and $\varepsilon = 0.035$

4. Numerical simulation and comparison with the experimental results

The numerical calculations were based on the artificially upstream flux vector splitting scheme (AUFS) for Euler equations, introduced by Sun and Takayama (2003). The scheme proved to be highly accurate, stable and robust in the considered configurations. In the following we describe the initial, boundary value problem investigated in the present numerical study.

We will consider propagation of strong shocks in a gas-filled thin chamber with various shapes of the outer boundary. The shock is assumed to be initiated by an impulsive high pressure in a thin annular zone adjacent to the outer boundary of the test section. The outer boundary of this zone is the reflector plate and the inner is a circle defined by the inner body of the shock tube. The inner of the chamber is initially kept at lower pressure. The complete two-dimensional flow in the chamber is then computed. This is certainly an approximation which disregards the details of the complex flow situation in the shock tube as the flow turns 90° from the annular section and enters test section. The validity of this approach was tested by comparison of the computational results with the experimental observations of the present study which proved to be good. The numerical model correlates well with the major features of the flow in various investigated configurations.

The process of convergence of the initial shock toward the center of the boundary as well as the following propagation of the outgoing reflected shock from the center of the chamber was studied in detail and the results compared to the experimental observations. The shape of the chamber together with the thin high pressure zone adjacent to the chamber boundary are shown schematically in Fig. 14.

The comparison with the experimental results has been carried out for the three cases shown in Fig. 14. In case (a) the shock is generated by means of an initially high pressure between the inner and outer circular boundary,

corresponding to the annular end of the inner body. In case (b) the outer boundary of the test section is formed as an octagon and in case (c) as a "smooth" pentagon.

In all three cases the pressure in the inner cylindrical part of the chamber was set to $p_1 = 13.3\ kPa$. This value was chosen to be the same as the one used in the experiment. The pressure in the driver section in the experiment was $p_4 = 112\ p_1$. In our case the losses in the straight portion of the tube are minimized, however we should expect greater losses due to the sharp 90° bend. The flow in the sharp 90° has been simulated numerically and the results indicate a significant drop on the Mach number after the turn. Calculations of the converging shock for various values of the initial pressure ratio in the chamber have been performed. One of the measured and calculated parameters of the complete flow is the average radius of the converging and reflected shock in the chamber as function of time. These curves were calculated for various initial pressure ratios at the boundary of the chamber starting from the maximum theoretical ratio $p_4/p_1 = 112$ and gradually decreasing this value in order to account for the pressure losses in the tube. The pressure ratio value that compared best with the experimental curves turned out to be about 30 % of the maximum value, giving $p_4/p_1 = 33.6$. This value was used in the calculations. Comparison of the calculated and experimental curves showing the shock radius as function of time for various initial configurations are shown in Fig. 15.

In case of a pentagonal and octagonal boundary the value of the radius in the experimental measurements as well as in calculations is chosen as the average shock radius at each time instant, that is $r = (r_{\max} + r_{\min})/2$. Shock positions of the converging shock at different locations in the chamber with an octagonal boundary are displayed in Fig. 16a. Fig. 16b shows the corresponding density profiles in the chamber at a certain instant of the process.

Fig. 17 shows comparison of the calculated shock profiles with the schlieren images at the corresponding time instants in the test section.

The calculated density contours for the outgoing shock in the case of an octagonal reflector are compared with the schlieren image in Fig. 18. The complicated flow situation with a circular shock front and an 8-point star-like profile is seen to be clearly reproduced in the numerical simulation.

As we can see from Fig. 14 the calculated and experimentally obtained values of the radii of the converging and diverging shock fronts compare well in all three geometrical configurations. It was mentioned in Section 3 that values of the radius as function of time for the converging shock have been compared with the similarity power law assumption both for the calculated and experimental values. Due to the single run procedure for each shock position it was not possible to make an accurate estimate of the power law exponent from

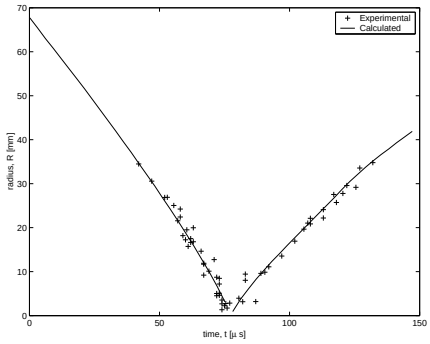

(a) Circular boundary

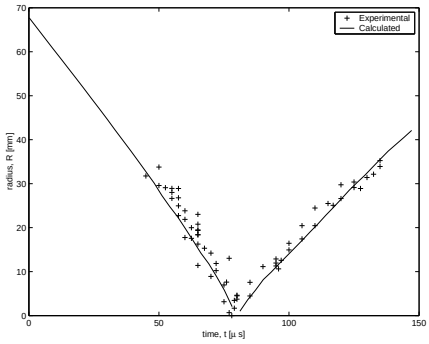

(b) Octagonal boundary

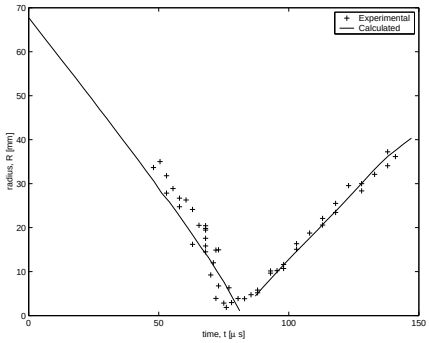

(c) Smooth pentagon

FIGURE 15. Calculated and measured values of the average shock radius in the chamber for $p_4/p_1 = 33.6$. (a) - circular boundary, (b)- octagonal boundary (c) - smooth pentagon.

the experimental data. The α value was however obtained from the numerical computations. The results are given in Table 2.

Shape	Pressure ratio	α
Circle	no counter pressure	0.832
Circle	$p_4/p_1 = 33.6$	0.857
Smooth pentagon	$p_4/p_1 = 33.6$	0.879
Octagon	$p_4/p_1 = 33.6$	0.883

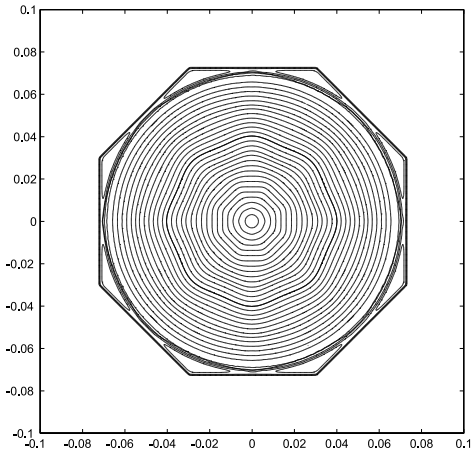

(a) Converging shock fronts

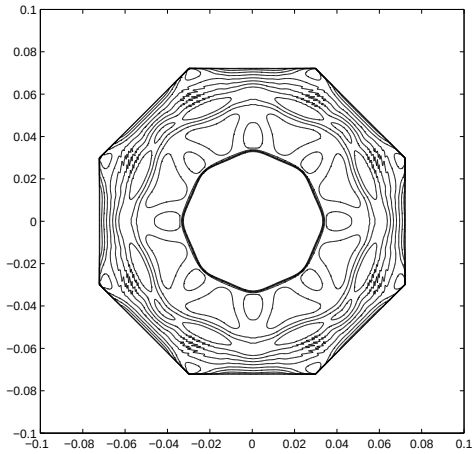

(b) Density contours at certain instant

FIGURE 16. Calculated converging shock in an octagonal chamber for $p_4/p_1 = 33.6$.

The α value for the case of a circular reflector with no counter pressure compares well with previous numerical results, see e.g. Takayama *et al.* (1984), Mishkin and Fujiumoto (1978) and experimental results of Takayma *et al.*

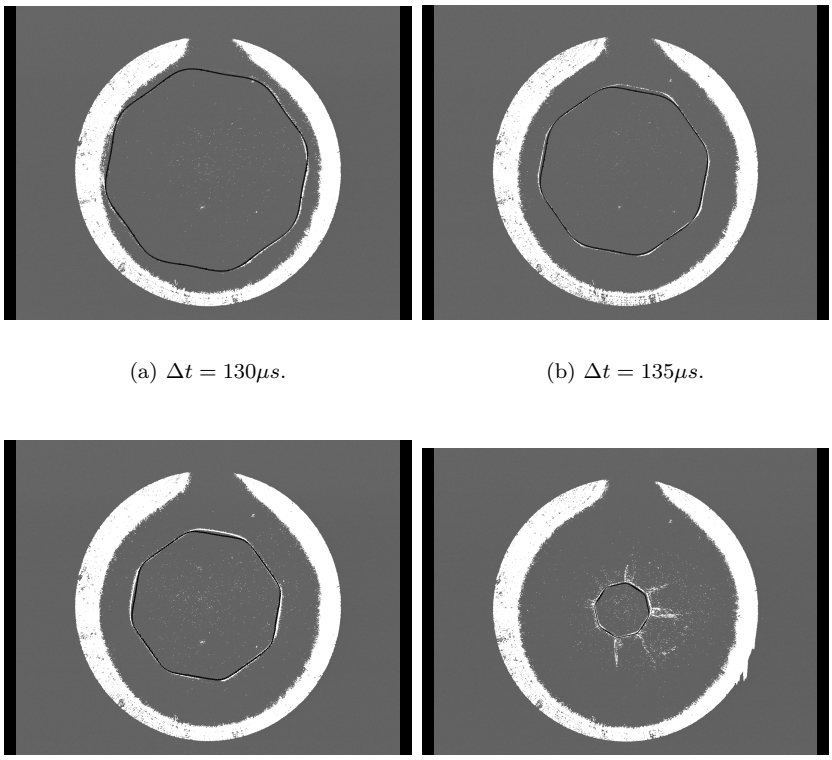

(a) $\Delta t = 130\mu s$. (b) $\Delta t = 135\mu s$.

(c) $\Delta t = 140\mu s$. (d) $\Delta t = 152\mu s$.

FIGURE 17. Comparison of the calculated shockwave profiles with the experimental schlieren images in the chamber with an octagonal boundary for $p_4/p_1 = 33.6$.

(1984). The lower values of the similarity exponent give higher values of the shock acceleration and thus higher velocity as the shock approaches the center of convergence. The calculated values indicate that the most favorable shape in terms of shock velocity and acceleration is the circular one.

There is however another parameter here which influences the converging shock velocity and thus the value of the similarity constant. This parameter is the distance from the inner circular end of the shock tube to the outer boundary of the chamber. For the pentagonal and octagonal case this distance will of course vary around the perimeter. If the distance is small the expansion wave, reflected from the chamber boundary will catch up with the converging shock

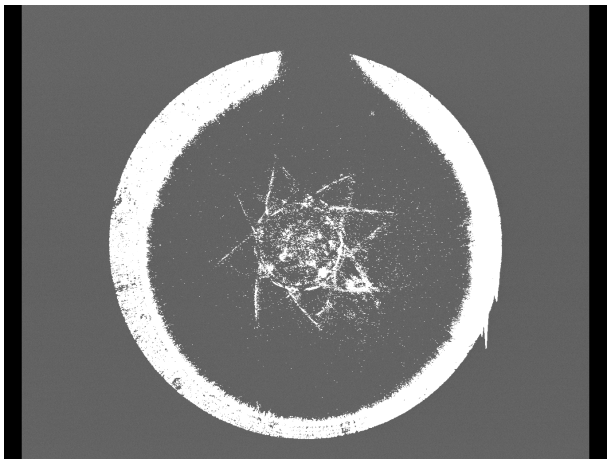

(a) Schlieren photograph of the flow for an outgoing shock

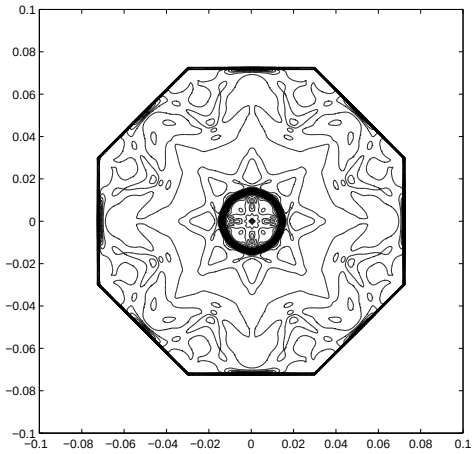

(b) Calculated density gradient contours for at outgoing shock

FIGURE 18. Comparison of the experimental and calculated density gradient profiles for an outgoing shock for $p_4/p_1 = 33.6$ in an octagonal chamber at $\Delta t = 230\mu s$.

and decrease its strength. This property is investigated numerically for the case of a circular boundary and the results are shown in Fig. 19.

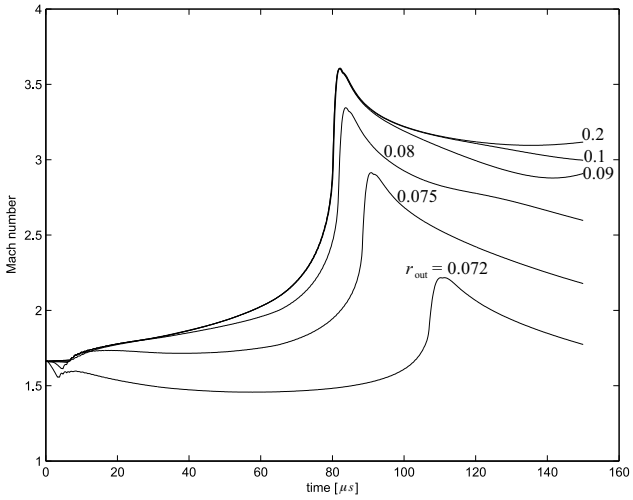

FIGURE 19. Influence of the high pressure zone thickness on the Mach number. The inner radius of the the high pressure zone is $r_{in} = 0.07m$ and the value of the outer radius is marked on each curve.

This figure shows the Mach number of the cylindrical shock as it is approaches the center of the chamber and then transforms to a reflected wave expanding from the center of convergence. The inner circular boundary of the high pressure zone has a fixed radius $r_{in} = 0.07m$ corresponding to the present experimental setup. The Mach number distribution is then calculated for various outer radii starting from $r_{out} = 0.072m$ and up to $r_{out} = 0.2m$. As we can see from the figure, in case of a thinnest zone the strength of the converging shock wave is severely decreased by the reflected expansion wave. This influence, however, decreases rapidly as the thickness of the zone is increased. For $r_{out} = 0.09m$ there is no influence of the reflected expansion wave on the converging shock.

In order to exclude the influence of the reflected expansion wave we have conducted calculations for a configuration with various outer boundaries but the same circular inner boundary and the same area of the high pressure zone for all cases. The results are displayed in Fig. 20. As we can see the maximum Mach number is obtained for a circular form, marked by $n = 0$ in the figure. This maximum is followed by an octagon, hexagon, pentagon and finally a square. As seen the deviation from the rest of the curves is largest for a square

reflector form giving a maximum mach number of $M_{max} = 3.35$ as compared with $M_{max} = 4.24$ for a circular form.

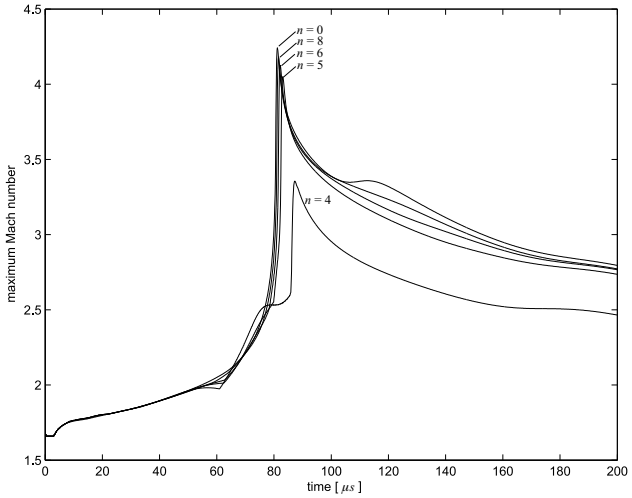

FIGURE 20. Influence of the form of the chamber boundary on the Mach number. Each curve is marked by a corresponding number of the polygon sides of the outer boundary. $n = 0$ corresponds to a circular boundary.

5. Conclusions

A new type of a a horizontal co-axial shock tube was used to investigate the properties of converging and reflected shocks with various initial shapes. The shape of the converging shock was generated by means of the reflector boundary in a thin cylindrical test section mounted at the rear part of the co-axial shock tube. Three various shapes of boundaries have been used in the present study - a circle, an octagon and a smooth pentagon. Numerical calculations have been performed to simulate the three described experimental configurations and the predictions of calculations have been compared with the experimental observations.

We summarize the major results of the present investigation.

(1) The initial form of the converging shock can be tailored by an appropriate choice of the form of the reflector boundary.

(2) The nonlinear dynamics of the shock convergence is observed in the present experimental study. The form of the shock undergoes a transformation from an original octagonal form through a double octagon back to a new octagon with an opposite orientation. This is due to the nonlinear coupling between the form of the shock and the velocity of shock propagation. The above

feature, previously shown only in the numerical simulations is thus confirmed experimentally in the present study. The same type of behavior is observed in the case of a pentagonal reflector boundary.

(3) The final form of the converging shock in the immediate vicinity of the convergence center is square-like for circular and octagonal reflector boundaries. This is believed to stem from the perturbations in the flow due to the set of four supports in the annular portion of the shock tube. The shock strength is increasing as it approaches the center of the cavity and the disturbances in the initial flow are amplified. In the immediate vicinity of the center of convergence the form of the shock is mainly determined by the the disturbances in the flow field. In the present case the shock was observed to obtain a square-like form very close to the convergence center. This is in agreement with the previous experimental studies.

(4) The reflected shock initially has a circular symmetry for all three reflectors. It retains its circular symmetry in the case of the circular reflector. In the case of the octagonal and pentagonal reflector the form of outgoing shock is influenced by the flow field created by the converging shock. In the octagonal case the shock is transformed to an octagon-like form while in the case of a pentagon it attains a pentagon-like shape. This shows the influence of the flow ahead of the shock on the shape of the reflected shock.

(5) The numerical simulation of the flow in the convergence chamber was performed by the numerical solution of the full set of Euler equations. The numerical calculations were based on the artificially upstream flux vector splitting scheme (AUFS), introduced by Sun and Takayama (2003). Several flow parameters obtained from the numerical computations have been compared with the experimental data. The first one is the average radius of the converging and reflected shocks as function of time. The experimental data was obtained from the schlieren images of the shocks. Also the shape of the shock fronts in the test section at various instants of the convergence and reflection processes as well as the density profiles obtained by means of the numerical calculations were compared with the schlieren images. The numerical results were found to be in good agreement with the experimental data and were also able to reproduce the major features of the flow in the chamber. Numerical results indicate further that the maximum Mach number at the center of the chamber is obtained for the circular reflector and is lower for a reflector with a polygonal form, decreasing with the number of sides of a polygon.

6. Acknowledgements

The authors would like to thank Mr Ulf Landén and Mr Marcus Gällstedt at KTH Mechanics for skillful construction of the new shock tube facility. This work has been financially supported by The Swedish Research Council (VR).

This is gratefully acknowledged. The funding from the Göran Gustafsson Foundation provided means for the construction of the shock tube and for acquisition of the experimental equipment which is gratefully acknowledged.

References

Apazidis N, Lesser MB (1996) On generation and convergence of polygonal-shaped shock waves. J. Fluid Mech. **309**: 301-319.

Apazidis N, Lesser MB, Tillmark N, Johansson B. (2002) An experimental and theoretical study of converging polygonal shock waves. Shock waves. **12**: 39-58.

Guderley G (1942) Starke kugelige und zylindrische Verdichtungsstöße in der Nähe des Kugelmittelpunktes bzw. der Zylinderachse. Luftfahrt Forsch, **19**: 302-312.

Mishkin E, Fujimoto Y (1978) Analysis of a cylindrical implodimg shock wave. J. Fluid Mech. **89**: 61-78.

Perry RW , Kantrowitz A (1951) The production and stability of converging shock waves. J. Appl. Phys. **22**: 878-886.

Schwendeman DW , Whitham GB (1987) On converging shock waves. Proc. R. Soc. Lond. A **413**: 297-311.

Sturtevant B , Kulkarny VA (1976) The focusing of weak shock waves. J. Fluid Mech. **73**: 651-671.

Sun M, Takayama K (2003) An artificially upstream flux vector splitting scheme for the Euler equations. J. Comput. Phys. **189**: 305-329.

Takayama K, Onodera O, Hoshizawa Y (1984) Experiments on the stability of converging cylindrical shock waves. Theor. Appl. Mech. **32**: 117-127.

Takayama K, Kleine H, Gröning H (1987) An experimental investigation of the stability of converging cylindrical shock waves in air. Exp. Fluids **5**: 315-322.

Watanabe M, Takayama K (1991) Stability of converging cylindrical shock waves. Shock waves. **1**: 149-160.

Watanabe M, Onodera O, Takayama K (1995) *Shock Waves @ Marseille IV.*,Shock wave focusing in a vertical annular shock tube, Editors Brun R, Dimitrescu LZ. Springer-Verlag, 99-104.

2

Paper 2

The production of strong converging shocks

By Veronica Eliasson

KTH Mechanics, SE-100 44 Stockholm, Sweden

Submitted to *AIP Conference Series*

Converging and reflecting strong shock waves are investigated experimentally in a horizontal co-axial shock tube. The shock tube has a test section mounted at the end of the tube. Two different methods to produce various geometrical shapes of shock waves are tested. In the first method the reflector boundary of the test section is exchangeable and four different reflectors are used: a circle, a smooth pentagon, a heptagon and an octagon. It is shown that the form of the converging shock wave is influenced both by the shape of the reflector boundary and by the nonlinear dynamics between the shape of the shock and the velocity of the shock front. Further, the reflected outgoing shock wave is affected by the shape of the reflector through the flow ahead of the shock front. In the second method we use cylindrical obstacles, placed in the test section at various positions and patterns, to create disturbances in the flow that will shape the shock wave. It is shown that it is possible to shape the shock wave in a desired way with these obstacles. The influence of the supports of the inner body of the co-axial shock tube is also investigated. A square shaped shock wave is observed close to the center of convergence for the circular and octagonal reflectors but not in any other setups. This square-like shape is believed to be caused by the supports for the inner body.

1. Introduction

Shock wave focusing has been investigated experimentally since the beginning of the 1950's. Still, it's an interesting research area with unsolved questions. High pressures and temperatures may be achieved in a region of gas compressed by a converging shock wave. This feature in connection with various technological applications, ranging from investigation of cavitation damage near material surfaces to applications in medicine and drug industry, is one of the main reasons for continuing interest in the problem of shock focusing. The highly nonlinear nature of the process presents a major challenge to its study. At the same time it serves as a source of the non-triviality of this phenomenon. Two aspects of a converging shock are of special interest. The first one being the connection between the local strength of the shock and the shape evolution of

the converging shock front. The second issue, which is however closely related to the first one is the question of the stability of converging shocks.

Further, a cylindrical shock wave is very sensitive to disturbances and will change its form when encountering a disturbance. Takayama K. *et al.* (1984), Takayama K. *et al.* (1987) and Watanabe M. & Takayama K. (1991) studied cylindrical shock wave focusing in horizontal annular shock tubes. An interesting discovery was the formation of triangular or square formed shocks when the shock reached the final stage of focusing. This disturbance was found to be introduced by the number of supports (3 or 4) for the annular part of the shock tube. To create shock waves without disturbances Watanabe M. *et al.* (1995) used a vertical co-axial shock tube without supports. The results showed that cylindrical shocks converged more uniformly than in horizontal shock tubes, used in previous studies.

Analytical and numerical results from Schwendeman D.W. & Whitham G.B. (1987) showed that if an n-gonal shaped shock wave is formed it will repeat itself during the focusing process. This was confirmed numerically by Apazidis N. & Lesser M.B. (1996) and Apazidis N. *et al.* (2002) for a smooth pentagonal converging shock wave.

In the present study we investigate experimentally the focusing and reflection of strong shocks. The experiments were performed in a new shock tube facility at the department of Mechanics, KTH. The shock tube is a horizontal co-axial tube. A plane shock wave transforms into an annular shape and is then focused and reflected in the test section mounted at the end of the tube. The outer boundary of the test section is exchangeable and various geometrical shapes of the reflector can be chosen.

We apply two different methods to create various geometrical shapes of shock waves. In the first method we choose a specific shape of the outer boundary of the test section. Four boundaries with various shapes have been tested in these experiments: a circular, a smooth pentagonal, a heptagonal and an octagonal boundary. In the second method cylindrical obstacles are placed in the test section. We use cylinders of different sizes, placed at various positions and patterns. These cylinders create disturbances in the flow and make it possible to shape the shock wave in a desired way.

The experimental setup consists of a laser (the light source), a horizontal shock tube and a schlieren optics system. The shock tube has a test section where shock waves are focused and reflected. The process is visualized by the schlieren system with a camera. The experimental setup is shown in Fig. 1.

1.1. *The shock tube*

The 2.4 m long circular shock tube (with diameter $d = 80$ mm) consists of a high pressure part and a low pressure part separated by a 0.5 mm thick aluminum membrane. A schematic illustration of the shock tube and its main

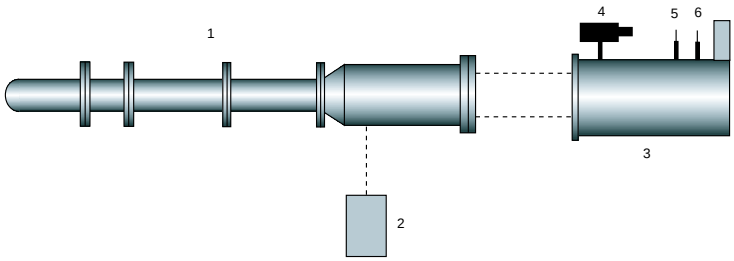

FIGURE 1. Schematic overview of the experimental setup: 1. Shock tube, 2. Pulse laser, 3. Schlieren optics, 4. PCO CCD camera, 5. Lens, 6. Schlieren edge.

parts is shown in Fig. 2. The first step to create a shock wave is to evacuate the low pressure part of gas. Then the high pressure part is filled with gas and at a certain pressure difference between the two parts the membrane bursts and a shock wave is formed. To control the membrane opening, a knife cross is placed at the inlet of the low pressure part. The knife-cross helps the membrane to open evenly. The shock wave becomes planar in the inlet section of the low pressure part, then enters the transformation section and becomes annular. This is done by a conically diverging section where the diameter increases from

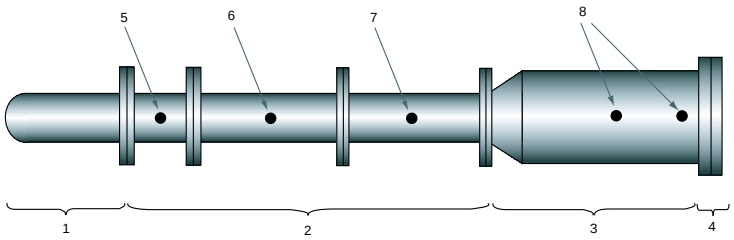

FIGURE 2. Schematic overview of the shock tube setup: 1. High pressure part, 2. Low pressure part: inlet section, 3. Low pressure part: transformation section, 4. Low pressure part: test section, 5. Low pressure sensor, 6. Vacuum valve, 7. Vacuum pump, 8. Shock speed sensors.

80 mm to 160 mm. The cross-section area is constant from the inlet section through the transformation section. An inner body is mounted coaxially in the interior of the outer tube, forming the annular section. The 490 mm long inner body (d =140 mm) is mounted with two sets of four supports. The supports are shaped as wing profiles in order to minimize the disturbances in the flow. The second set of supports is angularly displaced 45° relative to the first set. The plane test section is mounted directly at the end of the annular section. Hence, the shock wave enters the test section via a sharp 90° bend and the

focusing and reflection process begins. The outer boundary of the test section is exchangeable and various geometrical shapes of the reflector can be chosen. In the present study four reflectors have been used: a circle, a pentagon, a heptagon and an octagon.

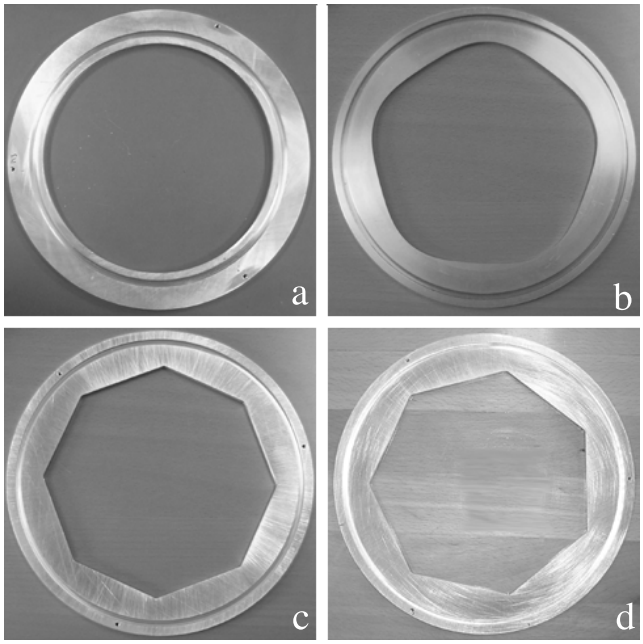

FIGURE 3. The four reflectors used in the present experiment.

The present experiments uses air as gas in both the high and low pressure part of the tube. The pressure in the low pressure part is 13.3 kPa and in the high pressure part about 1500 kPa. This produces strong shocks at Mach number 2.3.

2. Experimental Results

The present experimental setup allows only one photograph per run in the shock tube. The visualization process is made by a schlieren system with a CCD camera (SensiCam, 12 bits, 1280 x 1024 pixels, pixel size 6.7 x 6.7 $\cdot 10^{-6}$m, CCD). The light source consists of an Nd:Yag (NewWave Orion) laser with single shot operation. The focusing and reflection process is resolved in time by single exposures taken at different time delays. The camera and the light source are triggered by sensors placed at the annular part of the shock tube and a time delay unit (Stanford Research System, DG 535) is used to take the photo at the predetermined position.

Typical sets of images of the converging and reflection process are seen in Fig. 5 and Fig. 4.

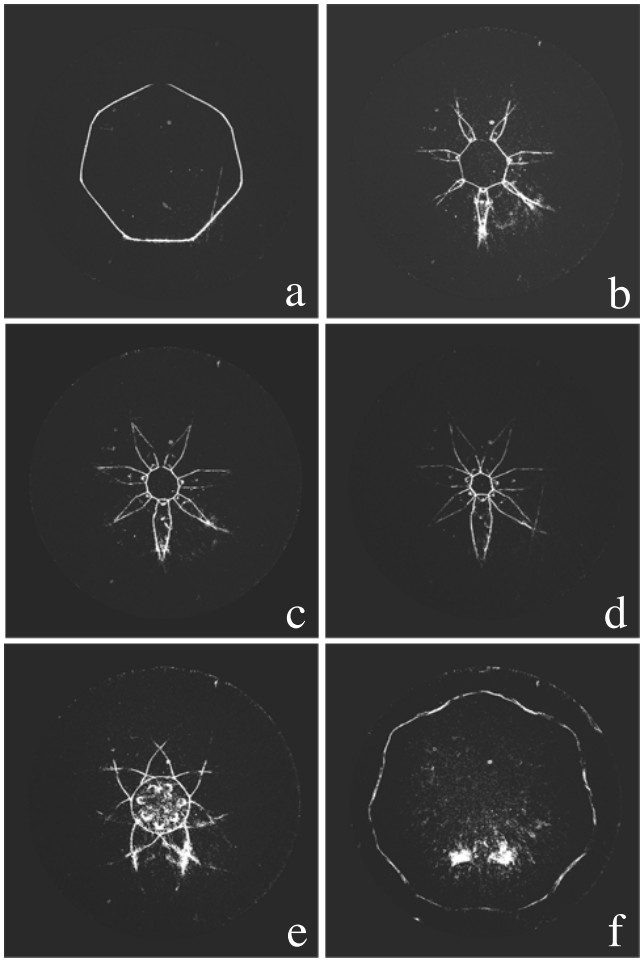

FIGURE 4. Shock waves created with the heptagonal reflector boundary. The time difference between the first and the last schlieren photograph is $75 \cdot 10^{-6} s$.

A series of schlieren photographs with the heptagonal reflector boundary is shown in Fig. 5. At first a heptagonal shock wave, oriented in the same direction as the reflector boundary, is created, see Fig. 5(a). Then it transforms into a double-heptagon and back to a heptagonal shock wave but oriented opposite to the former one, i.e. the corners have developed into plane sides and the plane sides into corners, see Fig. 5(b). This procedure continues during the

whole convergence process. When the shock wave starts to reflect it first has a circular shape. After a while it transforms into a heptagonal shape since it is influenced by the flow ahead of the shock front.

In Fig. 4 the octagonal reflector is used. At first an octagonal shaped shock wave is created, Fig. 4(a). It then transforms into a double-octagon and then back again to an octagon. This time it is oriented opposite to the initial shape, see Fig. 4(b). This was earlier predicted by Apazidis N. & Lesser M.B. (1996) and Schwendeman D.W. & Whitham G.B. (1987) using numerical analysis. It is due to the nonlinear coupling between the shape of the shock wave and the velocity of the shock propagation that causes this behavior. Regions with high curvature travel faster than the plane parts of the shock which leads to the reconfiguring and reorientation process. The reflected shock wave is at first circular, Fig. 4(c), but after some time it is influenced by the flow ahead of it and transforms into an octagonal shape again.

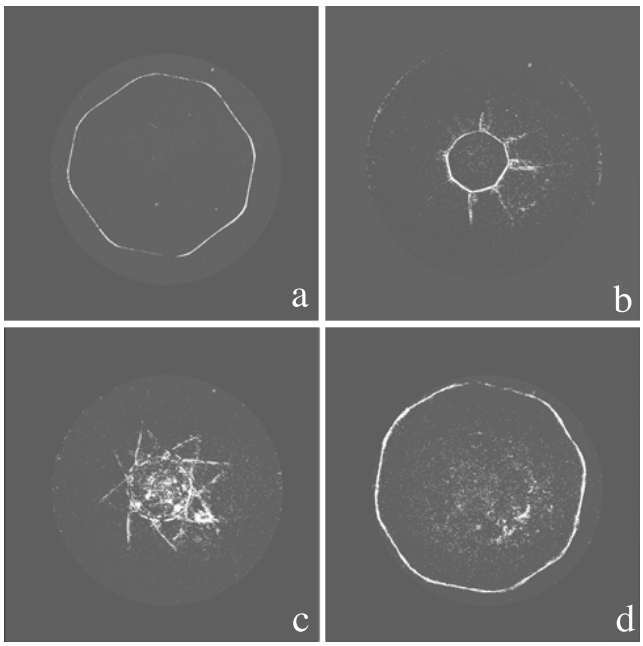

FIGURE 5. Shock waves created with the octagonal reflector boundary, (a)-(b) are converging and (c)-(d) are diverging. The time difference between (a) and (d) is $85 \cdot 10^{-6} s$.

The second method to shape the shock wave is to place cylindrical obstacles in a specific pattern in the test section. The cylinders create disturbances in the flow and hence it is possible to shape the shock wave in a desired way. A circular reflector boundary is used in this case. In Fig. 6 we show the result

when 8 cylinders (d = 15 mm) are placed in an octagonal pattern at radial position r = 46 mm. At first the shock wave obtains an octagonal shape with sides that are convex forward, Fig. 6(a). Then the sides get plane and the shock transforms into a double-octagon Fig. 6(b) and back to an octagonal shape which is reoriented, Fig. 6(c). In Fig. 6(d) the shape of the reflected shock wave is circular.

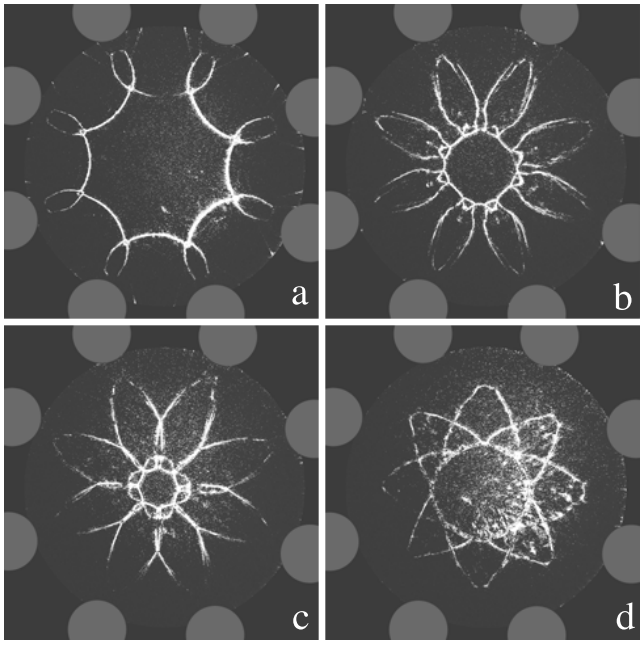

FIGURE 6. Schlieren photographs of shock waves at different time instants passing eight cylinders, (d=15 mm). The filled grey circles show the positions for the cylindrical obstacles. (a)-(b) are converging and (c)-(d) are reflecting. The time difference between (a) and (d) is $60 \cdot 10^{-6} s$.

The influence of the supports for the inner body is investigated. At first two of the downstream supports where tilted so that they occupied a larger cross-section area. This resulted in a non-symmetrical square shaped shock wave close to the vicinity of the center of convergence. Then the supports where tilted back in their original position to minimize the disturbances in the flow field. The square shaped shock was still present but this time its form was more symmetrical than before. Schlieren photographs of the square shaped shock waves are shown in Fig. 7. In Fig. 7(a) and (b) the circular reflector boundary is used and in Fig. 7(c) and (d) the octagonal reflector boundary is used. In (a) and (c) the supports are tilted and in (b) and (d) they are in original

position. The square shaped shock wave is only observed for the circular and octagonal reflectors and not for the pentagonal and the heptagonal reflectors. For the pentagonal and the heptagonal reflectors the shock wave follows the procedure of transforming and reconfiguring as long as we can see it.

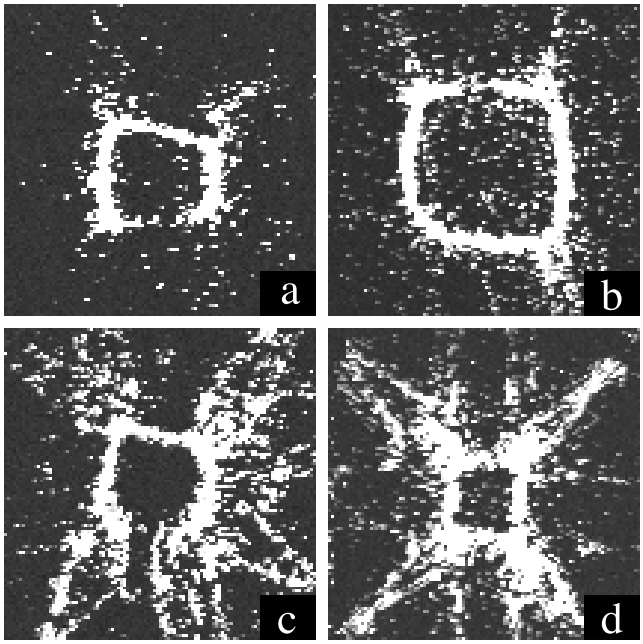

FIGURE 7. Square shaped shock waves close to the vicinity of the center of convergence. The square shaped shock is due to the supports for the inner body. The circular reflector is used for (a) and (b) and an octagonal reflector for (c) and (d).

3. Conclusions

We summarize the major results as follows:

(1) The initial form of the converging shock can be tailored by an appropriate choice of the form of the reflector boundary or by introducing obstacles in a specific pattern in the flow.

(2) The nonlinear dynamics of the shock convergence is observed in the present experimental study. The form of the shock undergoes a transformation from an original heptagonal form through a double-heptagon back to a new heptagon with an opposite orientation. This behavior is also observed when the outer boundary is octagonal and pentagonal and also for the case when 8 cylindrical obstacles are introduced in the flow.

(3) The final form of the converging shock is square-like for the case when a circular and octagonal reflector is used. The square like shape is believed to be caused by the supports for the inner body of the co-axial shock tube. It is not observed for the pentagonal or heptagonal reflectors. The artificially introduced disturbances are stronger than the disturbances caused by the four supports for the inner body since the previously observed square-like shape no longer exists, i.e. the octagonal shaped shock wave, created by the eight obstacles, is visible until the shock wave converges.

(4) The reflected shock initially has a circular symmetry for all four reflectors. It retains its circular symmetry in the case of the circular reflector. For the three other reflectors (pentagonal, heptagonal and octagonal) the form of the outgoing shock is influenced by the flow field created by the converging shock. This shows the influence of the flow ahead of the shock on the shape of the reflected shock. This behavior is observed when different reflector boundaries are used and not when obstacles are present in the flow. The reason for this is that no photographs where taken with a large time delay for the case with obstacles.

Acknowledgments

The author would like to thank Dr Nicholas Apazidis, Dr Nils Tillmark and Prof. Martin Lesser for valuable comments and ideas. 21st Century COE of Flow Dynamics is acknowledged for the invitation and financial support for ICFD2005.

References

Apazidis N. & Lesser M.B. (1996) On generation and convergence of polygonal-shaped shock waves. J. Fluid Mech. **309**: 301-319.

Apazidis N., Lesser M.B., Tillmark N. & Johansson B. (2002) An experimental and theoretical study of converging polygonal shock waves. Shock waves. **12**: 39-58.

Schwendeman D.W. & Whitham G.B. (1987) On converging shock waves. Proc. R. Soc. Lond. A **413**: 297-311.

Takayama K., Onodera O. & Hoshizawa Y. (1984) Experiments on the stability of converging cylindrical shock waves. Theor. Appl. Mech. **32**: 117-127.

Takayama K., Kleine H. & Gröning H. (1987) An experimental investigation of the stability of converging cylindrical shock waves in air. Exp. Fluids **5**: 315-322.

Watanabe M. & Takayama K. (1991) Stability of converging cylindrical shock waves. *Shock waves.* **1**: 149-160.

Watanabe M., Onodera O., &Takayama K. (1995) *Shock Waves @ Marseille IV.*, Shock wave focusing in a vertical annular shock tube, Editors Brun R. & Dimitrescu L.Z. Springer-Verlag, 99-104.

3

Paper 3

Controlling the form of strong converging shocks by means of disturbances

By V. Eliasson, N. Apazidis and N. Tillmark

KTH Mechanics, SE-100 44 Stockholm, Sweden

To be submitted

Influence of artificially introduced disturbances on the behavior of strong converging circular shocks is investigated experimentally and numerically. Cylindrical shocks are generated in a shock tube with an annular section and focused in a test section, a thin chamber mounted at the end of the section. Cylindrical objects, causing disturbances in the flow are placed at different locations and in various patterns in the test section. Their influence on the convergence and reflection process is investigated. It is found that disturbances arranged in a symmetrical pattern will produce a converging shock with a symmetric shape. For example a square formation will produce a square-like shock and an octagon formation a shock with an octagonal boundary. This introduces an alternative way of tailoring the form of a converging shock instead of using a specific form of a reflector boundary. Influence of disturbances arranged in non-symmetric patterns on the flow is also investigated.

1. Introduction

Focusing of shock waves can be used to generate high temperatures and pressures. This together with many technological applications is one of the main reason for continuing research in this area. A challenging problem in shock wave focusing is to produce focusing without disturbances in the flow. It is known that a cylindrical shock wave is very sensitive to perturbations and will change its form when encountering a disturbance. It is therefore important to have knowledge of the influence of disturbances on the process of shock convergence and reflection. The influence of obstacles on the flow is closely related to two interesting problems. The first problem being the relation between the shape and the local strength of the shock front, i.e. parts of the shock with a high curvature will travel faster than the plane parts and this will lead to a transformation and reorientation of the shock. The second problem concerns with the stability of the converging shock.

A classic example where a shock wave is passing an obstacle is diffraction over various objects. Bryson and Gross (1960) investigated diffraction of plane

strong shocks by cones, a cylinder and a sphere. Detailed schlieren photographs of the diffraction shows the regular reflection, Mach reflections, vortexes, triple points and the interconnection of these features. Bryson and Gross compared experimental results with Whitham's theory (1957, 1958, 1959) to a good agreement.

Takayama *et al.* (1984) used a horizontal shock tube and introduced disturbances in the flow in the form of rods with three different diameters. Experiments showed that the disturbance behind the shock front was more significant when rods with larger diameter where used. The shock tube was equipped with supports for the inner body and a so called mode 4 instability was observed, even in the case when large artificial disturbances where introduced in the flow.

In 1987 Takayama *et al.* used two different annular horizontal shock tubes to produce converging shock waves. Both shock tubes where equipped with n supports of the inner body and hence an n-mode instability, depending on the n supports, was observed during the convergence process. To test the influence of an initial disturbance 12 cylindrical rods where placed in the test section in one of the shock tubes (which had 4 supports for the inner body). At first the shock front was deformed by the rods but when the shock wave approached the center of convergence the 4-mode appeared again. It was concluded that it was not possible to suppress the disturbance caused by the supports by adding artificial disturbances.

Schwendeman and Whitham (1987) used the approximate theory of Whitham (1957), (geometrical shock dynamics), to study the behavior of converging cylindrical shocks. They showed that a regular polygon will keep reconfiguring with successive intervals and that the shock Mach number will increase exactly as that for a circular converging shock. They also showed that perturbed polygonal shaped shock waves, with smooth corners as well as without plane sides, first form plane sides and sharp corners. Then the shock wave starts to reconfigure until it reaches the center of convergence and starts to reflect. This behavior was later confirmed by Apazidis & Lesser (1996) and Apazidis *et al.* (2002) for a smooth pentagonal converging shock wave.

Watanabe *et al.* (1995) used a vertical annular shock tube without supports for the inner body to produce cylindrical converging shock waves. The results showed that the cylindrical shock waves tend to keep their form more uniformly than in horizontal shock tubes with supports. Still, when the shock wave reached the center of convergence it was not perfectly cylindrical. This was believed to be caused by small changes of the area in the co-axial channel between the inner and outer body of the shock tube. Watanabe *et al.* placed cylindrical rods upstream of the test section. Using different combinations of the number of rods they observed that smaller mode number disturbances were stronger than higher mode numbers.

In a previous paper by Eliasson *et al.* (2005) strong shock waves of various shapes where produced by changing the outer boundary of the test section in the horizontal annular shock tube. For the first time it was experimentally confirmed that octagonal and pentagonal converging shock waves will reorient and repeat themselves during the focusing process. This is due to the non-linear dynamics of the shock propagation and stems from the fact that portions of the shock with high curvature move faster than the plane sides. The shock wave will reorient itself when corners transform into plane sides and the plane sides into corners.

In this paper a new way of producing converging shock waves of various forms is investigated. Using the same shock tube as in Eliasson *et al.* (2005) but instead of changing the shape of the outer boundary of the test section cylindrical rods are placed in the inner of test section. The rods are placed in a number of various positions and patterns. The cylindrical rods create disturbances in the flow so that it is possible to shape the shock in a desired way. The present experiments investigate how the focusing and reflection process of a shock wave is influenced by introducing disturbances in the flow field. Numerical calculations are based on the artificially upstream vector splitting scheme (AUFS) for Euler equations introduced by Sun and Takayama (2003). The calculations are compared to experimental results and show good agreement.

The rest of this paper is organized as follows, in section 2 the experimental setup, consisting of the shock tube setup, the visualization technique and the artificial disturbances, is explained. In section 3 the experimental results are presented and in 4 the numerical results are showed and compared to experimental results. In section 5 we conclude and summarize the main results of the present study.

2. Experimental setup

The experimental setup consists of a laser (the light source), a horizontal shock tube and a schlieren optics system. The shock tube has a test section where shock waves are focused and reflected. The process is visualized by the schlieren system with a camera. The experimental setup is shown in Fig. 1.

2.1. *The shock tube*

The 2.4 m long circular shock tube with a diameter of 80 mm consists of a high pressure part and a low pressure part separated by a 0.5 mm aluminum membrane. A schematic illustration of the shock tube and its main parts is shown in Fig. 2. The first step to create a shock wave is to evacuate the low pressure part from air. Then the high pressure part is filled with gas and at a certain pressure difference between the two parts the membrane bursts and a shock wave is formed. To control the membrane opening, a knife-cross is placed at the inlet of the low pressure part. The knife-cross helps the membrane to

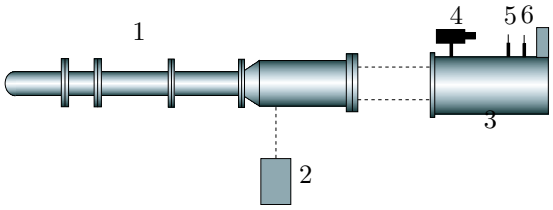

FIGURE 1. Schematic overview of the experimental setup: 1. Shock tube, 2. Pulse laser, 3. Schlieren optics, 4. PCO CCD camera, 5. Lens, 6. Schlieren edge.

open evenly. The shock wave becomes planar in the inlet section of the low pressure part, then enters the transformation section and becomes annular.

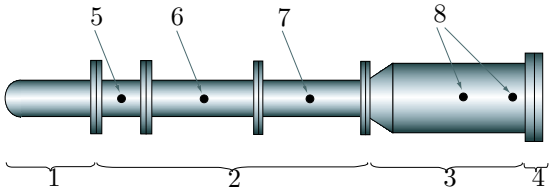

FIGURE 2. Schematic overview of the shock tube setup: 1. High pressure part, 2. Low pressure part: inlet section, 3. Low pressure part: transformation section, 4. Low pressure part: test section, 5. Low pressure sensor, 6. Vacuum valve, 7. Vacuum pump, 8. Shock speed sensors.

This is achieved by a conically diverging section where the diameter increases from 80 mm to 160 mm, see Fig. 3. The cross-section area is kept constant from the inlet section through the transformation section. An inner body is mounted coaxially in the interior of the outer tube, forming the annular section. The 490 mm long inner body with a diameter of 140 mm is mounted with two sets of four supports. The supports are shaped as wing profiles in order to minimize the disturbances in the flow. The second set of supports is angularly displaced 45° relative to the first set. The plane test section is mounted directly at the end of the annular section. Hence, the shock wave enters the test section via a sharp 90° bend and the focusing and reflection process begins. The gap between the two facing glass windows in the test section is 5 *mm* and therefore the cross section area is half of that in the annular part. The outer boundary of the test section is circular throughout all experiments. The present experimental study uses air as gas in both the high and low pressure part of the tube. The pressure in the low pressure part is 13.3 kPa and in the high pressure part about 1500 kPa. This pressure difference produces strong shocks at Mach number 2.3.

The shock speed, U_s, is measured by sensors placed in the annular section. The temperature jump from the passage of the shock wave triggers the sensors and the accuracy of the shock speed estimations is within 0.5%.

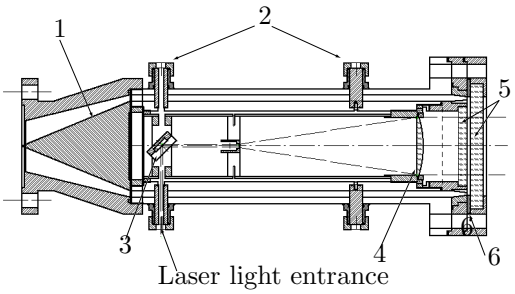

FIGURE 3. The annular part of the shock tube: 1. Inner body with a cone, 2. Supports, 3. Mirror, 4. Lens, 5. Glass windows for visualization, 6. Test section where the cylindrical rods are positioned.

2.2. *The shock visualization*

A Nd:Yag (NewWave Orion) laser that provides single shot operation, with 5 ns long light pulses is used as a light source for the schlieren optics. The laser is mounted outside the shock tube and the light beam enters the shock tube perpendicular to its axis. The light beam is then deflected in the axial direction by a mirror placed in the inner body, see Fig. 3. To damp spurious reflections inside the inner body the walls are coated with non-reflective material. To produce a parallel light for the schlieren optics an adjustable beam expander is placed inside the inner body. The parallel light passes through the test section and is then focused by the schlieren optics. A pin head with a diameter of 1.0 mm is used as schlieren edge. It intercepts parts of the light before it reaches the camera (SensiCam, 12 bits, 1280 x 1024 pixels, pixel size 6.7 x 6.7 μm, CCD). The camera and the laser are triggered by the same signal from the shock speed sensors. A delay unit (Stanford Research System, DG535) is used to delay the signal with a predetermined value to take images at different positions in the test section.

2.3. *Artificial disturbances*

Disturbances in the flow field were produced by 1-16 cylinders with three different diameters; 7.5, 10 and 15 mm. The cylinders were arranged in various patterns and at various positions in the test section. The cylinders were placed at two radial positions, $r_1 = 46.25$ mm and $r_2 = 66.25$ mm in both regular and irregular patterns using a template with holes in as shown in Fig. 4 (a).

In Fig. 4 (b) an example were 16 cylinders with diameters of 10 mm or 15 mm are placed in a circle with $r = r_1$.

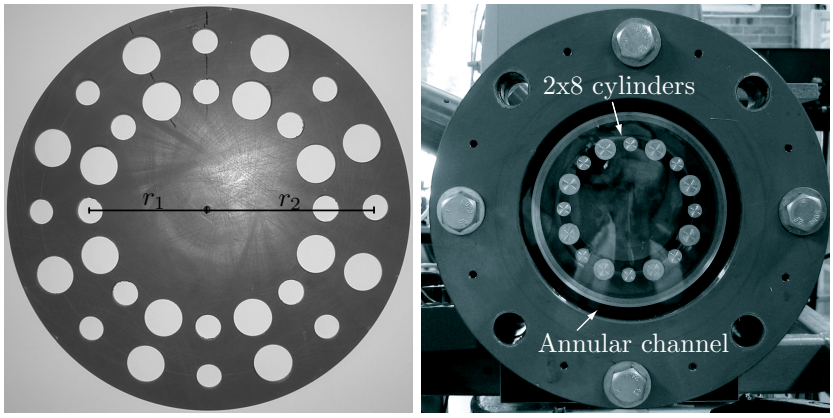

(a) (b)

FIGURE 4. (a) Template for cylinder positioning, $r_1 = 46.25$ mm and $r_2 = 66.25$ mm. (b) Rear part of the shock tube with 2x8 cylinders placed in the test section at $r = r_1$.

3. Experimental Results

It has been verified by cold wire measurements that the temperature in the shock tube is constant one minute after the evacuation of air from the low pressure part is completed. Hence the speed of sound in the low pressure part is known and thus the Mach number of the shock wave. A plot of the temperature as a function of time during the evacuation phase can be found in Fig. 5. Before the first peak (I), the pressure is 100 mm Hg in the low pressure part. Then air is let in at (II). At (III) the vacuum pump is started and air is evacuated and when the pressure in the low pressure part reaches 100 mm Hg the pump is shut down (IV).

A cylindrical shock wave is disturbed by placing cylindrical obstacles in the flow. The disturbed shock wave tends to produce plane sides and corners. Results show that a regular pattern of disturbances produces a regular shock wave with plane sides and corners which will repeat its shape in successive intervals. It is possible to create shock waves of various shapes, for example octagons, by using obstacles. The results agree with earlier analytical, numerical and experimental results obtained by Schwendeman *et al.* (1987), Apazidis *et al.* (2002) and Eliasson *et al.* (2005). These investigations show that regular polygonal

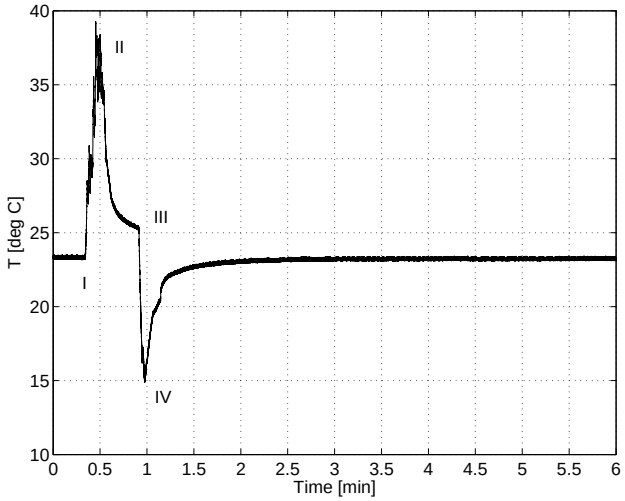

FIGURE 5. Measurements of the temperature in the low pressure part during evacuation.

shock waves will repeat their form in successive intervals. The disturbance on the shock wave depends on the size of the obstacle. Cylinders with a larger diameter give more significant disturbances. This agrees with the results of Takayama *et al.* (1987). The obstacle will also delay the parts of the shock wave after interaction. Due to restrictions in the experimental equipment it is only possible to take one photograph per run in the shock tube in the present study.

We start by placing a single cylinder with a diameter of 15 mm at $r_1 = 46.25$ mm. In Fig. 6 a schlieren photograph shows the converging shock wave after the passage of the single cylinder. A reflected shock wave (RC) is created when the converging shock hits the cylinder. Mach shocks and the triple point (TP) between these and the converging shock (CS) are seen in Fig. 6. Comparison with photographs from Bryson and Gross (1960) showing diffraction on a cylinder by a plane shock wave illustrate similar behavior. The major difference is the shape of the incoming, reflected and converging shock wave. Photographs of the converging shock wave at different time instants are taken and displayed in the same figure in Fig. 7. Here it is possible to compare the position of the different parts of the shock.

Two cylindrical obstacles with diameters of 15 mm are placed at $r_1 = 46.25$ mm opposite each other. Several images of the converging process are taken and shown in the same figure in Fig. 8. Here it is clearly seen that the shock wave is delayed when passing over an obstacle. The time delay, denoted

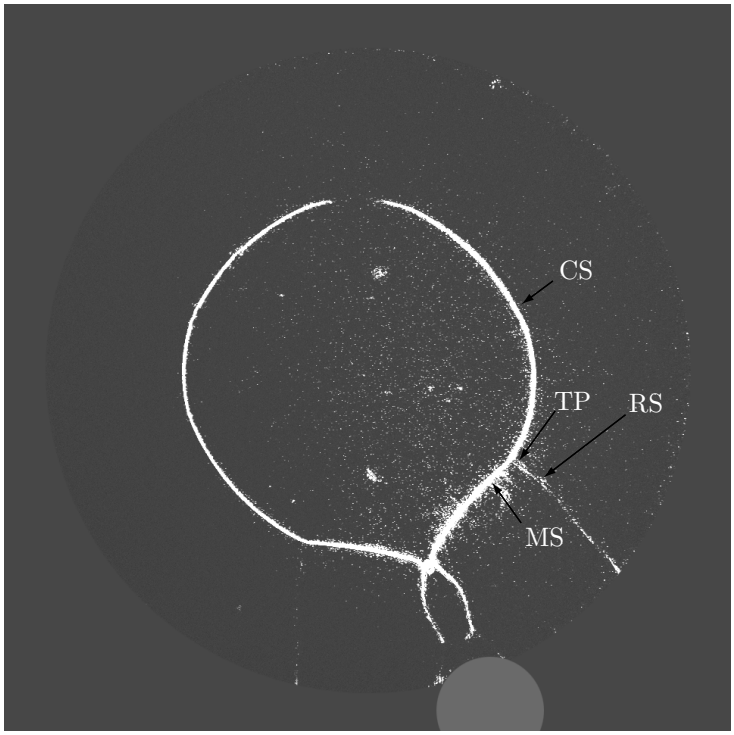

FIGURE 6. Schlieren photograph of a shock wave passing a single cylinder, (ϕ=15 mm). M_S=3.2. CS, converging cylindrical shock, RS, reflected shock from the cylinder, MS, Mach shock and TP, tripple point. The filled grey circle show the position of the cylindrical obstacle.

Δt, is the time from the instant when the shock passes the second sensor to the moment when the photograph is taken. Perry and Kantrowitz (1951) noted that the center of a shock wave which passed over an obstacle was shifted toward the disturbed side. This asymmetry is also observed in the present study, see Fig. 8.

To compare the effect of the size of the diameter on the shock shape, one of the two cylinders was replaced by a smaller one, with a diameter of 7.5 mm. Four different time instants are shown in Fig. 9. It is now possible to see how the diameter of the cylinder affects the shock wave. Behind the smaller cylinder a second Mach shock and triple point is visible. This could also be seen in the schlieren photographs of diffraction over a cylinder from Bryson and Gross (1960) when the incoming shock wave had passed about 0.5 to 1.0 diameters

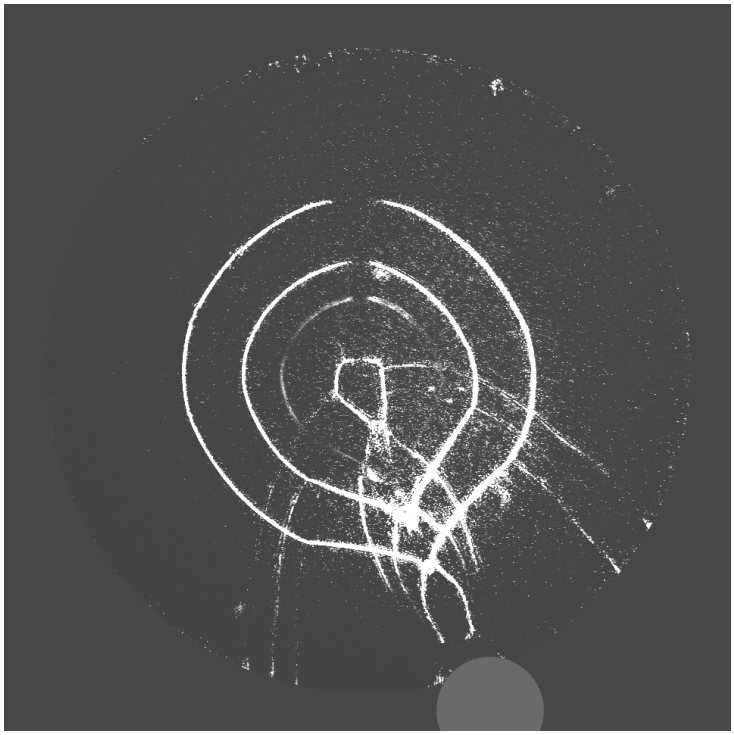

FIGURE 7. Schlieren photograph of four shock waves at different time instants passing a single cylinder, (ϕ=15 mm). M_S=3.2. The filled grey circle show the position of the cylindrical obstacle.

behind the cylinder. The second Mach shock results from the collision between the first two Mach shocks.

Three cylindrical obstacles, with diameters of 15 mm, are placed at $r_1 =$ 46.25 mm with an angle of 90° between each other. Several images of the converging process are taken and shown in the same figure in Fig. 10. Plane sides are developing after the shock wave has passed the obstacles. The original circular shape is lost even for the undisturbed side when the shock wave approaches the center. It is also seen that the undisturbed part of the shock travels faster than the disturbed one.

To create square like shock waves four cylinders, with diameters of 15 mm, are placed at $r_1 = 46.25$ mm at the corners of a square formation. Schlieren images of the converging process at different time instants are shown in Fig. 11. At first eight sides, which are convex forward, are forming an octagon with

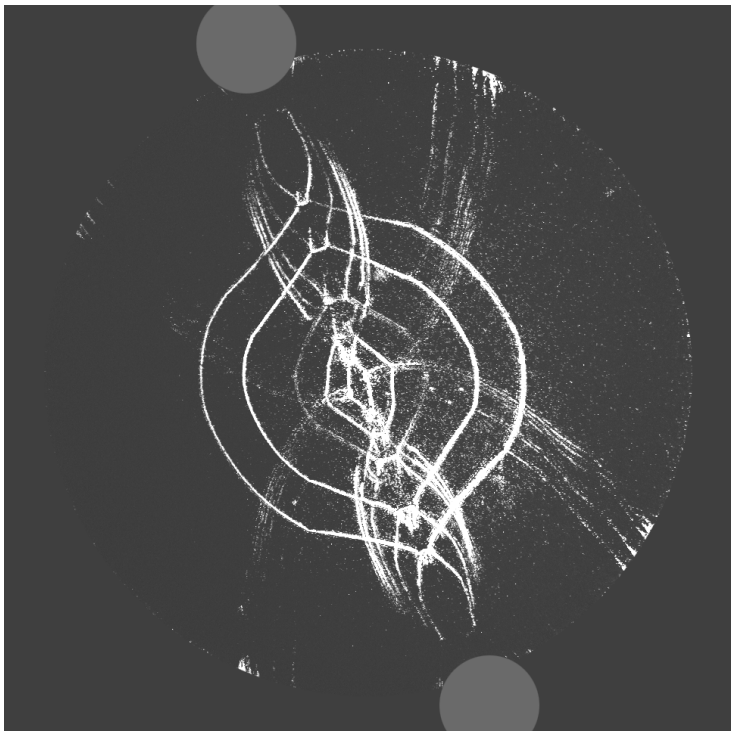

FIGURE 8. Schlieren photograph of converging shock waves at five different instants. Two cylindrical obstacles with diameters of 15 mm are placed opposite each other. The filled grey circles show the positions of the cylindrical obstacles.

square-like shape. As the shock wave approaches the center the sides get plane and the octagon is replaced by a square.

Fig. 12 shows the deviation of the radius of the shock wave normalized with the mean radius for Δt=200 μs, Δt=205 μs, Δt=210 μs and Δt=215 μs for the case with four cylindrical obstacles. In the first frame, Δt=200 μs, eight sides are seen forming a slightly disturbed octagonal shape. At a later moment the shock wave sides become more planar.

Eight cylinders, with diameters of 15 mm, are placed at $r_1 = 46.25$ mm in an octagonal pattern to create octagonally shaped shock waves. At first the shock wave becomes octagonal, Fig. 13(a), (b) and then it transforms into an double octagon Fig. 13(c). After some time the shock wave transforms back to an octagon again Fig. 13(d). The second octagonally shaped shock wave is oriented opposite with respect to the first one. Photographs of the reflected shock wave Fig. 13(f), (g) show that a circular shape is obtained in the

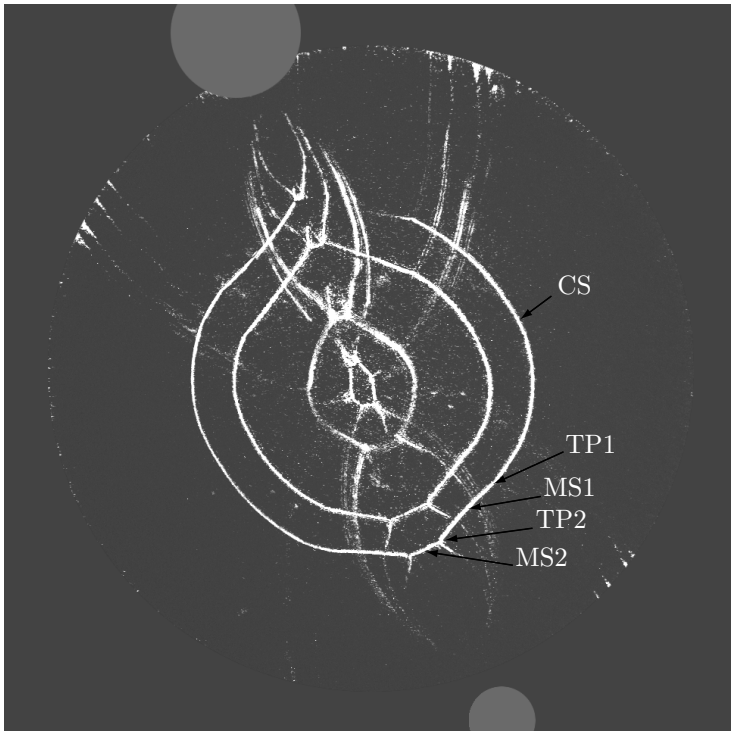

FIGURE 9. Schlieren photograph of four shock waves at different time instants passing two cylinders, (ϕ=15 mm and 7.5 mm). M_S=3.2. CS, converging cylindrical shock, RS, reflected shock from the cylinder, MS, Mach shock and TP, triple point. The filled grey circles show the positions of the cylindrical obstacles.

early stages of the reflection process. It is known from the earlier experiments (Eliasson *et al.* (2005)) the shock will later be influenced by the incoming flow and resume an octagonal shape.

To investigate the influence of the size of cylindrical object for a more complicated pattern eight cylinders with diameters of 15 mm and eight cylinders with diameters of 10 mm where placed in two symmetric octagonal patterns, see Fig. 14. At first the influence from all 16 cylinders is present. The shock wave consists of 16 concave sides but with the shape of an octagon. When the shock wave is approaching the center the disturbances from the larger cylinders overtake the disturbances created by the smaller ones and again an octagonally shaped shock wave with plane sides is formed.

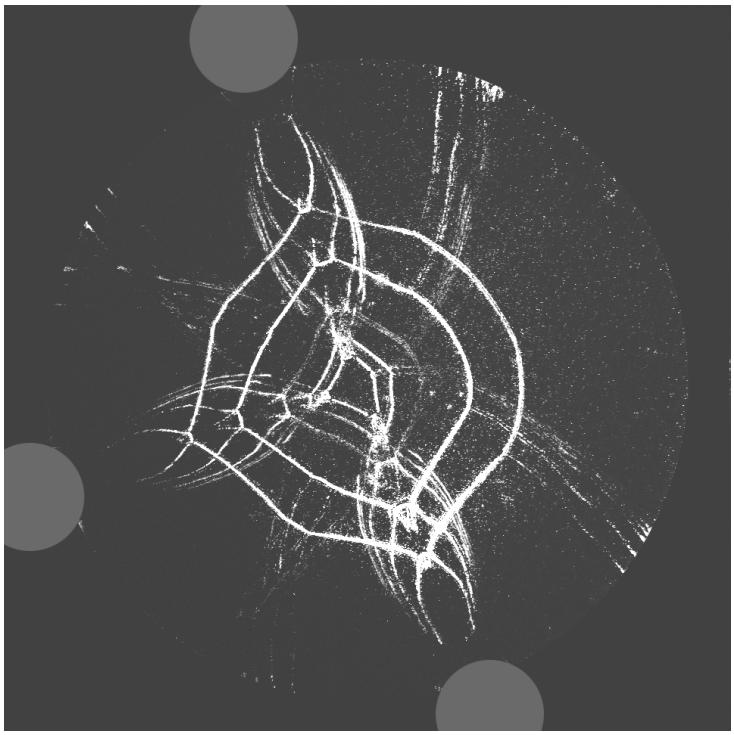

FIGURE 10. Schlieren photographs of five shock waves at different time instants passing three cylinders, with diameters of 15 mm. The filled grey circles show the positions of the cylindrical obstacles.

By placing many obstacles close to each other and leaving the rest of the test section free it was possible to see that the disturbed part of the shock was delayed. Three cylinders with diameters of 15 mm, 2 cylinders with diameters of 10 mm where placed at $r_1 = 46.25$ mm and 3 cylinders with with diameters of 7.5 mm at $r_2 = 66.25$ mm, see Fig. 15. The smallest cylinders where placed at the same angular position as the largest cylinders and are not seen in the figure.

By finding the edges of each shock wave from the schlieren images and calculating a center based on these edges it is possible to see how much the center is shifted for the individual shock wave. For each shock wave the calculated center positions are placed at the same point, a common origin, and then displayed in the same figure as the schlieren photographs of the shock waves, see Fig. 16. If there was no shift of the center of the shock wave, the calculated edges and the schlieren image would overlap exactly. The calculated edges

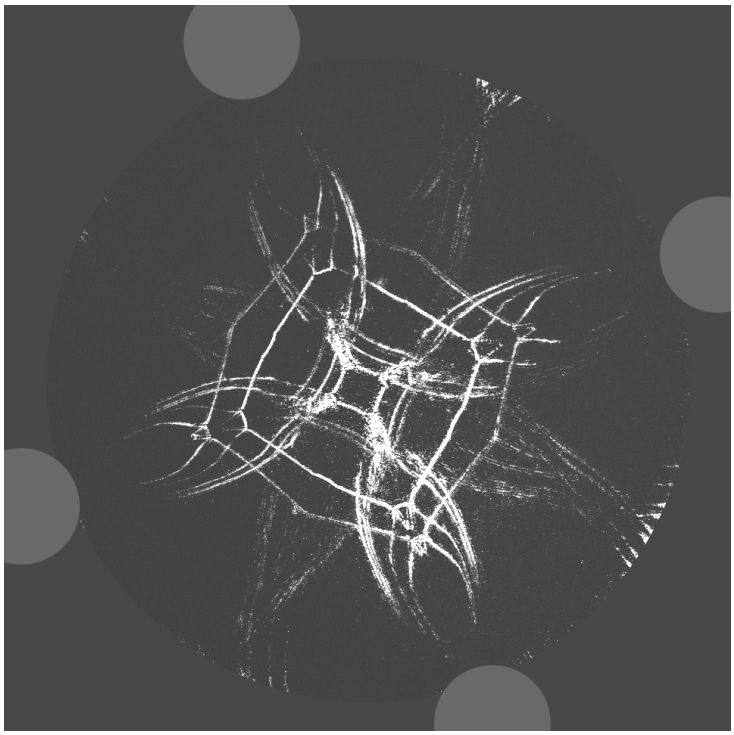

FIGURE 11. Schlieren photographs of five shock waves at different time instants passing four cylinders, with diameters of 15 mm. The filled grey circles are the cylindrical obstacles.

for the first two shock waves, corresponding to 200, 210 μs, overlap with the schlieren images. The calculated edge for the third shock wave, 215 μs, does not overlap perfectly and from this figure it is possible to see that the center of the shock wave has moved. There is a slight shift toward the side where the obstacles are placed and this observation agrees with previous observations made by Perry and Kantrowits (1951).

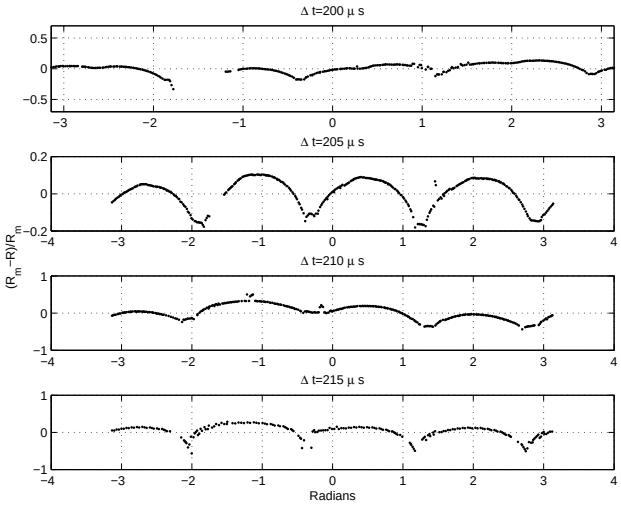

FIGURE 12. The deviation from the mean radius normalized with the mean radius for the case with four cylinders placed at the corners of a square. The time delay, Δt, for the individual shock waves are 200, 205, 210, 212.5 and 215 μs respectively. 200 μs represent the largest one. Observe that the scale is not the same in all four graphs.

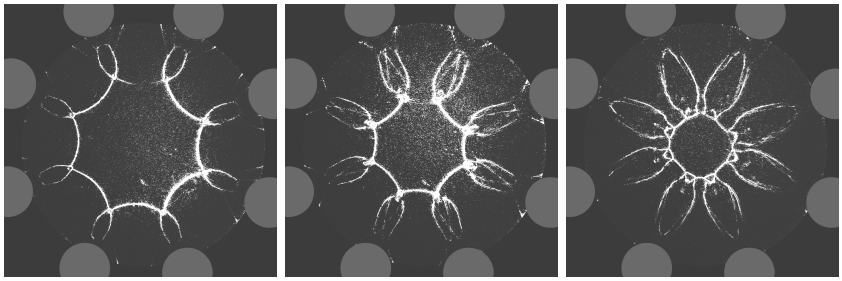

(a) Δt=200 μs. (b) Δt=205 μs. (c) Δt=210 μs.

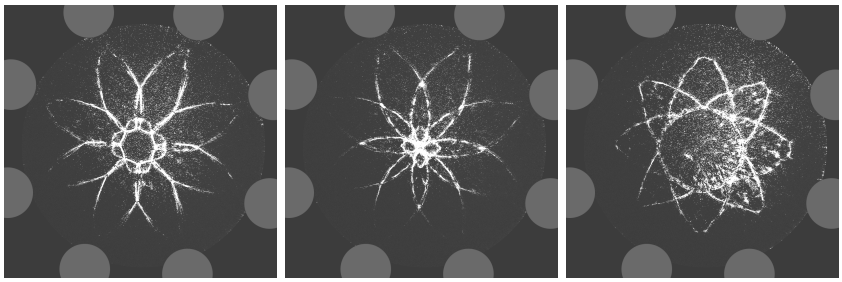

(d) Δt=216.5 μs. (e) Δt=217.5 μs. (f) Δt=240 μs.

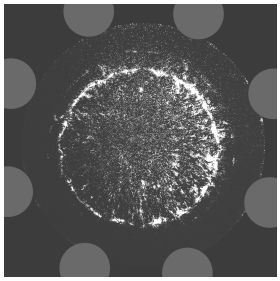

(g) Δt=260 μs.

FIGURE 13. Schlieren photographs of shock waves at different time instants passing eight cylinders, with diameters of 15 mm. The filled grey circles show the positions of the cylindrical obstacles.

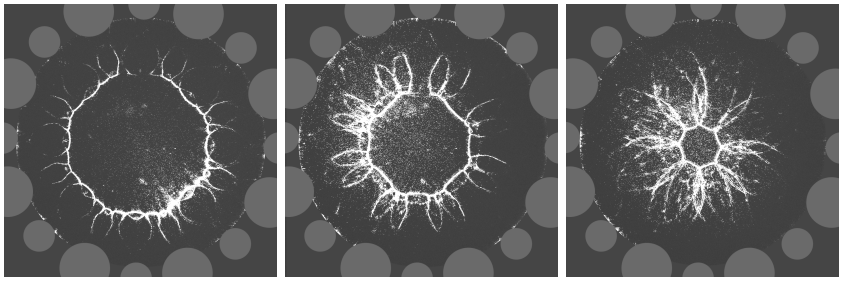

(a) Δt=200 μs. (b) Δt=205 μs. (c) Δt=210 μs.

FIGURE 14. Schlieren photographs of shock waves at three different time instants passing 16 cylinders, with diameters of 15 mm and 10 mm. The filled grey circles show the positions of the cylindrical obstacles.

(a) Δt=200 μs. (b) Δt=210 μs. (c) Δt=215 μs.

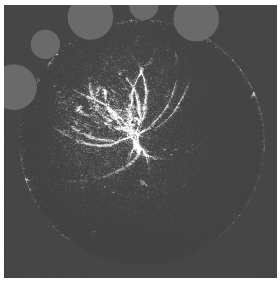

(d) Δt=217 μs.

FIGURE 15. The shock wave at four different time instants, M=2.3. The filled grey circles show the positions of the cylindrical obstacles.

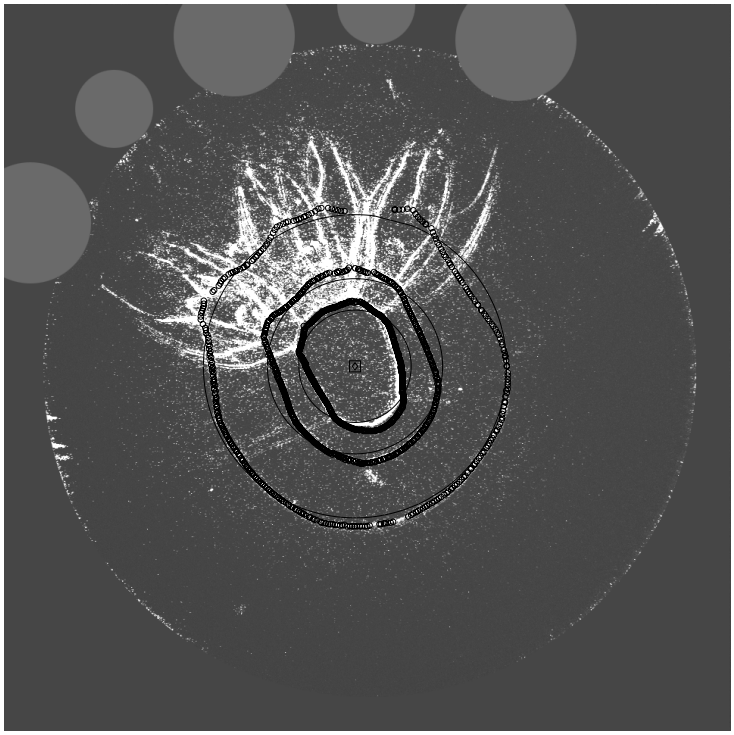

FIGURE 16. Schlieren photographs of the three converging shock waves, (same as in Fig. 15), a calculated edge of the shock wave and center point. The filled grey circles show the positions of the cylindrical obstacles. Three additional cylinders (d=7.5 mm) are not seen in the figure, placed outside the cylinders with d=15 mm.

4. Numerical Results

In a previous work, Eliasson *et al.* (2005) used the artificially upstream flux vector splitting scheme (AUFS) for Euler equations, introduced by Sun and Takayama (2003) to conduct the numerical study of the problem. In the present work this scheme once again proved to be a robust, stable and accurate numerical tool, able to predict and reproduce the major features of the shock focusing process in the present case.

In the numerical study we consider the propagation of a strong shock in a thin gas-filled test section, representing the test section in the experimental setup. The shock is assumed to be created by an impulsive high pressure in a thin annular zone between between two cylindrical boundaries. One of which is outer boundary of the test section while the other is the inner circular end of the annular part of the shock tube. The inner of the test section is initially kept at lower pressure and a number of cylindrical obstacles of various radii is placed in several patterns in the test section. This initial and boundary value problem is solved numerically and the complete two-dimensional flow in the test section is computed.

In all three cases the pressure in the inner cylindrical part of the test section was set to $p_1 = 13.3kPa$. This value was chosen to be the same as the one used in the experiment. The pressure in the driver section in the experiment was $p_4 = 112\ p_1$.

Although the losses in the straight portion of the tube are minimized, we should expect greater losses due to the sharp 90° bend.Numerical results for various values of the initial pressure ratio in the test section have been compared with the experimental data. One of the measured and calculated parameters of the complete flow was the average radius of the converging and reflected shock in the test section as function of time. These curves were calculated for various initial pressure ratios at the boundary of the test section starting from the maximum theoretical ratio $p_4/p_1 = 112$ and gradually decreasing this value in order to account for the pressure losses in the tube. The pressure ratio value that compared best with the experimental curves turned out to be about 30 % of the maximum value, giving $p_4/p_1 = 33.6$. This value was used in the present calculations as well.

The process of convergence of the initial cylindrical shock in the test section with cylindrical obstacles placed in various patterns as well as the following process of propagation of the outgoing reflected shock from the center of the test section is studied in detail and the results are compared with the experimental observations. The shape of the test section in the present case of a circular boundary together with the thin high pressure zone adjacent to the test section boundary and a typical configuration of cylindrical obstacles are schematically shown in Fig. 17.

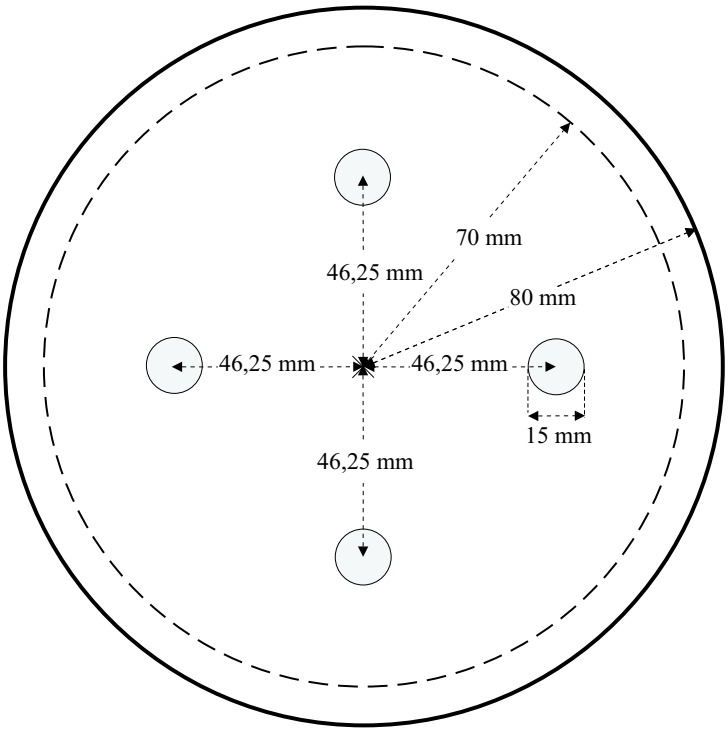

FIGURE 17. The outer cylindrical test section boundary with the thin adjacent initial high pressure zone and four cylindrical obstacles.

Results of a typical calculation illustrating the density gradient profiles at various positions in the test section for the case of four cylindrical disturbances is shown in Fig. 18. In this case four cylindrical obstacles are placed in the test section forming a square pattern. A square-like pattern is seen to be formed after the shock has passed the four cylindrical disturbances. The sides of the square are convex forward in the same way as in the experimental schlieren images as shown in Fig. 11. As the shock propagates toward the center of the test section the sides become planar and a square-shaped shock is formed.

The comparison with the experimental results has been carried out for four cases with one, two, four and eight cylindrical obstacles and the results are shown in Figs. 19-22. These figures show that the numerical calculations based on the AUSF scheme are able to reproduce the main features of the shock propagation in the test section. As seen from these figures the form of converging shocks compares well with the calculated shock fronts in these configurations.

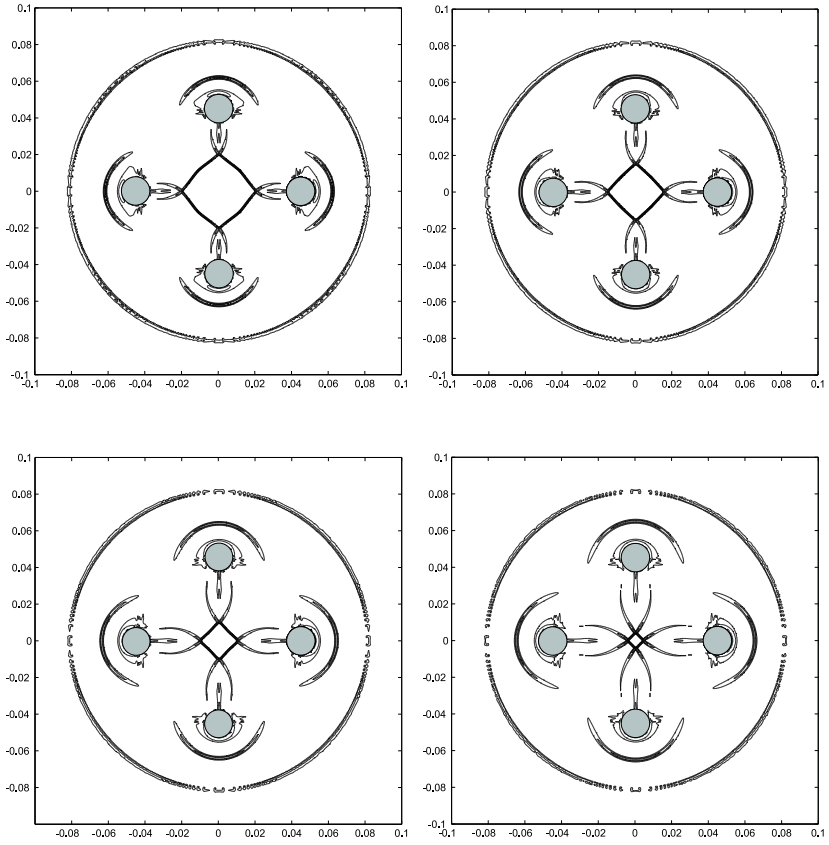

FIGURE 18. Density gradient profiles at various positions in the test section for the case of four cylindrical disturbances.

Fig. 19 shows comparison of the calculated shock profiles with the schlieren images at the corresponding positions in the test section.

Figures 21 and 22 show that it is possible to obtain converging shocks with polygonal form by means of cylindrical disturbances placed in the test section. In Fig. 21 four cylindrical disturbances are placed symmetrically in the test section and the form of the converging shock front is shaped as a square, while in Fig. 22 an octagonal form is produced by means of 8 cylinders. An alternative way of shaping a converging shock front is by using an appropriate form of the reflector boundary, as it was reported in our previous work, Eliasson *et al.* (2005). The present method appears to be more simple in terms of practical applications. There is however a question of losses due to disturbances in

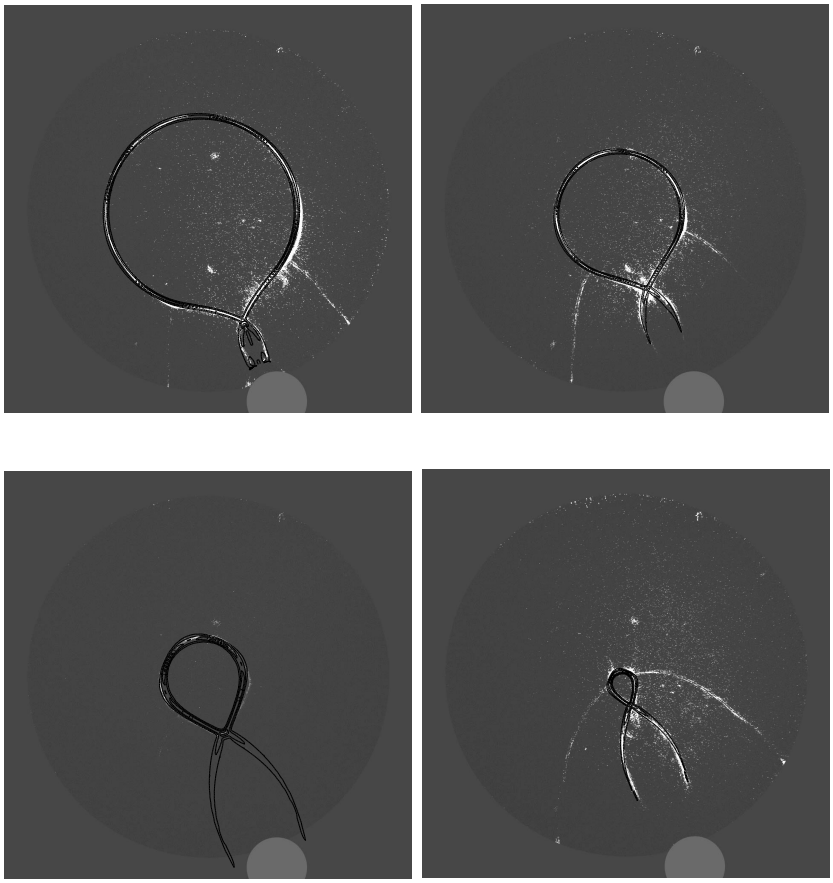

FIGURE 19. Comparison of the calculated shockwave profiles with the experimental schlieren images in the test section with one cylindrical disturbance for $p_4/p_1 = 33.6$.

the flow. In other words one would like to compare the development of the maximum Mach number during the convergence process in both cases. This comparison is given in Fig. 23 and shows that the maximum Mach number (at a certain time over the total test section) is higher in the case of an octagonal reflector as compared to eight cylindrical disturbances each with an diameter of 15 mm.

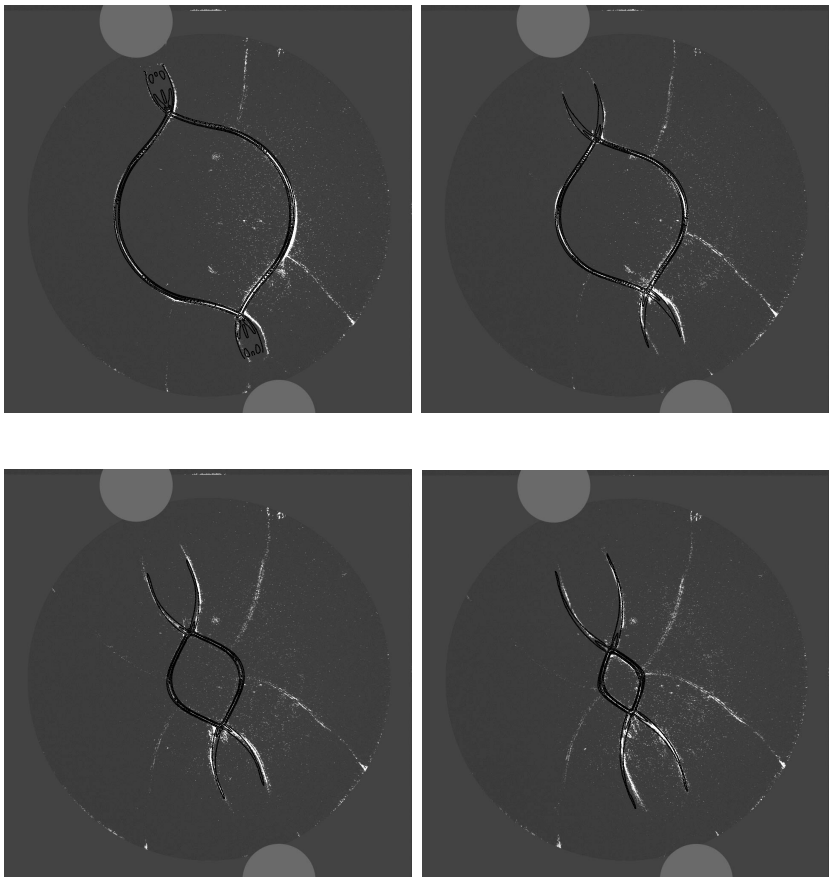

FIGURE 20. Comparison of the calculated shockwave profiles with the experimental schlieren images at various positions in the test section with two cylindrical disturbances for $p_4/p_1 = 33.6$.

5. Conclusions

A horizontal co-axial shock tube was used to investigate the properties of strong converging and reflected shock waves. The cylindrical shock wave was disturbed by circular cylinders. Three different sizes of cylinders have been used. The cylinders where placed in a various number of patterns. A numerical study has been performed and the results compared to the experimental observations. The main results of the present investigation can be summarized as follows.

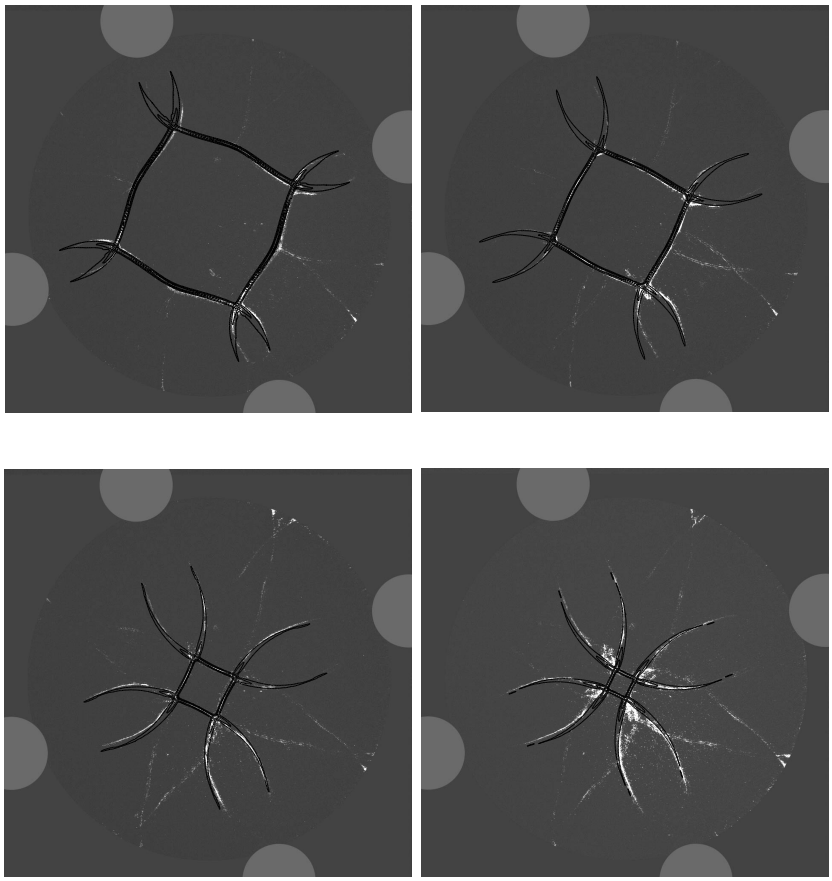

FIGURE 21. Comparison of the calculated shockwave profiles with the experimental schlieren images at various positions in the test section with four cylindrical disturbances for $p_4/p_1 = 33.6$.

(1) It is possible to produce shock waves of various shapes in a desired way by introducing obstacles in the flow. The present method may be easier to implement than to change the boundary of the test section as it was done in earlier experiments by Eliasson *et al.* (2005). Since a converging cylindrical shock wave is unstable, it is easy to disturb it and transform the shape of the shock.

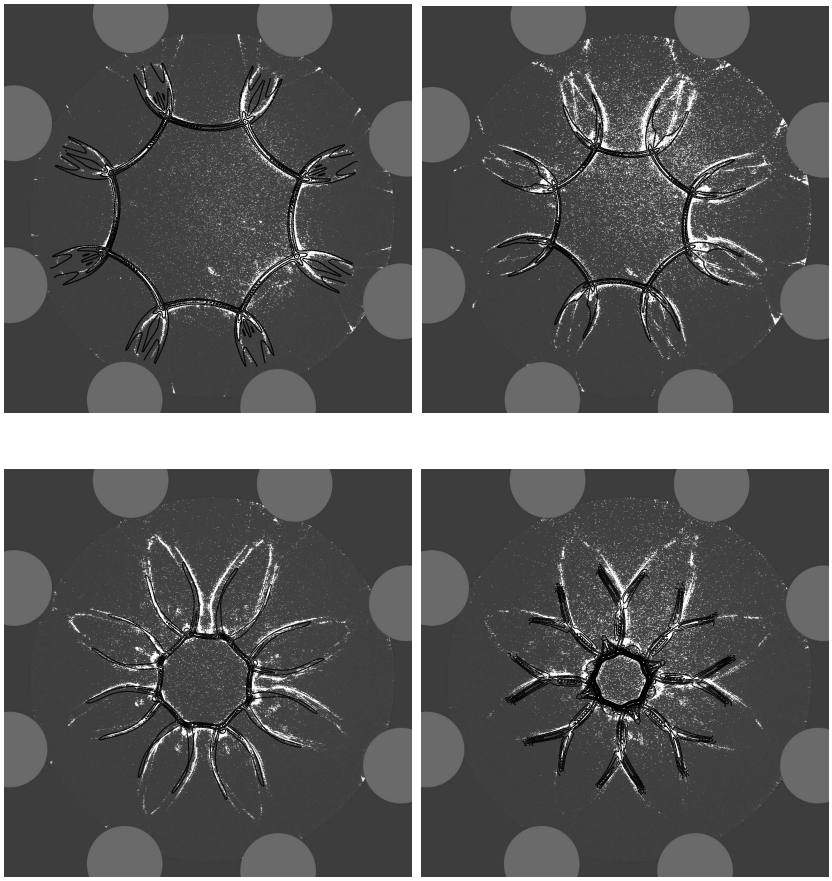

FIGURE 22. Comparison of the calculated shockwave profiles with the experimental schlieren images at various positions in the test section with eight cylindrical disturbances for $p_4/p_1 = 33.6$.

(2) The nonlinear dynamics of the shock becomes evident in the present experiments. An octagonally shaped shock wave transforms into a double octagon and then back again to an octagonal shape although oriented in the opposite direction.

(3) The artificially introduced disturbances are stronger than the disturbances caused by the four supports for the inner body. This means that close to the center of convergence we no longer see square-like shapes caused by the supports to inner body.

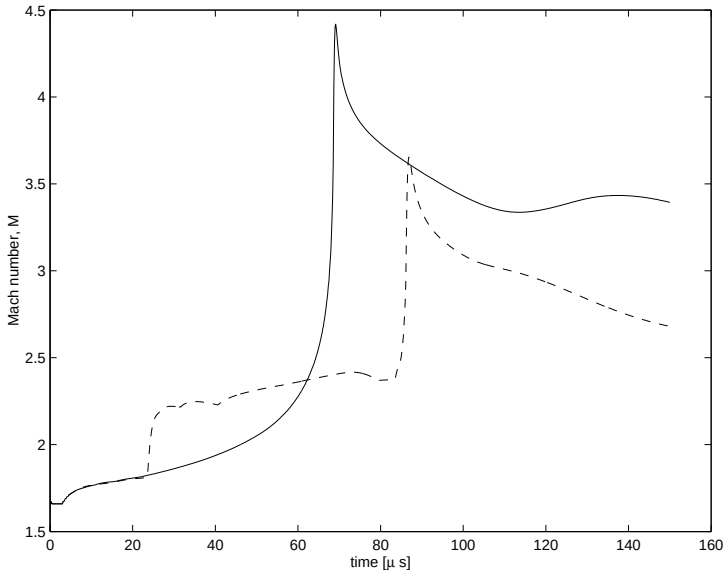

FIGURE 23. Comparison of the maximum Mach number in the test section for a shock produced by an octagonal boundary, solid line, vs eight cylindrical disturbances, dashed line

(4) The reflected shock wave is circular for all setups tested in the present experiments. However, no photographs where obtained as far out from the center to show if the reflected shock wave is influenced by the flow field created by the converging shock as earlier reported by Eliasson *et al.* (2005).

(5) Parts of the diffracted shock wave are delayed when passing over an obstacle. The center of the converging shock wave does shift slightly toward the disturbed side. However, the influence of the obstacle is greater on the shape of the shock than on the position of the shock center.

(6) Numerical analysis based on the AUFS scheme was able to reproduce the major features of the shock propagation process in the test section. The flow patterns produced in the calculations compare well with the experimental observations. This numerical tool may therefore serve as a starting point for the future experimental work as it has done in the present one.

6. Acknowledgements

This research was initiated in collaboration with Prof. Martin Lesser and his ideas and suggestions are gratefully acknowledged. The authors would like to thank Mr Ulf Landén at KTH Mechanics for careful construction of the cylindrical obstacles. We also would like to thank Dipl. Ing. Ramis Örlü for help with the cold wire temperature measurements. This work has been financially

supported by The Swedish Research Council (VR). This is gratefully acknowledged. The funding from the Göran Gustafsson Foundation provided means for the construction of the shock tube and for acquisition of the experimental equipment which is gratefully acknowledged.

References

Apazidis N, Lesser MB (1996) On generation and convergence of polygonal-shaped shock waves. J. Fluid Mech., **309**: 301-319.

Apazidis N, Lesser MB, Tillmark N, Johansson B. (2002) An experimental and theoretical study of converging polygonal shock waves. Shock waves., **12**: 39-58.

Bryson AE, Gross RWF (1960) Diffraction of strong shocks by cones, cylinders and spheres. Fluid Mech. **10**: 1-16.

Eliasson V, Apazidis N, Tillmark N, Lesser M (2005) Focusing of strong shocks in an annular shock tube. Accepted for publication in Shock waves

Guderley G (1942) Starke kugelige und zylindrische Verdichtungsstöße in der Nähe des Kugelmittelpunktes bzw. der Zylinderachse. Luftfahrt Forsch, **19**: 302-312.

Perry RW , Kantrowitz A (1951) The production and stability of converging shock waves. J. Appl. Phys. **22**: 878-886.

Schwendeman DW , Whitham GB (1987) On converging shock waves. Proc. R. Soc. Lond. A **413**: 297-311.

Sun M, Takayama K (2003) An artificially upstream flux vector splitting scheme for the Euler equations. J. Comput. Phys. **189**: 305-329.

Takayama K, Kleine H, Gröning H (1987) An experimental investigation of the stability of converging cylindrical shock waves in air. Exp. Fluids **5**: 315-322.

Watanabe M, Onodera O, Takayama K (1995) Shock wave focusing in a vertical annular shock tube *Shock Waves @ Marseille IV.*, Editors Brun R, Dimitrescu LZ. Springer-Verlag, 99-104.

Whitham G.B. (1957) A new apporach to problems of shock dynamics. Part 1. Two-dimensional problems.

Whitham G.B. (1958) On the propagation of shock waves through regions of non-uniform area or flow *J. Fluid Mech.* **4**, 337–360.

Whitham G.B. (1959) A new apporach to problems of shock dynamics. Part 2. Three-dimensional problems. *J. Fluid Mech.* **5**, 369–386.